

Laporan Akhir Projek Penyelidikan Jangka Pendek

Effect of Using Piezoelectric Fans on Cooling of Microelectronic Systems

By
Prof. Dr. Mohd Zulkifly Abdullah
Dr. Kamarul Ariffin Ahmad
Dr. Farzad Ismail
Dr. Muhammad Razi Abdul Rahman

TECHNICAL REPORT

ON

DEVELOPMENT AND PERFORMANCE ANALYSIS OF PIEZOELECTRIC FANS FOR COOLING OF MICROELECTRONIC SYSTEMS

BY

Mohd Zulkifly Abdullah Kamarul Arifin Ahmad Farzad Ismail Muhammad Razi Abdul Rahman

School of Mechanical & Aerospace Engineering,
Engineering Campus, Universiti Sains Malaysia, 14300 Nibong Tebal,
Penang, Malaysia.

Email: mezul@eng.usm.my

Tel: +6045996310

Fax: +6045941025

Summary

Piezoelectric fans can be used to generate airflow for cooling microelectronic devices. Their outstanding features include noise-free operation, low power consumption and suitability for confined spaces. This work presents experimental optimization of tip gap and orientation angle of three piezoelectric fans (multi-piezofan) to maximize the heat removal performance of finned heat sink used in microelectronic cooling. Design of experiments (DOE) approach was used for the optimization, and a three dimensional simulation using FLUENT 6.3.2 was carried out to better understand the flow induced by the multi-piezofan and the resulting heat transfer from the heat sink surface. For the optimization, the Central Composite Design (CCD) of response surface methodology (RSM) was exploited from the Design Expert software. In the numerical model, the flow induced by the piezofan was treated as incompressible and turbulent; the turbulence was taken care by the shear stress transport (SST) k- ω model. The experimental results are found to be in good agreement with the predictions. Out of 13 experimental trials determined by CCD, the optimum tip gap and fan orientation are found to be $\delta = 0.17$ and 90° respectively. At this condition, an enhancement in convective heat transfer coefficient exceeding 88% is achieved, compared to natural convection.

The output of the project:

- 1) Two PhD students One graduated 2011 and will be graduated in this October, 2012.
- 2) One MSc student- Ongoing.
- 3) 3 papers have been accepted in the International journal and 1 is under review.
- 4) 3 papers have been accepted in the International conference.
- 5) Experimental facility for piezoelectric study was developed in Aerodynamic Laboratory, school of Mechanical Engineering, Universiti Sains Malaysia.

1.0 Introduction

The field of electronics deals with the construction and utilization of devices that involve current flow through a vacuum, a gas or a semiconductor. The vacuum tube served as the foundation of the electronics industry until the 1950s. However, the invention of the transistor in 1948 marked the beginning of a new era in the electronic industry. The next turning point in electronics occurred in 1959 with the introduction of the integrated circuits (IC), where several components such as diodes, transistors, resistors, and capacitors are placed in a single chip.

Development of this pioneering technology formed the basis of large scale integration (LSI) devices in the 1970s and very large scale integration (VLSI) in the 1980s, and thereafter more advanced ultra large scale integration (ULSI) on a single chip. The semiconductor industry paving the way for Giga scale integration (GSI) and Tera scale integration (TSI), where billion and trillion of transistors may be integrated on a single-on-chip. These evolutions of microelectronic technology from a single transistor to many billions of transistors on a single chip are summarized in Figure 1.1(a-b) respectively. This trend conforms to the Moore's law according to which the number of transistors that can be placed inexpensively on an integrated circuit is doubled approximately every two years (Figure 1.2), and this will continue for several chip generations. As a result, the integration scale has become smaller and smaller.

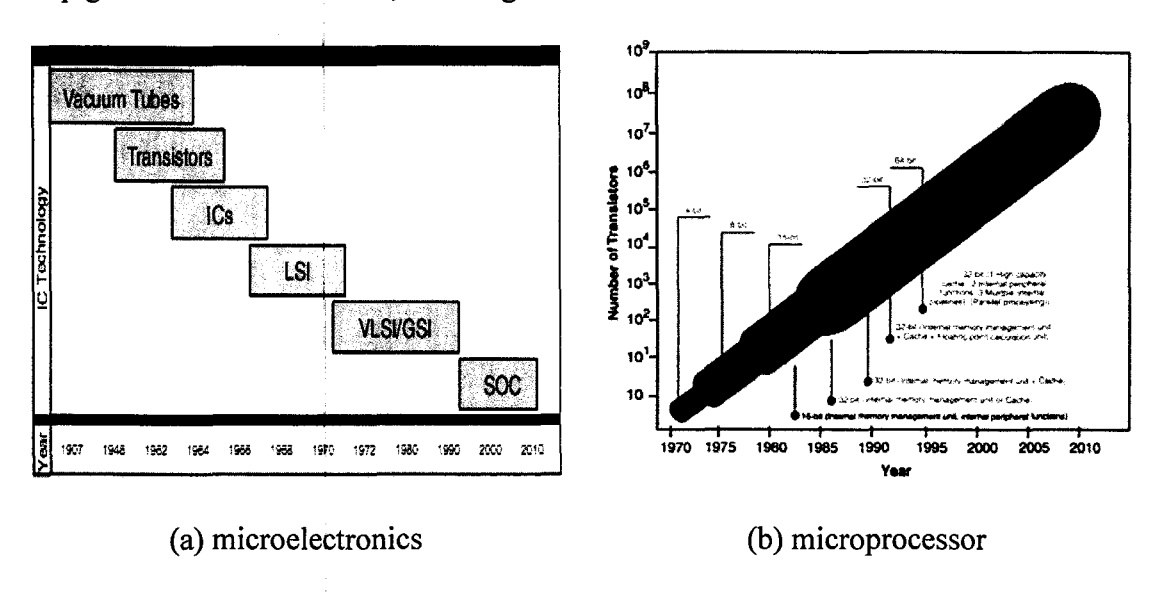


Figure 1.1 Evolution of microelectronics over the year (Tummala, 2001)

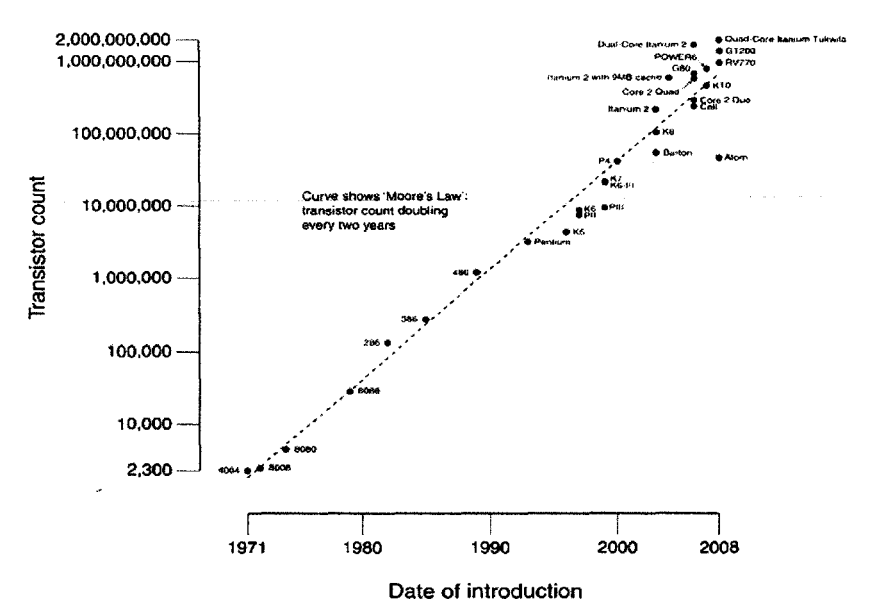


Figure 1.2 Plot of transistor counts against dates of introduction (www.wikipedia.com)

Theoretically, there is no limit to integrating multiple functions on a single chip giving rise to concepts such as System-on-Chip (SOC). The concept of SOC is integrated together the electrical, optical, mechanical, chemical and biological devices on a single chip. This includes processors and numerous digital peripherals. Figure 1.3 shows a personal handy phone system design by the SOC concept.

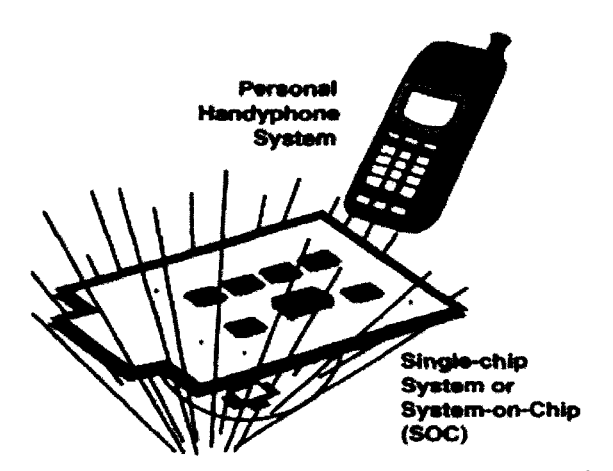


Figure 1.3 Personal handy phone system based on System-on-Chip (Tummala, 2001)

1.1 Thermal Management in Microelectronics

1.1.1 Thermal Management Issue

In the early stage of introduction of the transistor, it was touted as a device that produces no heat. This certainly was a fair statement, considering the huge amount of heat generated by vacuum tubes. But when thousand or even millions of such components are packed in a small volume, the heat generated increases to such high levels that its removal becomes a formidable task and a

major concern for the safety and reliability of the microelectronic devices. The heat fluxes in microelectronic devices encountered are in the range of less than 1 W/cm² to more than 100 W/cm². Heat is generated in a resistive element as long as current continues to flow through it. This creates a heat build-up and a subsequent temperature rise at and around the components until the component is destroyed unless heat is transferred away from it. The failure rate of electronic devices increases almost exponentially with the operating temperature as shown in Figure 1.4 (Cengel, 2003). This problem exists in almost all fields such as defense, aerospace, automotive, gas, remote sensing and micro processor.

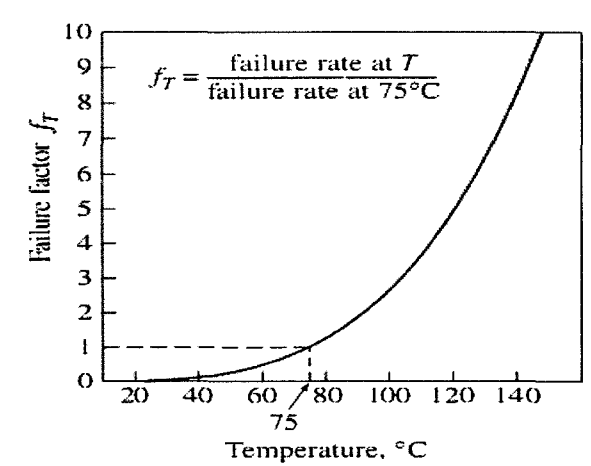


Figure 1.4 Failure rates of digital devices with the temperature (Cengel, 2003)

Managing heat flow and the negative effects of high temperatures on electrical packages needs to be considered during the package whole life cycle to ensure optimal performance and reliability. It is important that heat is managed to ensure robust assembly (i.e. solder joint interconnections) and avoid defects due to overheating (i.e. impact of higher lead-free reflow temperatures) during manufacturing and assembly. When the electronic package is placed in the field it is important to ensure that heat is controlled to ensure operating temperatures are within the specified values recommended by chip manufacturers. Unfortunately as transistors become smaller (but contain as billions or trillion transistors embedded on a single chip), the amount of power leaked is also increasing and this leads to increase power densities for future devices. Heat resulting from higher power density is becoming a critical issue in computer and semiconductor design. This growing thermal issue is causing distress due to:

- Shorter product lifetime: According to a rough estimation, a 10°C increment in the operating temperature can cause a reduction of 50% product lifetime.
- Increased operating cost: To maintain the device always cool, it requires more fans, which use more electricity and hence increase energy consumption and cost.
- Increase build cost: Even larger and more complex heat sinks fans and other thermal management solutions are driving up manufacturing costs.
- Consumer acceptance: More heat requires larger, faster and noisier fans. Consumers are reluctant to accept noisy products.

If thermal management is inadequate then premature device failure can be expected either by direct failure of the semiconductor or more likely by progressive accumulation of thermo mechanical damage and eventual cracking of interconnect structures (Kristiansen, 2001). Organizations such as US National Aeronautics and Space Administration (NASA) have

estimated that 50-90% of mission failure can be attributed to thermally induce interconnect failures (Bailey, 2008). Figure 1.5 shows the percentage of failures due to different environmental effects.

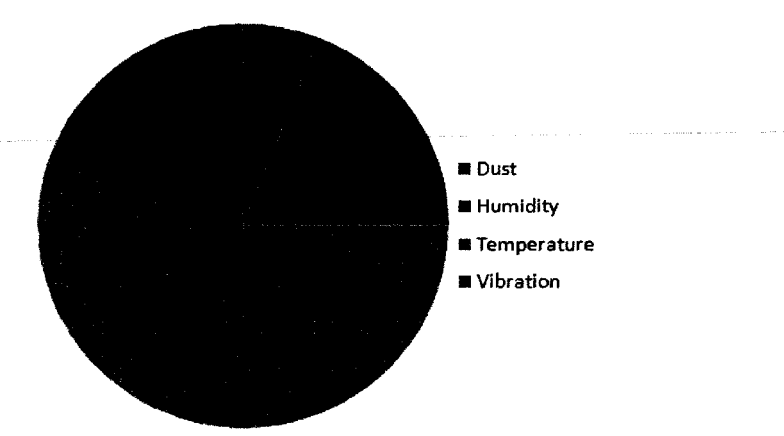


Figure 1.5 Causes for defects in defense related electronics (Bailey, 2008)

1.1.2 Thermal Management Solutions

The primary thermal management objective of the modern microelectronic package is to reduce the heat flux to a more manageable level while keeping its temperature below 100°C. Various methods have been proposed to overcome this issue. The definition of thermal management relates to techniques that enable the removal of heat from microelectronic devices with/without the need to apply external energy to do this. The solutions can be characterized as passive, active and combination of the two aforementioned or it may call as hybrid cooling (Ohadi and Qi, 2005).

The passive cooling technique is relatively reliable and simple to implement since there is no external power required. The primary mechanism of removing heat in this manner is through thermal conduction and radiation. However, the performance is limited for many high power applications. The main passive thermal management technologies are conduction (metal spreader, interface materials, adhesives, pads, pastes, and epoxy bond), natural convection (finned heat sinks, ventilation slots, and liquid immersion cooling), radiation (paints, coatings, mechanical surface treatments) and phase change (phase change materials, heat pipes, thermosyphons, and vapour chambers).

Meanwhile, the active thermal management techniques require input power to remove heat from a microelectronic device and hence have enhanced performance and capacity. It may extend the performance of microelectronic cooling systems; however, the system thermal impedances create bounds outside of which active cooling cannot offer improved thermal performance over passive cooling. The essential active technologies include forced convection (rotary fans, piezoelectric fans and nozzles), pumped loops (heat exchangers, cold plates and jet/spray), and refrigerators & coolers (vapour-compression, vortex, thermo acoustic, thermoelectric/Peltier). In general, adopting an active cooling technology for thermal management needs is more costly than passive approaches and it is well recognised that air cooling using conventional fan is reaching its limit for certain applications.

A hybrid thermal management technique combines passive and active cooling into a single package. The foremost hybrid thermal management technologies are natural and forced convection (heat sink and rotary fan), forced convection and phase change (jet impingement and micro channel, rotary fan and heat pipes/vapour chamber) and etc.

1.2 Introduction to Piezoelectric Fan

1.2.1 Piezoelectricity

The term of piezo actually comes from the Greek word "piezo," which means "squeeze" and the word piezoelectricity means electricity resulting from pressure. According to Duran and Moure (1986), Piezoelectricity is a phenomenon present in all crystals having a polar axis, and in those crystals where a polar axis is generated when subjected to mechanical stress, and it is the direct result of the piezoelectric effect. Pierre and Jacques Curie were the first discovered piezoelectricity when they discovered an unusual characteristic of certain crystalline minerals in the 1880s.

The piezoelectric materials can generate electricity when it squeezes, and expand or twist when electrified. Many substances can be piezoelectric, if they have the right shape. Salt, sugar, quartz and other common substances can form piezo crystals. A piezoelectric crystal is off-balance due to asymmetry which means one side has more atoms than the other. When the crystal is squeezed, an electric charge is created due to the increase of atomic imbalance. Electric current can be generated if both sides of the crystal are connected in a circuit. This effect can be understood as the linear electromechanical interaction between the mechanical and the electrical state in crystalline materials with no inversion symmetry (Gautschi, 2002). This is a reversible process, which means that materials exhibiting the direct piezoelectric effect also exhibit the reverse piezoelectric effect.

1.2.2 Piezoelectric Materials

In the 20th century, metal oxide-based piezoelectric ceramics and other manmade materials enabled designers to employ the piezoelectric effect and the inverse piezoelectric effect in many new applications. These materials generally are physically strong and chemically inert, and they are relatively inexpensive to manufacture. The composition, shape, and dimensions of a piezoelectric ceramic element can be tailored to meet the requirements of a specific purpose. Lead zirconate titanate (Pb[ZrxTi1-x]O3; 0<x<1), also called PZT, is a ceramic perovskite material that shows a marked piezoelectric effect. PZT-based compounds are composed of chemical elements such as lead and zirconium, and the chemical compounds such as titanate, which are combined under extremely high temperatures, and this is the most widely used piezoelectric ceramic material.

1.2.3 Types of Piezoelectric Structures

Normally three types of piezoelectric structures are available in the market, namely unimorph, bimorph and stack, as shown in Figure 1.7. Unimorph is a cantilever beam having one active layer bonded with piezoelectric and one inactive layer (i.e. non-piezoelectric material). Application of an electric field induces deformation in the active layer, thereby creating bending displacement in the cantilever. Bimorph is a cantilever beam which consists of two active layers namely piezoelectric layer and metal (piezo ceramic elements bonded together with a flexible metallic panel as its central electrode). These layers can produce a displacement by two

activations: first activation by a temperature change which causes one layer to expand more than the other, and the second by electrical activation which causes one layer to extend and the other layer to contract. Piezoelectric stack is a monolithic ceramic construction of many thin piezoceramic layers connected in parallel electrically. Its motion may be increased at the expense of force, by mechanical amplification. This stack offers a high energy density in a small package due to its superior compressive strength, and provides a high load bearing capability.

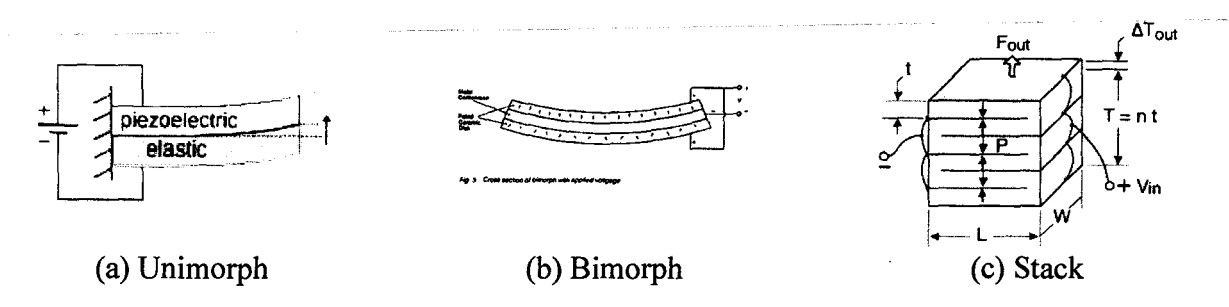


Figure 1.7 Type of piezoelectric

1.2.4 Piezoelectric Applications

A piezoelectric system can be constructed for almost all applications for which any other type of electromechanical transducer can be used. However, some limiting factors to be considered are size, weight, and cost of the system. Usually, piezo ceramic devices can be fitted into four general categories: generators, sensors, actuators, and transducers; the characteristics of each category are summarized here.

Piezoelectric ceramics can generate voltages sufficient enough to create spark across an electrode gap, and can be manipulated as igniters. The devices using this small scale power generation are fuel lighters, gas stoves, welding equipment etc. Piezoelectric ignition systems are small and simple, and have distinct advantages relative to alternative systems that include permanent magnets or high voltage transformers and capacitors. Alternatively, the electrical energy generated by a piezoelectric element can be stored.

Piezoelectric sensor is a device that converts a physical parameter, such as acceleration, force, strain or pressure, into an electrical signal. It has been successfully used in various applications, such as in medical, aerospace, nuclear instrumentation, and as a pressure sensor in the touch pads of mobile phones. In some sensors the physical parameter acts directly on the piezoelectric element; in other devices an acoustic signal establishes vibrations in the element and the vibrations are, in turn, converted into an electrical signal. Often, the system provides a visual, audible, or physical response to the input from the sensor; for example, automobile seatbelts lock in response to a rapid deceleration.

Piezoelectric actuator is a device which converts an electrical signal into controllable physical displacement. Displacement, force, frequency, weight and size are examples of the basic characteristics of any linear actuator. Piezoelectric actuators are used to control hydraulic valves, act as small-volume pumps or special-purpose motors, etc. A potentially important additional advantage of piezoelectric actuator is the absence of electromagnetic noise. Alternatively, if physical displacement is prevented, an actuator will develop a useable force.

Lastly, piezoelectric transducer is a device which transforms either mechanical or acoustic energy into electrical energy. An example of the high sensitivity of the piezoelectric transducer is microphones which converts sound pressure into electric voltage. They are compact, simple, and highly reliable, and minimal energy can produce a high level of sound. Because the piezoelectric effect is reversible, a transducer can both generate an ultrasound signal from electrical energy and convert the incoming sound into an electrical signal. Piezoelectric transducers are also used to generate ultrasonic vibrations for cleaning, atomizing liquids, drilling or milling ceramics or other difficult materials, welding plastics, medical diagnostics, etc.

1.2.5 Piezoelectric Fan (piezofan)

A piezoelectric fan (piezofan) is a resonant device which is used to move air due to induce oscillations in a cantilever beam that uses a ceramic material. Normally, it is fabricated by bonding a piezoelectric patch or several patches to a shim material cut to the desired shape and size, or by using the patch itself with no shim (blade) attached. When an alternating voltage is applied to the piezoelectric patch, it expands and contracts alternately like a hand-held fan with the same frequency as the input signal as shown in Figure 1.7. Typically, the alternating voltage is applied at a resonant frequency of the piezofan to maximize fan efficiency usually ranging from a few millimeters to 2.5 cm. Figure 1.8 shows a sample of piezofan available in the market.

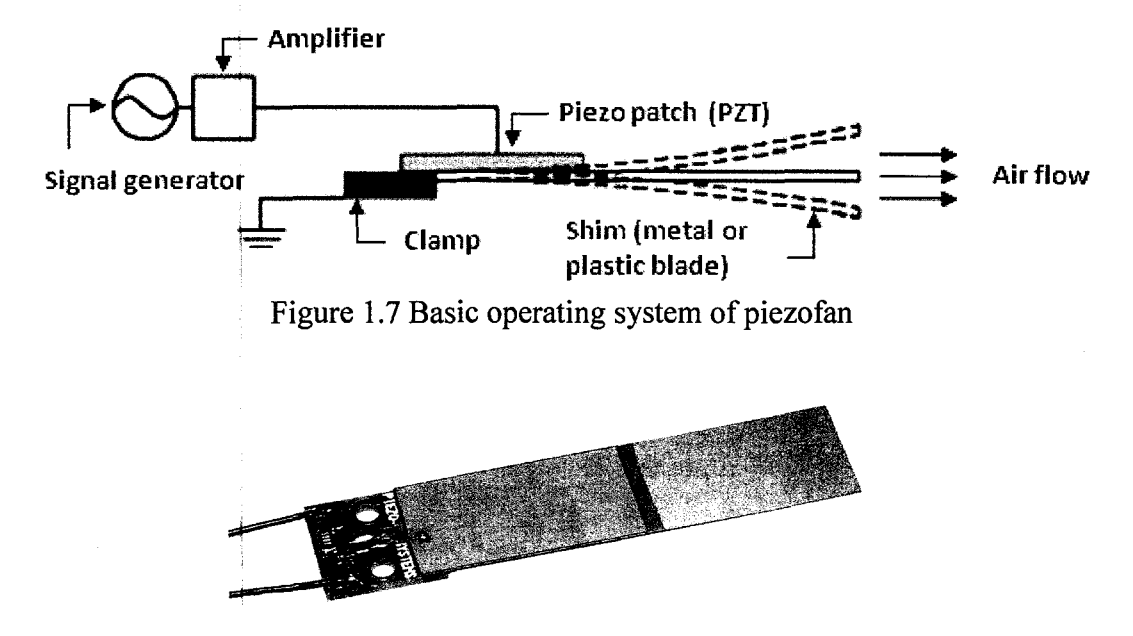


Figure 1.8 Picture of a piezofan (www.piezo.com)

1.3 Significance of Piezofan

Piezofan has received some attention for use in cooling applications throughout the last few decades. Characteristic of piezofans have made it more convenient to be used in microelectronic cooling application and it can be characterized as active cooling technique. The piezofan has very low power consumption; it does not require large amounts of power and typically operate in the range of 10 to 20 mW, less noise; most devices are driven at frequencies under 100 Hz so that the acoustic energy and noise levels are kept low such that their first mode of resonance is

outside the range of frequencies audible to the human ear in order to ensure silent operation (i.e., under 25 dBA) and high velocity airflow induced; small deflections in the piezoelectric patch are amplified to large values at the tip of the fan to create the stirring leading to air movement. It is well suited, especially for portable electronics cooling applications such as cell phones, laptops, PDAs etc.

1.4 Problem Statement

Advances in portable electronics to meet increasing consumer demand for smaller products with greater functionality have resulted in faster and more powerful electronic components to be installed into smaller spaces. Conventional methods of heat removal such as incorporation of heat sinks and rotational fans are thermally viable. However, a promising of an alternate technique of thermal management in term of minimized space, power, and noise requirements is more feasible to piezofan.

At the moment, there are extremely limited literatures on multi piezofan and combining piezofan with heat sink. Most of the previous researchers have considered a single piezofan except Kimber et al. (2009) who greatly reframe the work of Toda (1970 & 1971) by practically configured multiple piezofans in arrays. Acikalin et al. (2007) and Petroski et al. (2009) were the first to study on the effect of heat sink with piezofan on microelectronic cooling. However, their focus was limited over flat plate (Kimber, 2009) and laminar flow across the fins and a single fan was used (Acikalin et al., 2007 and Petroski et al., 2009). The present research is the first to utilize simple finned heat sink (two and four fins), with multi-piezofan. The piezofan tip gap and orientation angle are the two parameters investigated while the frequency is constant. In addition, the present study includes heat transfer optimization by using design of experiment (DOE) with respect to piezofan tip gap and orientation angle, in order to enhance the cooling. Furthermore, unlike the previous works, a detailed three-dimensional (3-D) numerical simulation is also performed to study the flow turbulence and heat sink temperature.

1.5 Objective of the Research

The present study is aimed to achieve the following objectives

- a. To study the effects of single-fan and multi-fans on the heat transfer performance of unfinned heat sink.
- b. To study the effect of tip gap and orientation angle of multifans on the thermal performances of unfinned and finned heat sinks, and to optimize them by using DOE approach.
- c. To study the effect of Reynolds number on the thermal performances of unfinned and finned heat sinks with multifans, with the optimum tip gap and orientation angle, in order to know the best Reynolds number.
- d. To compare the performance of finned heat sink with multifans, with the optimum tip gap and orientation angle, and the best Reynolds number, with that of finned heat sink with conventional rotary fan.
- e. To perform three dimensional numerical simulation to study the flow turbulence and temperatures of unfinned and finned heat sinks with multifans, and compare with the experimental results.

2.0 Literature Review

2.1 Cooling of Microelectronic Devices

Advances in the field of electronics have resulted in a significant increase in density integration, clock rates, and miniaturization of modern electronics. This resulted in dissipation of high heat flux, which linearly relates to the temperature at the chip level and creates thermal failures such as mechanical stresses, thermal debonding and thermal fracture. Managing temperature and its negative effects on electronic packages need to be considered, to ensure optimal performance and reliability (Bailey, 2008; Mochizuki, 2008).

Natural convection cooling is obviously advantageous for low power dissipating devices since it offers low-cost, energy-free, and noise-free operation (Tou et al., 1999; Adams et al., 1999). An additional means of passive cooling namely finned heat sink has been adapted (Ledezma and Bejan, 1995) since it provides a large surface area for the dissipation of heat and effectively reduces the thermal resistance (Ismail et al., 2008). Nevertheless, the rising demand for high performance and multi-functionality in electronic devices poses thermal challenges that may not be tackled by passive cooling techniques; this situation calls for active cooling techniques (Arularasan and Velraj, 2008). Table 2.1 summarizes a variety of novel alternative thermal solutions for electronics cooling.

Table 2.1 Various thermal solutions for electronics cooling

Type	Authors
Absorption heat pump	Drost and Friedrich (1997); Hu and Chao (2008)
Electro osmotic pumping	Jiang et al. (2002); Al-Rjoub et al. (2011)
Heat pipe	Harmand et al. (2011); Putra et al. (2011)
Impinging jet	Bintoro et al. (2005); Chang et al. (2007)
Integrated air and liquid micro pumps	Singhal et al. (2004); Liu et al. (2005)
Micro channel	Khaled and Vafai (2011); Chiu et al. (2011)
Thermoelectric micro cooler	Zhang et al. (2010); Huang et al. (2010)
Thermosyphon	Filippeschi (2011); Khodabandeh and Furberg (2010)
Vapor absorption	Kim et al. (2008); Kim et al. (2008)
Vapor chamber	Wong et al. (2011); Li and Chiang (2011)
Vapor compression	Wu and Do (2011): Ribeiro et al. (2010)

However, the choice of the cooling solution is dependent on factors such as heat flux, power consumption, space, weight, reliability, mobility, integration, maintenance, noise level and cost (Lasance, 1995; Garimella, 2006; Sauciuc, 2008; Mochizuki, 2011). Based on the works of Abdullah et al., (2008; 2009), piezofan is one of the best techniques that could cope up with these factors.

2.2 Experiments on Piezofan in Fluidic Studies

2.2.1 Single Fluidic

Toda (1979) conducted experiments with a piezofan, which was constructed as a multilayered PVF₂ bimorph cantilever. Simplified models for airflow and vibration were also presented. The observed resonance frequency was larger than the value predicted from theory, and this

difference increased as shorter fans were considered. However, their results showed good agreement with theory for airflow from longer fans (lower frequencies).

Yorinaga et al. (1985) introduced a new type of a piezofan that could supply sufficient and constant airflow without any structural destruction for a long time since the flexible beam resonated in large amplitude, and the bimorph vibrated with very small amplitude. They designed a modified bimorph based on the theory of a dynamic absorber and succeeded to obtain stable vibration and sufficient airflow. Yoo et al. (1994) fabricated various kinds of piezofans for application to a component cooling apparatus. The piezoelectric ceramic subtracts were manufactured by using a PZ'T-5 raw materials. They concluded that, the resonance frequency of the vibrating plate was decreased with the increasing plate length under a constant piezoelectric ceramic length, wind velocity was increased with the increasing applied voltage and displacement appeared large in case of phosphor copper with excellent elastic properties.

Several types of piezofans had been developed and investigated by Yoo et al. (2000). Fans were made from bronze, brass, aluminum with PZT patches and lengths from 32 to 35 mm. All fans were operated at 60 Hz and at two voltage levels, 110 and 220 VAC, which produced different vibration amplitudes and airflow rates. The measured air velocity was found to be highly dependent on the maximum tip velocity. They also found that the most effective fan was made from a phosphor bronze shim and with PZT in a bimorph configuration whose width was equal to that of the piezoelectric patch.

Loh et al. (2002) visualized acoustic streaming near the beam. The beam was excited at 28.4 kHz with the vibration amplitude of 10 mm. Acetone was sprayed onto the vibrating beam, produced small droplets and follows the airflow pattern near the beam until it completely evaporates. Unique features of acoustic streaming were observed; air rised above the antinodes and descended toward the node, and two distinctive circular airflows within the half-wavelength of the beam. They also viewed that clearer acoustic streaming when bigger vibration amplitude was used.

Acikalin and co-workers (2003) conducted flow visualization experiments to gain insight on the flow induced by piezofans. The piezofan with 60 Hz actuation was located at the center of the domain and sandwiched between a black bottom surface, transparent acrylic top sheet, with the side walls were kept sufficiently away from the fan to reduce interference effects on the flow field. A baffle was placed along the axis of the fan spaning the full length of the setup. A laser sheet illuminated the field from the side, parallel to the top Plexiglas surface, and smoke was seeded from a theatrical fog generator. A digital video camera was placed above the setup to capture the scattered light from the smoke particles in the domain. This work was extended by Acikalin et al., (2004) for additional visualization experiments. A piezofan actuated at 20Hz was placed inside a clear acrylic enclosure. Both observations found that suction occured near the clamp and near the tip of the piezofan. and two circulation zones having opposite directions were generated on each side.

Kim et al. (2004) investigated the flow field created by a vibrating plate using phase-resolved particle image velocimetry (PIV) and smoke visualization techniques. The actuated cantilever was 31 mm long and vibrated at 180 Hz with tip displacements ranging from 0.74 to 1.4 mm.

Counter-rotating vortices were shed each time the beam passed the original position i.e. at twice the vibration frequency. Between these two vortices and just beyond the tip, a region was formed where the maximum fluid velocity occurred, and was found to be roughly four times that of the maximum tip velocity. They also found that the flow field was two-dimensional near the cantilever tip and became more complex and three-dimensional further downstream.

Wait et al. (2007) experimented piezofan at the higher resonance modes by varying its length. Detailed flow visualizations were performed to understand both the transient and steady-state fluid motion around the piezofan. The setup was quite similar to that of Acikalin et al. (2003). They observed that the flow patterns at different resonance modes changed according to the deformation mode shape of the piezofan. Areas of recirculation were created between two nodes of the piezofan and vortices were shed from the tip. The bulk fluid motion decreased as the mode number increased due to the decrease in amplitude. Additionally, as the motion of the piezofan became more complex along the length of the blade, different portions of the fan blade moving in opposing directions tend to counteract, rather than augmenting the flow. It was also observed that decreasing the length of the fan decreased the flow volume due to smaller amplitude of vibration, and lesser surface area available to "push" the fluid.

Abdullah et al. carried out experimental analyses on the piezofan in the horizontal (2008, 2009) and vertical (2012) orientations with certain gaps. The flow measurements were carried out at different piezofan gap by using a particle image velocimetry (PIV) system. The corn oil was atomized into the clear glass tunnel, while a laser sheet was illuminated through double pulse YAG laser. The induced velocity was captured by a CCD camera, which was synchronized and controlled by the computer via the PIV controller unit. They observed that induced velocity was very much depending on its direction of movement and gap.

Acikalin and Garimella (2009) conducted flow visualization and PIV experiments in a liquid at an amplitude of 1.5 mm (peak-peak) at two different gaps. The dielectric liquid was used for submersion of the whole setup, including the piezofan. A piezofan was sandwiched between two transparent acrylic plates, clamped by a copper block and positioned at the center of the setup. A light sheet generated from a diode-pumped Nd:YVO₄ laser using a cylindrical aspheric lens with a hyperbolic profile illuminated the mid-plane of the experimental setup. A high-speed camera captured top-view images of the flow field. Flour particles were used as tracers to visualize the flow patterns. For both the gaps, the shapes of the streamlines were very similar for the regions close to the piezofan but not near the piezofan tip. Two separation flows were observed; fluid approached the fan and fluid entered the domain and ejected from the heater surface. Eastman and Kimber (2009) analyzed the flow field of a piezofan in a glass enclosure using PIV for a range of Reynolds numbers. It was found that larger Reynolds number gave a more repeatable and predictable vortex path. It was also observed that lower amplitudes tend to give a stronger flow in the x-direction as well as having a higher overall flow velocity in a 2-D view.

Kim et al. (2011) investigated the velocity field around a vibrating cantilever plate using phase-locked PIV. Experiments were performed at three different Reynolds numbers based on the tip amplitude and frequency of the cantilever. The averaged vector fields showed that a pseudo-jet flow was dominated by vortical structures.

2.2.2 Fluidic Coupling

Majority of previous studies have considered single fan. However, the studies of multi-fan are still lacking. It is practically important to configure multi-fan, and the complexity increases substantially in describing the structural, fluidic, and heat transfer behavior.

Ihara and Watanabe (1994) investigated flow field generated from single and two flexible cantilevers for in-phase and out-of-phase vibration at three different pitches. These cantilevers were sandwiched between two parallel plates to approximate a two-dimensional flow field as shown in Figure 2.1. The smoke wire method was employed for flow visualization. Comparisons of flow field and volumetric flow rate have been made. The volumetric flow rate for in-phase vibration of two cantilevers was found to be approximately double that of a single cantilever.

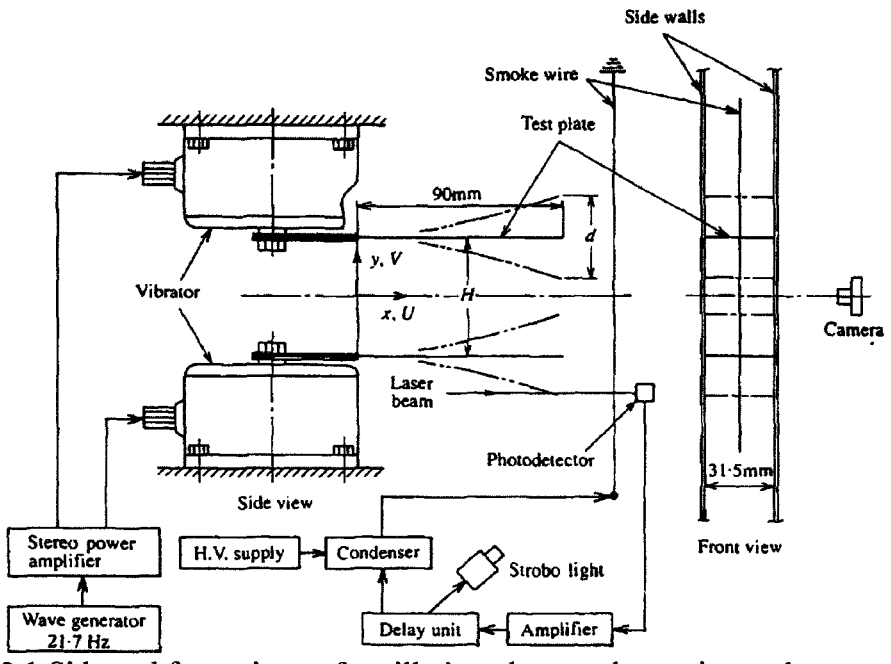


Figure 2.1 Side and front views of oscillating plates and experimental arrangement (Ihara and Watanabe, 1994)

Schmidt (1994) performed mass transfer measurements on a vertical surface mounted near two piezofans. The fan pitch was kept constant and vibrated out of phase. Power-law correlations were found to reasonably describe both maximum and surface-averaged Sherwood numbers for three different distances from the vertical surface. The contours of Sherwood numbers formed symmetrically about the midpoint of fan separation in each case. Obviously, changes in fan vibration parameters influenced the flow field and heat transfer performance. A number of studies have shown that the presence of a second oscillating beam could alter the vibration characteristics of a vibrating cantilever.

Linderman et al. (2005) analyzed flow rates produced by single and linear array of vibrating beams in a channel. It has been observed that the flow rate for the single cantilever varied linearly with frequency, length, and vibration amplitude and the flow rate was nearly tripled

whenever three fans placed in series. However, the fan's pitch variable was neglected and the interaction between neighboring fans was not captured. Kimber et al. (2006) measured resonance frequency and quality factors for fans vibrating in air and observed a decrease in viscous drag when the fans vibrated in phase. Larger vibration amplitudes of the fans were found for a given input signal relative to a single fan.

Kimber et al. (2006) presented experiments on multi-fan in air and within a vacuum chamber to isolate the source of coupling. Two piezofans were mounted in a vacuum chamber and excited in-phase at a frequency of 60 Hz at four discrete amplitudes and two fan pitches. Optical viewport provided the capability to capture vibration signals. The result showed that the amplitudes were nearly double regardless of whether a single fan or two fans considered. In contrast, the vibration amplitude for two fans under atmospheric conditions was found larger compared to that of the single fan.

Kimber et al. (2008) studied the effect of pressure and flow rate generated from vibrating cantilevers. Design tools similar to the often-used fan laws were proposed in order to predict the pressure and flow rate. The effect of proximity of surrounding walls to the piezofan was also studied by using three enclosures of different sizes. It was found that the performance was highly dependent on both the vibration amplitude and frequency. They also developed predictive relationships to describe the experimental trends, provided insight into the sensitivities of pressure and flow rate to these operating parameters. The tip velocity contributed a nearly quadratic dependence on flow rate, while the vibration frequency extremely influenced in determining the pressure. It was also found that a large enclosure had relatively little influence on the pressure or flow rate; as the size of the enclosure became smaller, only pressure was adversely affected and the inlet flow was found to be freely open for experiencing the largest amplitude to ensure the largest flow rate possible. Kimber et al. (2010a) performed further investigation, for the aforementioned effect. Direct comparison was made between two commercial axial fans, in terms of overall performance, and the efficiency with which energy was imparted to the fluid. It was observed that piezofans were nearly 10 times more efficient in converting the input power to useful energy imparted to the fluid.

Kimber et al. (2010b) experimentally quantified the fluid loading (added mass and damping) on arrays of cantilevers vibrating face-to-face and edge-to-edge. Two sets of experiments were conducted; in air and vacuum. The effect of air resonance frequency and flow rate for a range of pitches and input voltages were determined. They observed a substantial decrease in the fluid damping with in-phase vibration, while the converse was true with out-of-phase vibration for the face-to-face orientation. The edge-to-edge, out-of-phase vibration exhibited a decrease in fluid damping, and in-phase vibration caused an increase.

2.3 Experiments on Piezofan in Heat Transfer

2.3.1 Single-fan

Toda (1981) was the first who studied piezofan exclusively on heat transfer enhancement, targeted on a heated surface. The piezofan vibrated at 13 Hz with maximum airflow velocity of 1.4 m/s, caused 17°C decrease in temperature on the power transistor panel of a TV receiver. In addition, the temperature inside the receiver was also reduced by 5°C.

Kimber et al. (2007) measured the local heat transfer characteristics of piezofans by using infrared camera. The experimental setup included a film plate, coated on both sides with a thin layer of Krylon #1602 black paint with constant heat flux surface mounted in a vertical position on an optical table. A piezofan was mounted normal to the heat source, with one side linearly adjustable, while a laser displacement sensor captured the vibration signal of the fan tip. A plexiglass enclosure was built around the entire setup to isolate it from extraneous flows within the room. Four vibration amplitudes with certain distance gaps and amplitudes were considered. They found that the thermal map of the local heat transfer coefficient transitioned from a lobed shape at small gaps to an almost circular shape at intermediate gaps and became elliptical in shape at larger gaps. In addition, the value of optimum gap was dependent on the vibration amplitude. They proposed a predictive correlation for stagnation-region and area-averaged local Nusselt numbers.

Abdullah et al. carried out the effect of tip gap on the piezofan in horizontal (2008, 2009) and vertical (2012) orientations. Two heat sources in in-line arrangement (2008, 2009) and single heat source (2012) were used in the experiment. The result showed that there existed a certain tip gap at which the piezofan could remove maximum heat from the heat source.

Liu et al. (2009) investigated the thermal performance of piezofans with various blade geometries. They also considered the influence of geometric parameters such as the horizontal/vertical arrangement, and location of the piezofan. Experiments were performed in an environmental chamber with room temperature at 25°C. It consisted of an aluminum plate attached on Kapton heater with an identical size as the test plate with the power inputs ranging from 3-15 W by a DC power supply, and an insulation box. The heat transfer performance for vertical arrangement showed a symmetrical distribution and peaked at the center region whereas the horizontal arrangement possessed an asymmetrical distribution and showed an early peak.

2.3.2 Multi-piezofan

Local and average heat transfer coefficients on a vertical surface cooled by a piezofan were evaluated by Schmidt (1994) using the naphthalene sublimation technique. The piezofan blades vibrated out of phase, and the fan frequency pitch was kept constant. A rectangular hole was made at the centre of the Plexiglas sheet and three cast naphthalene plates were installed side by side in this hole during the test runs. Power law correlations were found to reasonably describe both maximum and surface-averaged Sherwood numbers for three separate distances from the vertical surface. The local Sherwood number indicated the surface locations where the fan provided the most effective cooling. The maximum coefficient occurred at the midpoint of the fan blade for all the three fan-to-surface separations.

Kimber et al. (2006) conducted an experimental study for a pair of piezofans in horizontal and vertical orientations. The piezofans pitch and tip gap were the primary factors considered in this investigation. They found that the vibration amplitude increased dramatically for in-phase vibration in the horizontal orientation, whereas the reverse effect was observed for out-of-phase vibration. However, for vertical orientation, out-of-phase vibration produced the highest vibration amplitude. The performance was greatest when the piezofans were closest with smallest fan pitch to the heat source. Ironically, it decreased the coverage area and average heat

transfer coefficient. Nevertheless, both orientations demonstrated significant increase in the thermal performance compared to the single-fan.

Kimber and Garimella (2009) quantified the influence of each operational parameter such as vibration frequency, amplitude and geometry of the vibrating cantilever beam and its relative impact on thermal performance. Different fans, with fundamental resonance frequencies ranging from 60 to 250 Hz, were considered. The performance of the piezofans was maximized at a particular value of the tip gap and the heat transfer rate depended only on the frequency and amplitude of oscillation. Correlations were developed based on dimensionless parameters, which successfully predicted the thermal performance.

2.4 Numerical Works on the Piezofan

2.4.1 Structural and Dynamics Studies

The structural and dynamic aspects of piezofans have also been studied in detail. Lerch (1990) presented a method for the analysis of piezoelectric media based on finite element (FE) calculations. The distinction of their calculation scheme was the capability of computing transient responses and of handling structures with non-uniform damping where the damping coefficients might differ from element to element.

A closed-form of experiment, analytical and FE solution of the dynamic response of a resonant, composite piezoelectric beam was developed for the optimization of piezofans with two symmetrically placed piezoelectric patches (Bürmann et al. 2003). They found that the optimal values were different depending on whether the optimization criterion was posed in terms of maximal electromechanical coupling factor (EMCF) and maximal tip deflection and rotation at resonance. Basak et al. (2005) performed a similar analysis to the more complicated and practically relevant case of finite beams in both symmetric and asymmetric configurations. It was shown that the configuration (symmetric or asymmetric), the choice of materials, specific length and thickness ratios influence the EMCF for certain bending-dominated modes of the structures.

Huang et al. (2004) studied the tip-deflection of a piezoelectric bimorph cantilever in the static state. They found that the tip-deflection of the serial bender was half of that of the parallel bender at the same geometric size and same voltage in the standard operation. The tip-deflections of the benders were proportional to the electric potential difference and the square of the ratio of length to the thickness, and have no relation with the width. In 'electrical pre-stress' operation case, the tip-deflection of parallel bender was proportional to the difference between the electric fields of the two layers.

Wait et al. (2007) used FE modeling and experimental impedance measurements on piezoceramic structure to demonstrate that the EMCF in certain modes could be better than in the first bending mode; however, losses were also shown to be higher at those modes. Additionally, the overall power consumption of the piezofans was also found to increase with increase of the mode number. A 3-D FE with fluid structure interaction (FSI) model has been developed by Basak et al. (2006) to predict the hydrodynamic loading of microcantilevers in viscous fluids. They found that microcantilever damping was arisen from localized fluid shear near the edges of the microcantilever in an infinite medium. However, the damping occurred due to a combination

of squeeze film effects and viscous shear near the edges whenever closer to the surface. As the structural modeling of the piezofan is beyond the scope of the present work it will not be discussed further.

2.4.2 Fluid Flow and Heat Transfer

The 2-D flow field generated from two piezofans was analyzed by Ihara and Watanabe (1994). The discrete vortex method combined with the singularity method was employed in their numerical simulations. The particle movements obtained from numerical simulations were coincident with the experiment for single plate oscillation and two-plate in-phase oscillation. However, the particle movements were coincident qualitatively in the case of two-plate counterphase oscillation, but not quantitatively.

Loh et al. (2002) developed analytical model based on Nyborg's formulation using successive approximation method along with CFD simulation. The gap between the two plates was small (2–20 mm), and the fluid was assumed as laminar and incompressible flow. Two distinctive acoustic streaming patterns in half-wavelength of the flexural vibrations were observed, which agreed well with the theory. However, the acoustic streaming patterns agreed well with the theory but overestimated in the streaming velocity to the fact that compressible flow that occur at high frequencies was excluded in the model.

Hosaka and Itao (2002) investigated coupled vibrations of two cantilever arrays with low vibration amplitudes. The vibration coupling amplitude and damping ratio were derived by replacing the beam with strings of spheres and combining the airflow force of the spheres with ordinary beam equations. They found that coupling amplitude increased as the beam size, beam gap, internal friction, and the difference in the resonant frequencies of the beams decreased and the damping ratio increased as the beam size was reduced. This theory was verified with actual-size and enlarged model experiments.

Acikalin et al. (2003) developed two-dimensional models to describe the acoustic streaming flow induced by an infinite and finite, baffled piezofan vibrating at 60 Hz with vibration amplitude of 0.8 mm. The method of successive approximations was first used to derive analytical closed-form solutions and no closed-form solution was developed to solve the resulting perturbation equations. The agreement between experiment and numerical simulation was seen to be quite good, although the size and location of the outer streaming nodes were slightly different from the predicted values. The discrepancies were attributed to the following factors: the assumption of 2-D flow in the model, the baffle used in the experiments were not ideal, errors in the model related to perturbation and incompressibility assumptions and errors resulting from the numerical methods employed.

Wan and Kuznetsov (2003) studied numerically the efficiency of acoustic streaming for enhancing heat transfer between two parallel beams. A perturbation method was employed to analyze the acoustic streaming in the gap between two beams; one was vibrated while the other was stationary, with heater attached onto it. The compressible Navier–Stokes equations were decomposed into the first-order acoustic and second order streaming equations with steady state energy equation associated. These equations were discretized by the finite-difference method on a uniform mesh. Cooling effect due to acoustic streaming was observed, and it was suggested to

utilize higher (ultrasonic) vibration frequency or vibration amplitude in conjunction with a heat sink for cooling of computer chips in future.

Florio and Harnoy (2005) conducted 2-D numerical studies on the feasibility of using the vibrating plate (piezofan) for cooling electronic components at closed proximity. The system consist of a vertical channel formed by an oscillating surface and a parallel, fixed, constant heat flux surface (electronic component). Squeeze film assumptions were adopted for the velocity field, while the temperature field was carried out using a modification of Patankar's SIMPLER finite-volume scheme along with backward-difference implicit time discretization scheme. The Gauss-Seidel iteration method were employed to solve the discretized finite-volume equations. However, the effects of natural convection and fluid inertia were neglected. The Nusselt number was enhanced five times compared to the reference natural convection condition. The cooling effect was not just on the oscillation amplitude ratio, but also increased with the oscillation frequency.

This model was modified by Florio and Harnoy (2006), who investigated the effect of one insulated wall and a short, thin oscillating piezofan at a mean clearance in a similar channel through a 2-D numerical model using the FE technique. They observed that the oscillations increased the local velocities by drawing cooler fluid towards the clearance, forcing heated fluid from the clearance, and initiating the interaction of different flow streams. Additionally, the natural convection currents carried away heat from the oscillating plate and heat source and delivered cooler fluid to the area near the plate while the fluid inertia promoted the mixing of flow streams at different temperature levels.

Florio and Harnoy (2007a) updated their previous study (Florio and Harnoy, 2005) to include the effect of natural convection and fluid inertia. The combination of the oscillations, the natural convection, the fluid inertia, and other flow drivers produced up to a 340% increase in the local heat transfer coefficient. Their study was extended (Florio and Harnoy, 2007b) by inserting two rectangular heat sources on a vertical mounting board, and a cross-flow opening in the mounting board area between the two heat sources with a number of different positions considered. In this 2-D parametric FE study, the oscillating plate was rigid and moved in the transverse direction, perpendicular to the plane of the channel walls and the top surfaces of the heat sources. It was observed that the cooling effect was most influenced by the proper positioning of the vibrating plate relative to the heat sources and the opening for a given heat source array. Florio and Harnoy (2007c) conducted extra research on possibilities of using a vibrating plate to enhance natural convection cooling of a discrete heat source. The results suggested that a parameter and configuration dependent optimum clearance space existed for a given displacement amplitude and frequency that was related to the degree of constriction of the flow around the heat source caused by the positioning of the plate near the heat source.

Wan et al. (2005) investigated forced convection in a narrow channel by a vibrating piezoelectric bimorph. The Navier-Stokes equations were decomposed into the acoustic equations and the streaming equations by the perturbation method. All governing equations were discretized by finite volume method (FVM) and Gauss-Seidel iteration method. In addition, the SIMPLER method was utilized in solving the acoustic streaming Equations. The flow field showed the

combination of symmetric and counter-rotational eddies which occupied the whole channel width, was in agreement with the experimental results.

Basak and Raman (2006) employed a boundary integral technique to solve the unsteady Stokes equations. The orientation was same as that considered by Hosaka and Itao (2002). They studied the coupling fan parameters such as separation distance (fan pitch), frequency, and relative amplitude and phase between neighboring beams (either it could constructively or destructively interfere). They also provided guidelines on how to suit microscale cantilever arrays, either weak or strong coupling of amplitude were targeted.

Acikalin et al. (2007) used FLUENT simulation software in order to predict the fluid flow and heat transfer induced by a piezofan. Investigations were made on the frequency offset, fan amplitude, and the distance between the fan and heat source. In their 2-D simulation, the bouoyancy effects and clamp of fan were omitted, and frequency was rounded to 62.5 Hz. A slender beam model for the displacement of the piezofan suggested by Basak et al. (2005) was used at the first mode shape. In order to reduce the number of deforming cells, the fluid domain was divided into two regions; first fluid domain included the deforming beam and second fluid region was characterized by stationary fluid cells that interacted with the first region through the fluid interface. Smoothing and remeshing were chosen from the three dynamic meshing mechanisms. Local circulation regions were developed when the heat source was closed to the fan and optimal conditions were occurred when the fan operated at resonance and oriented normally to the heat source.

Zaitsev et al. (2007) simulated 3D turbulent flows around bodies subjected to vortex-induced and forced vibration. The deforming mesh approach namely ALE formulation was used to simulate the flow around vibrating bodies, while the hydrodynamic force computed was used to predict the body motion/deformation. The RANS/LES vortex-resolving approach was selected in the turbulence model. They observed 3-D interaction of the vortices shed from the tip and two side edges of the blade, and concluded that 2-D formulation was unable to provide an adequate simulation of the jet formation.

Abdullah et al. studied sinusoidal moving of piezofan tip in horizontal (2008, 2009) and vertical (2012) orientations. The FLUENT 6.3 software was used in the 2D (2008, 2009) and 3D (2012) simulations to predict the heat transfer coefficient and the flow fields, using dynamic mesh option to simulate the piezofan swinging phenomenon. They observed that the induced flow by piezofan was an unsteady phenomenon and much dependent on the fan swinging. The temperature on the heat source decreased gradually due to the double vortices that appeared over the heat source and slowly moved away by the subsequent airflow. They also concluded that certain tip gap was crucial on the temperature of the heat source.

Acikalin and Garimella (2009) investigated the effect of amplitude of the piezofan and the tip gap by 2-D and 3-D simulations. Laminar incompressible flow with no radiation contribution and precluded buoyancy-induced convection were assumed. A seventh-order least squares polynomial fit was used to represent the mode shape and describe the location of the piezofan in time. Four amplitudes of the piezofan were considered. However, only one 3-D model was selected for the validity of the assumption of two-dimensionality. The optimum gap

was predicted to be approximately 2.5 mm. However, there were under and over predictions of the Nusselt number for largest and smallest amplitudes respectively. The predictions agreed within $\pm 20\%$ of the heat transfer experiments, except for the case with the smallest amplitude and largest gap. They also reported that beyond a gap-amplitude ratio of 2, the flow could no longer be assumed 2-D.

2.5 Optimization of the Piezofan

Both experimental and numerical approaches are the most common practices of the researchers to determine the best parameters. In these conventional approaches, one experimental/simulation factor is varied at a time (OFAT) while the other parameters are fixed (Acikalin, 2004). Complex design of the experimental system may lead to number of assumptions. This usually leads neither to an optimum solution, nor does it allow parametric interactions to be explored. Therefore, alternative techniques to determine the optimum results in less time are desirable.

Burmann et al. (2003) presented optimization of piezofans with two symmetrically placed piezoelectric patches by using an analytical Bernoulli–Euler model and a FE model of the composite beam. Their objective was to maximize the EMCF. It was indicated that the optimal values of patch-to-beam ratio, patch location and patch-to-beam thickness were different depending on the optimization criteria (maximal EMCF and tip deflection, and rotation at resonance). However, for the forced vibration response, it required accurate damping models to realize physically acceptable optimal designs.

Acikalin et al. (2004) also performed EMCF optimization based on length and patch placement to the thickness ratio. It could be seen that the EMCF was more sensitive to variations in the length ratio than the thickness ratio. It was also noted that the optimal geometries for maximal EMCF depended on the combination of materials used for the piezoelectric patch and the fan blade, and placement of the patch flush to the fixed end of the cantilever. Dynamic responses of asymmetric and symmetric piezoelectric configurations were studied by Basak et al. (2005) using analytical field equations and Hamilton's principle on one side patch. The optimal geometries such as patch-to-beam length and thickness ratios to maximize EMCF were also identified with maximum EMCF. It was shown that depending on the configuration (symmetric or asymmetric) and the choice of materials, specific length and thickness ratios maximized the EMCF.

Kim et al. (2005) focused on the optimization of piezofan design by using Evolution Strategy (ES). The piezofan was composed of one elastic body and two elastic materials. The four parameteres considered to maximize the displacement at the tip of piezofan were length, thickness, material and elasticity. It was analyzed by using 3-D FE method, and good match with the experiment was observed. Based on the appropriate parameters suggested by the ES, the optimal design was $29.9 \times 4 \times 0.407$ mm with the maximum displacement of 7.36×10^{-4} m under resonance frequency 459 Hz which was first mode frequency when the applied voltage was 1V.

Ramana et al. (2007) presented numerical study on cantilever piezofans to understand their mechanical behavior and to aid in design-optimization. The effects of various parameters such as length, thickness, location of the piezoelectric metal layer, temperature, damping ratio, and

electric field on the vibration characteristics were investigated and consolidated through artificial neural networks. Optimal geometrical dimensions for maximum performance were then obtained using genetic algorithm. They observed that with the increase in thickness ratio, the tip-deflection increased but resonance frequency decreased. A material with higher piezoelectric matrix and lower elasticity stiffness matrix was required in choosing a good piezoceramic material. The proper length of bimorph might contribute a higher surface velocity. Deflection of the bimorph greatly influenced the temperature behavior of the piezoelectric strain coefficient and the applied electric field affected only tip-deflection.

Acikalin et al. (2004, 2007) studied the effect of varying the piezofan amplitude, the gap between piezofan and the heat source, the length, frequency offset from resonance, and the piezofan offset from the center of the heat source to assess the cooling potential of the fans. The design of experiments (DOE) approach was used in the experiment in order to obtain the optimum value of those parameters. Three different configurations of the piezofan and heat source were considered as shown in Figure 2.2. In the first two configurations, the position of the fan relative to the heat source was changed (2004), while in the third, a fin was included on the heat source, with the fan position being held the same as in the first case (2007). Based on their analysis, DOE revealed that the piezofan frequency offset from resonance, and the piezofan amplitude was the critical parameter.

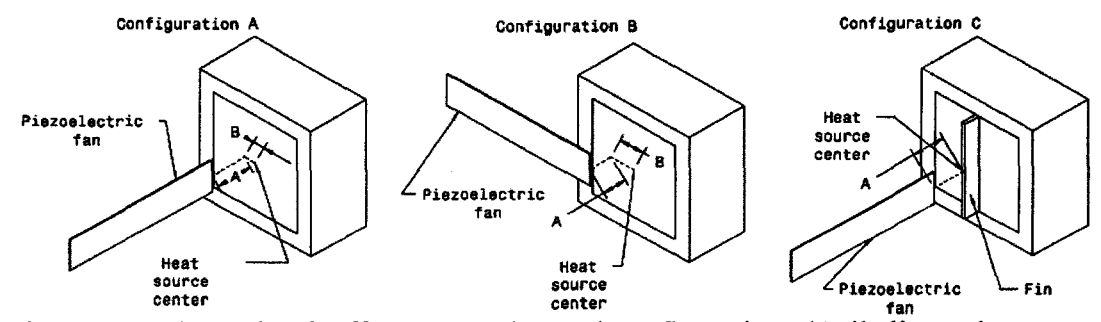


Figure 2.2 Schematic of different experimental configurations (Acikalin et al., 2007)

Petroski et al. (2010) conducted a two-level three-factorial DOE; power and amplitude of piezofan were set as factors and thermal resistance as response. A system of piezofan and a heat sink were presented as a more efficient method of system cooling. They also proposed a volumetric coefficient of performance (COP), which allowed the piezofan and heat sink system volume to be compared against the heat dissipating capacity of a similar heat sink of the same volume for natural convection. The piezofan system was shown to have a COP of five times the typical natural convection solution and less variation in the system thermal resistance.

2.6 Application of Piezofan in Electronic Cooling

Açikalin et al. (2004) were the first to study the possibility of implementing piezofans in electronic systems. A piezofan with a resonant frequency of 20 Hz was placed in an enclosure with small aluminum heat sink attached on heater, which has similar in size of cellular phone and a commercially available laptop. Four different positions of piezofan as shown in Figure 2.3 were studied. Significant localized cooling was found at the right of piezofan position, and the convective heat transfer coefficients was enhancemed more than 100%.

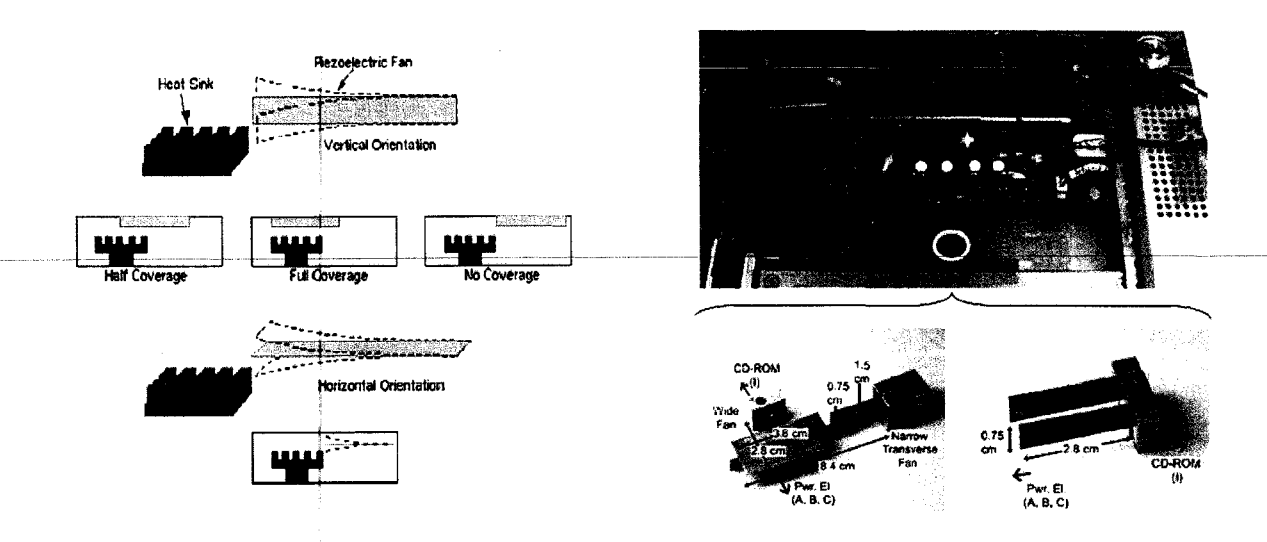


Figure 2.4 Piezoefan used in the portable products cooling experiment (Acikalın et al., 2004)

Sauciuc et al. (2006) studied the application of piezofan in the low form factor. They conducted two experiments; Piezofan was combined with heat sink at first and then with spreader in an enclosure. A significant reduction in thermal resistance was observed compared to natural convection, Moreover, the power consumption was greatly reduced in comparison with the axial fans and blowers of similar size and comparable performance.

Ng et al. (2010) investigated the possibility of installation of piezofan in the notebook. The cooling characteristics of piezofan were studied first in terms of blade length, thickness, operating frequency, amplitude and sound level. It was found that the cooling performance of piezofan was better when it was shorter, thicker and operated with higher input voltage at higher resonance frequency and larger vibration amplitude. They also observed that sound level was proportional with resonance frequency and input voltage. A piezofan prototype was installed into a 13" thin and light notebook with 18W processor TDP low power platform. Thermal test results indicated comparable temperature readings between piezofan and blower fan, and it was feasible to be implemented in notebook system to achieve low power consumption and acoustic noise.

Tseng et al. (2010) developed and tested piezofans for the cooling possibilities of in compact cooling modules according to the demands of mobile electronics with multiple heat sources, low cost PC and LED modules. They also used FEM for design support, the demands for long life and compact size. It was noted that the temperature was tremendously decreased for all the modules. Additionally, the noise of the piezofan was 24-29 dBA where it was very quiet. The power consumption was 11 mW, about 1/20 that of the axial fan or the blower with the same cooling performance. They also observed that the design support successfully helped to prevent the crack generation on the piezoelectric element.

Recently, Zhang et al. (2011) simulated the airflow velocity field generated by piezofans using 3D FSI method in the light emitting diodes (LED) package. The airflow generated by the periodic deformation of the blade was treated by the FEM structural solver. A Multi-field solver was used to obtain the two-way coupling of structural solver and CFD solver. The calculated velocity near the tip of the piezofan agreed well with the measured data, and was proposed for LED cooling.

3.0 Experimental setup and procedure

Figure 3.1 shows the experimental apparatus used in the present study. The test section of size $800 \text{ mm} \times 120 \text{ mm} \times 250 \text{ mm}$ is made from clear glass. The electronic package is mimicked as a heater (size $30 \text{ mm} \times 30 \text{ mm} \times 3 \text{ mm}$) into which a constant heat flux of 9166.7 W/m² is applied. One side of the heater is embedded on a wood platform which also serves as thermal insulator, while the other side is pasted to the heat sink bottom surface, by using RS® heat sink compound which has high thermal conductivity.

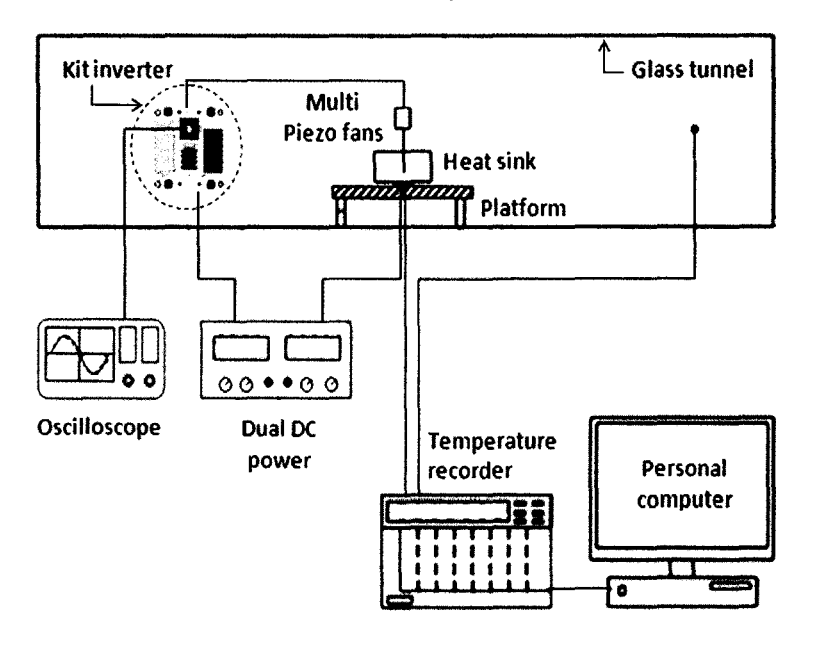
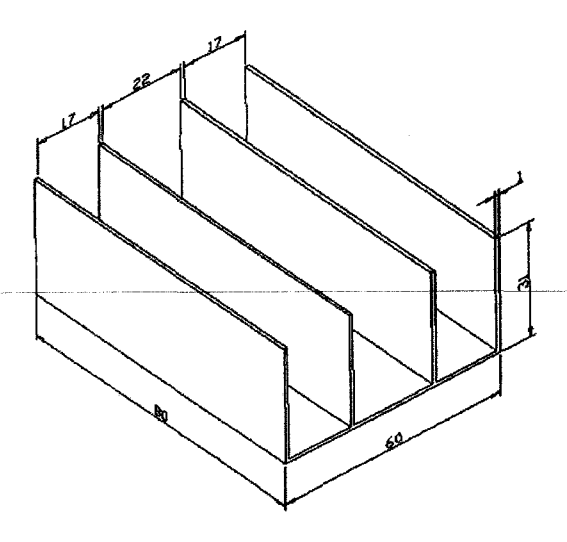


Figure 3.1 Experimental setup used in the present study.

The target being cooled is aluminum heat sink (Figure 3.2a), which has dimensions of 80 mm \times 60 mm \times 1 mm, and is provided with four fins of 1 mm thick and 30 mm high. Nine K-type thermocouples are used to monitor temperatures at critical locations as shown in Figure 3.2 (b-c). The temperatures are displayed and recorded by the computer by means of data logger, for each minute during the experiment.



(a) Heat sink

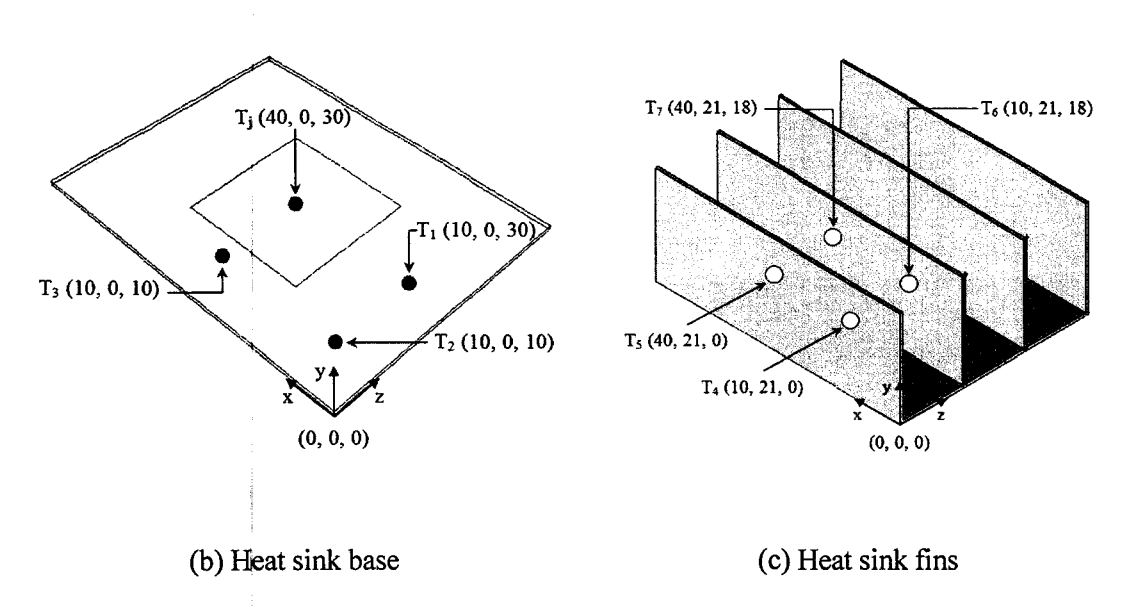


Figure 3.2 Schematic of the heat sink with thermocouple locations (all dimension in mm and not in scale)

The multi-piezofan consists of three piezoelectric fans that can be oriented at angles of 0° to 90° as shown in Figure 3.3 (fins are excluded from heat sink for viewing G and α); Table 1 shows the specifications of the piezofan (PiezoSystem Inc, USA). The oscillating drive signal to match the resonant frequency of the beam was provided by means of an inverter circuit. In the reminder of this article a normalized tip gap (δ) will be used, which is defined as the ratio of fin height (H_f) to the tip gap (G).

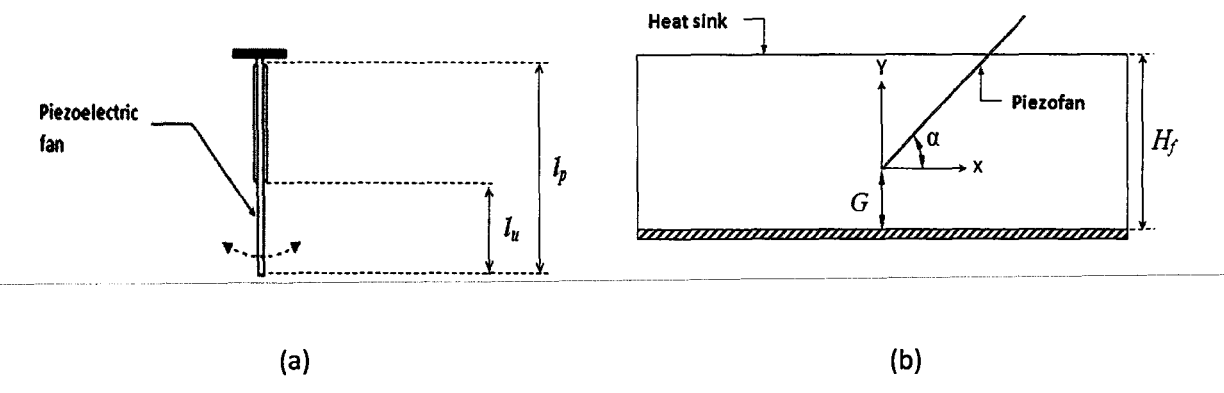


Figure 3.3 (a) Fan height and (b) tip gap and angle between fan and heat sink base

Table 1 Specifications of the piezoelectric fan

Specification	Value		
Material	Stainless steel		
Fan size (mm)	$47 (l_P) \times 12 (w_P) \times 0.4 (t_P)$		
Resonant frequency (Hz)	111		
Power consumption of fan and circuit (mW)	42		
Fan weight (gm)	2.0		

A laser displacement system (KEYENCE LK-G152) was used to measure the deflection produced by the piezoelectric fan. The experimental setup is shown in Figure 3.4. The laser beam was pointed on the tip of piezofan which was mounted vertically. When the piezofan swung left and right, the IMC DAQ system recorded the displacement and its frequency from peak-to-peak position to the initial position and stored in the computer. The heat sink - pizofan assembly was perfectly isolated from external disturbances by means of a large transparent housing fixed on a rigid platform.

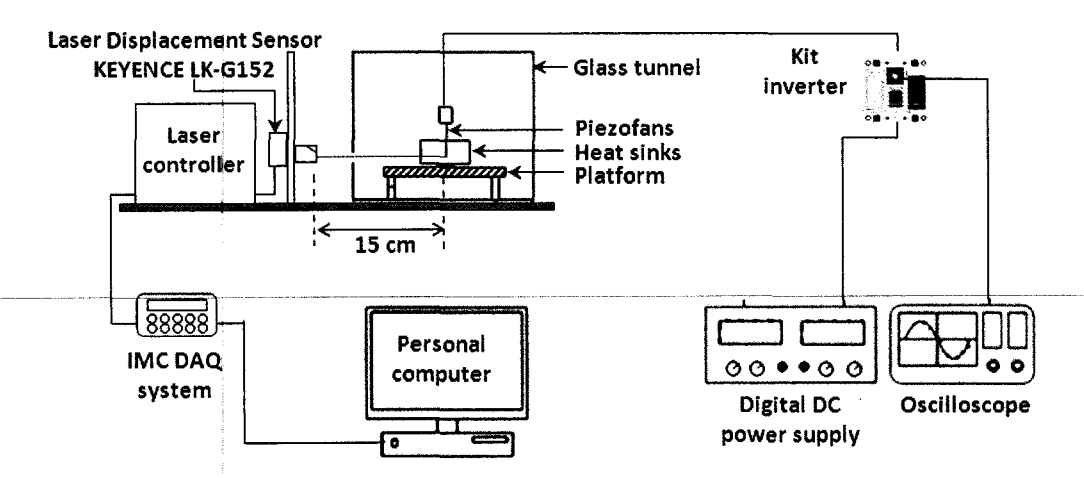


Figure 3.4. Vibration parameter experimental setup using laser displacement sensors to measure vibration signals for piezofans

In this study, Central Composite Design (CCD), the most widely used approach of Response Surface Methodology (RSM), was employed to optimize δ and α with the objective of maximizing temperature drop (ΔT); the entire DOE procedure was facilitated by the 'Design Expert 6' software, similar to the published work [18].

4. Modeling

4.1 Computational domain

The 3D model used in this simulation consisted of a heater, simple heat sink and three piezoelectric fans. Fig. 5 shows multi-piezofan are mounted in vertical (Fig. 4.1a) and horizontal (Fig. 4.1b) positions. The size of heat source was similar to the heater used in the experiment.

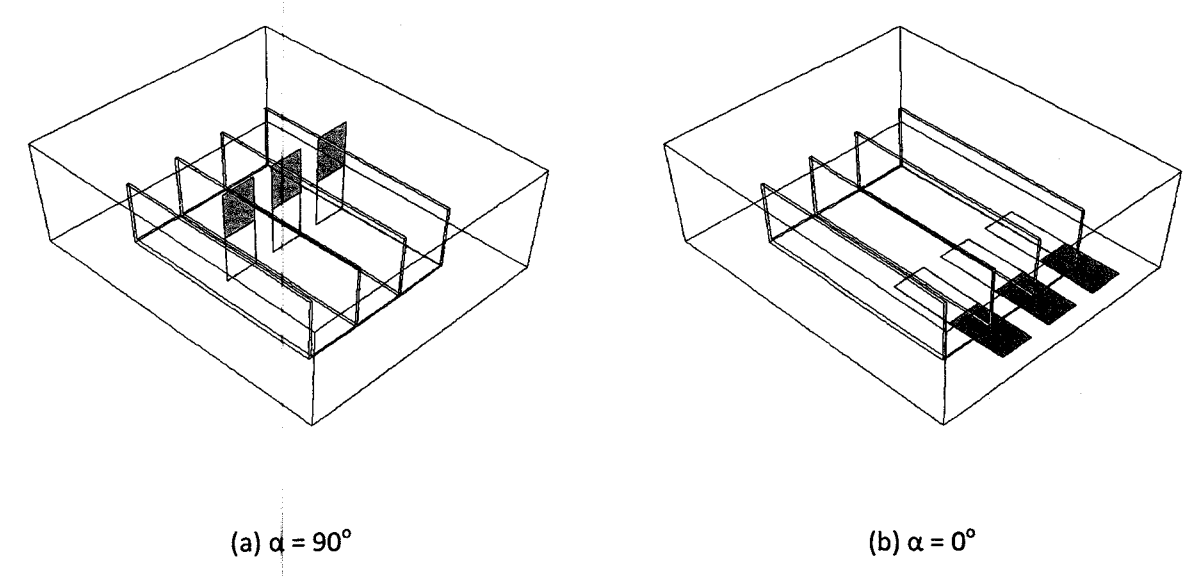


Figure 4.1 Positions of multi-piezofan

The volume of the computational domain was 120 mm × 100 mm × 46.1 mm which included heater, heat sink and multi-fans. The clamp of the piezoelectric fan was neglected. The fan boundary was modeled as a moving adiabatic wall whose location in time was set by a UDF in FLUENT. The fan was modeled as infinitesimally thin wall with no thermal conduction allowed through it. No-slip boundary conditions were applied to the walls such as platform and heat sink. Other boundaries were treated as pressure boundaries, permitting the air flow inward or outward direction. A combination of tetrahedral and quad literal elements (about half million) were used for meshing (see Figure 4.2).

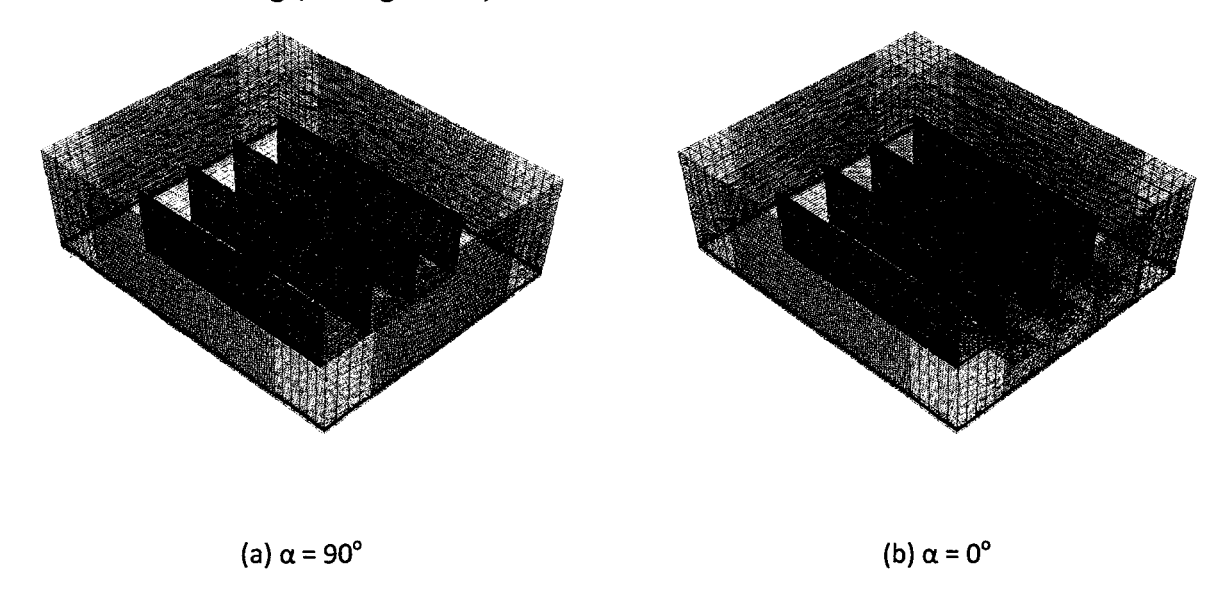


Figure 4.2 The meshed models

The fluid domain was divided into two regions namely region 'a' and region 'b as shown in Figure 4.3. The boundary of these two regions is imposed as a fluid interface. The purpose of fluid interface is to avoid damaged fluid cells since region 'a' of the fluid domain includes the deforming beam (piezoelectric fan). The fluid cells can be greatly skewed due to its movement. This technique can overcome the problem by flagging the cells from one side of the interface as deforming cells. In addition, only single cell spacing was included from the tip of the beam to the fluid interface to avoid stretching, which may lead the fail of fluid cells. Region 'b' is distinguished by stationary fluid cells that interact with region 'a' through the fluid interface. FLUENT offers many options on the dynamic mesh mechanism, but only smoothing and remeshing mechanism were chosen. Smoothing considers the movement of the fluid zone to be a spring-like deformation while, remeshing is used to remesh the cells if their new volume is smaller than the prescribed value. More explanation of these mechanisms can be obtained from FLUENT [19]. However, the disadvantage of fluid interface is minor discontinuities in contour plots at the interfacial line may be printed.

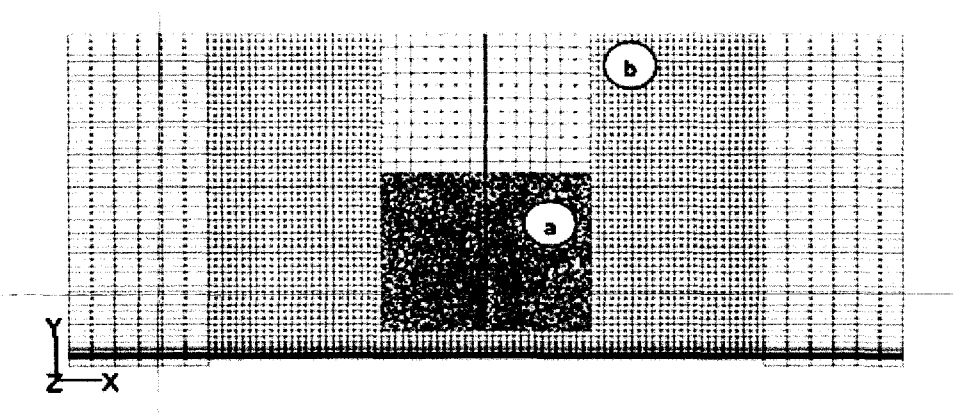


Figure 4.3 Mesh generation regions

4.2 Mathematical model

The flow was assumed incompressible and turbulent. The governing equations employed in FLUENT, for describing the transient fluid flow are as follows:

Continuity:

$$\frac{\partial \rho}{\partial t} + \frac{\partial}{\partial x_i} (\rho u_i) = 0 \tag{2}$$

Momentum (non-accelerating reference frame):

$$\frac{\partial}{\partial t}(\rho u_i) + \frac{\partial}{\partial x_j}(\rho u_i u_j) = -\frac{\partial P}{\partial x_j} + \frac{\partial \tau_{ij}}{\partial x_j} + \rho g_i + F_i$$
(3)

where; ρ is the fluid density, P is the pressure in the fluid, τ_{ij} is the viscous stress tensor and g_i and F_i are the gravitational acceleration and external body force in the *i*-direction, respectively.

However, FLUENT allows the user to simulate moving and deforming domains through the use of user define function (UDF). Dynamic meshes can be used to model flow where the shape of the domain is changing with time due to motion of the domain boundaries. The integral form of the transport equation for a general scalar (Φ) , on an arbitrary control volume (V), on a moving mesh is written as:

$$\frac{d}{dt} \int_{V} \rho \Phi dV + \int_{dV} \rho \Phi (\vec{u} - \vec{u}_g) dA = \int_{dV} \Gamma \nabla \Phi dA + \int_{V} S_{\Phi} dV$$
(9)

where \vec{u} is the flow velocity vector and \vec{u}_g is the grid velocity of the moving meshes. The first and second terms on the left are the time derivative and the convective terms. The terms on the right are the diffusive and the source terms. Γ is the diffusion coefficient and S_{Φ} is the source term of Φ . ∂V represents the boundary of the control volume V and dA is the area movement.

Fluid energy:

$$\frac{\partial}{\partial t}(\rho E) + \frac{\partial}{\partial x_i} \left(u_i(\rho E + P) \right) = \frac{\partial}{\partial x_j} \left(k_{eff} \frac{\partial T}{\partial x_i} - \sum_{j'} h_{j'} J_{j'} + u_j \left(\tau_{ij} \right)_{eff} \right) + S_h \tag{4}$$

where k_{eff} is the effective conductivity ($k_f + k_t$, where k_t is the turbulent thermal conductivity, defined according to the turbulence model being used), and J_j is diffusion flux of species. The first three terms on the right-hands side of equation (4) represent energy transfer due to conduction, species diffusion, and viscous dissipation, respectively. S_h includes heat of chemical reaction, and any other volumetric heat sources defined. E is the total energy of moving fluid per unit mass and is defined as:

$$E = e + \frac{u_i^2}{2} = h - \frac{P}{\rho} + \frac{u_i^2}{2} \tag{5}$$

where e is the fluids internal energy per unit mass and h the sensible enthalpy. For an incompressible fluid the viscous dissipation terms are neglected because the amount of energy produced by the viscous stress will be too small compared to the other sources of energy.

Solid energy:

$$\frac{\partial}{\partial t}(\rho h) + \frac{\partial}{\partial x_i}(\rho u_i) = \frac{\partial}{\partial x_i} \left(k_s \frac{\partial T}{\partial x_i} \right) + \dot{q}^{"} \tag{6}$$

where $\dot{q}^{""}$ is the volumetric heat source. The second term on the left-hand side of equation (6) represents convective energy transfer due to rotational or translational motion of the solids; in this study, it is always set to zero since the solid boundaries are motionless. The first term on the right-hand side is the heat flux due to conduction.

The shear stress transport (SST) k- ω model as expressed in equations (7) and (8) is used to describe the flow induced by the piezofan, which has local turbulence.

$$\frac{\partial}{\partial t}(\rho k) + \frac{\partial}{\partial x_i}(\rho k u_i) = \frac{\partial}{\partial x_j} + \left(\Gamma_k \frac{\partial k}{\partial x_j}\right) + \tilde{G}_k - Y_k + S_k \tag{7}$$

$$\frac{\partial}{\partial t}(\rho\omega) + \frac{\partial}{\partial x_i}(\rho\omega u_i) = \frac{\partial}{\partial x_j} + \left(\Gamma_\omega \frac{\partial\omega}{\partial x_j}\right) + \tilde{G}_\omega - Y_\omega + D_\omega + S_\omega \tag{8}$$

where, \tilde{G}_k represents the generation of turbulence kinetic energy due to mean velocity gradients, G_{ω} denotes the generation of ω , and Γ_k and Γ_{ω} are the effective diffusivity of k and ω , respectively. Y_k and Y_{ω} are terms for the dissipations of k and ω respectively, due to turbulence. D_{ω} is the cross-diffusion term, and S_k and S_{ω} are user-defined source terms.

In present study, the mode shape of a piezoelectric fan is approximated by that of a clamped-free beam [20]. Assuming a sinusoidal driving, position of the beam is given by:

$$w(x,t) = A_f \cdot \begin{bmatrix} (\sin(\beta l_u) - \sinh(\beta l_u))(\sin(\beta x) - \sinh(\beta x)) \\ +(\cos(\beta l_u) - \cosh(\beta l_u))(\cos(\beta x) - \cosh(\beta x)) \end{bmatrix} \cdot \sin(\omega_b t)$$
(10)

Differentiating this equation with respect to time gives the velocity of the beam,

$$\dot{w}(x,t) = A_f \cdot \begin{bmatrix} (\sin(\beta l_u) - \sinh(\beta l_u))(\sin(\beta x) - \sinh(\beta x)) \\ +(\cos(\beta l_u) - \cosh(\beta l_u))(\cos(\beta x) - \cosh(\beta x)) \end{bmatrix} \cdot \omega_b \cos(\omega_b t)$$
(11)

where β values can be calculated from the frequency equation

$$\cos(\beta l_u) \cdot \cosh(\beta l_u) = -1 \tag{12}$$

This must be solved numerically and yields infinity solutions of β . The β value corresponding to the first mode shape is

$$\beta = \frac{1.875}{l_y} \tag{13}$$

4.3 Simulation

The first-order upwind discretization scheme is used both for momentum and energy equations, with the SIMPLE scheme for pressure-velocity coupling. For the treatment of the turbulent flow at the near-wall region (heat sink surface), the y⁺ value is set as 1. The beam is assumed to vibrate at a frequency of 100Hz; this round off (compared to the experimental value of 111Hz) is made for achieving numerical stability. Time-step size of 0.0001s is chosen for all the cases, with 100 time steps per cycle of fan vibration. This value is arrived at after three attempts to check the trend and proximity with the profiles investigated; for instance, the trials are done by increasing the mesh elements and decreasing the time steps. However, a problem arose when the mesh elements were increased, due to the negative volume or less memory detected in FLUENT during analysis. This problem is typically found in dynamic meshing setup. The total duration of the simulation is selected such that the temperature reaches a steady value during this period. It took 5,000 iterations, which corresponds to approximately three days of computation time per each case on a Pentium DualCore processor (each 2.8 GHz) computer with 2.0 GB of memory.

5. Results and discussion

5.1 Experimental results

5.1.1 Effect of multi-piezofan on temperature

In the present configuration, as the fans are separated by the fins, the resonance of amplitude could be neglected. The transient temperature distributions at different locations of the heat sink, with and without piezofans, are shown in Figure 5.1. First of all, keeping the fans off, the heater is turned on (time t = 0), and the temperature is monitored; the steady state is reached at around t = 80 min. At this condition, the piezo fans are turned on and a new steady state is reached at around 100min. The multi-piezofan is seen to cause a maximum of 22% reduction in temperature relative to natural convection.

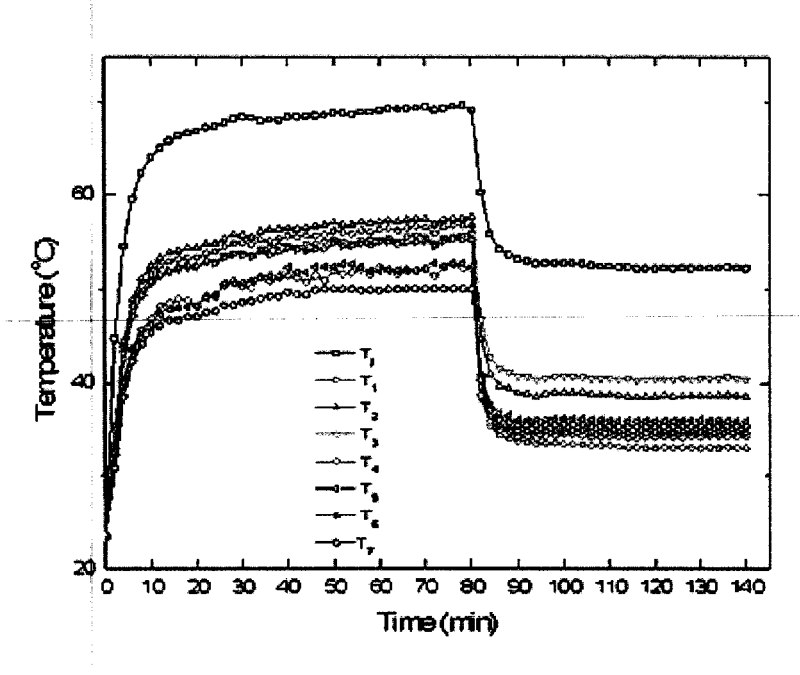


Figure 5.1 Effect of multi-piezofan on the heat sink temperature

5.1.2 Results of DOE analysis

A total of 13 runs obtained from the CCD, and the corresponding responses are shown in Table 2. It is observed that, the temperature drop (ΔT) due to the presence of multi-piezofan varies between 15.53°C and 18.08°C.

T 11 A D	1	C	1100		1
I able 7 Resi	nance values	tor	different	experimental	CONditions
1 4010 2 1303	polise values	IVI	different	Oxportitiontal	Conditions

Run no.	Factor A: α	Factor B: δ	Response 1: ΔT (°C)
ì	45.00	0.33	16.6001
2	45.00	0.33	15.9593
3	90.00	0.33	16.2903
4	45.00	0.33	15.9389
5	45.00	0.5	15.7593
6	45.00	0.33	16.069
7	90.00	0.50	15.5258
8	0.00	0.17	17.3071
9	45.00	0.17	17.7892
10	45.00	0.33	15.6737
11	90.00	0.17	18.08
12	0.00	0.50	16.2365
13	0.00	0.33	15.5283

Table 3 shows the analysis of variance (ANOVA) of regression parameters of the predicted response surface quadratic model for ΔT . The value of correlation coefficient obtained for ΔT is $R^2 = 0.9203$.

Table 3 Summary of ANOVA of the quadratic model for ΔT

Source	Sum of squares	Degree of freedom	Mean square	<i>F</i> - value	Prob > F	
Model	10.24	5	2.05	20.56	0.0005	
	1.01		1.01	10.14	0.0154	
δ	7.99	1	7.99	80.18	< 0.0001	
α^2	0.31	1	0.31	3.11	0.1212	
δ^2	0.38	1	0.38	3.78	0.0930	
$\alpha\delta$	0.14	1	0.14	1.37	0.2797	
Residual	0.7	7	0.1			
Lack of fit	0.36	3	0.12	1.42	0.611	
Pure error	0.34	4	0.084			
SD = 0.32	= 0.32		$R^2_{\text{adj}} = 0.8907$	Adeq. Pro 15.099	ecision =	

The final regression model, in terms of their coded factors, is expressed by the following second-order polynomial equation (Eq. 14).

$$\Delta T = 15.79 + 0.41\alpha - 1.15\delta + 0.33\alpha^2 + 0.37\delta^2 - 0.18\alpha\delta \tag{14}$$

In order to ensure that the selected model adequately represents the real system, the diagnostic plots such as normal probability plots of the studentized residuals, as well as the predicted versus actual value plots, are plotted as shown in Figures 5.2 and 5.3 respectively. It can be observed that the data is almost normally distributed even though there is some scattering which is acceptable. The predicted and experimental values of ΔT are in good agreement as shown in Figure 5.2.

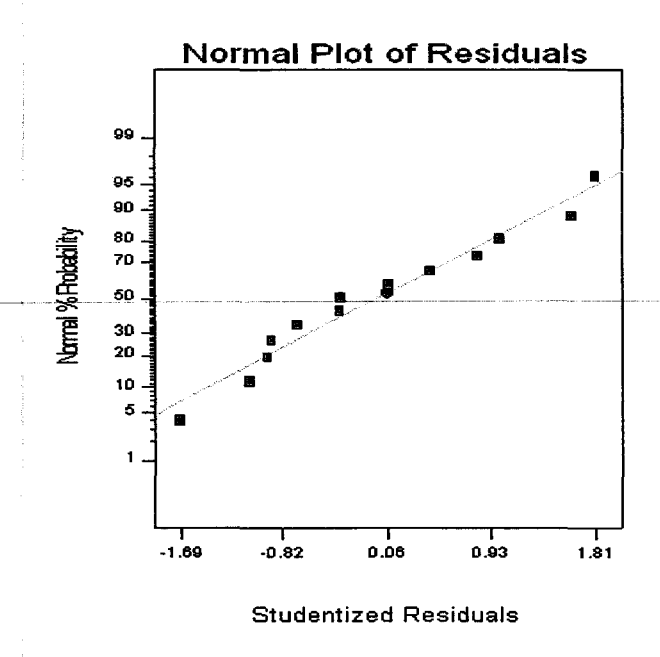


Figure 5.2 Normal probability plot of the studentized residual for heat removal

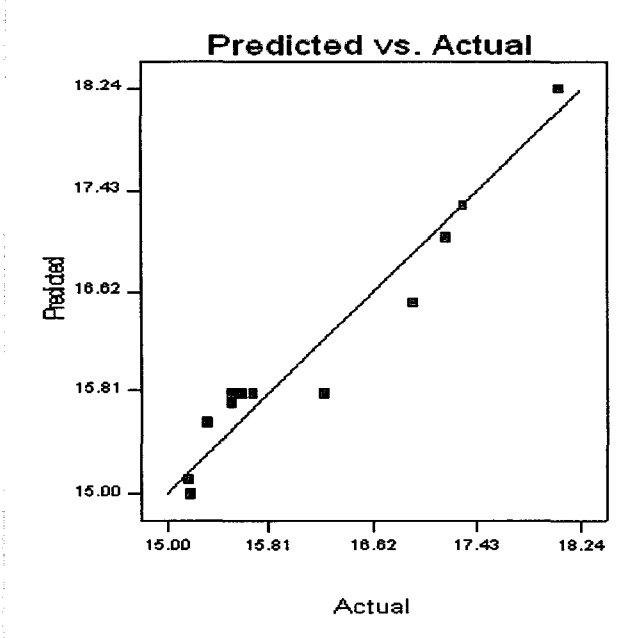


Figure 5.3 Comparison of actual and predicted ΔT

The 3D response surface and contour plots of the quadratic model as shown in Fig. 5.4, demonstrate the interactive relationship between δ and α on ΔT . The maximum ΔT observed is 18.2337°C at $\delta = 0.17$ and $\alpha = 90^{\circ}$, while the minimum ΔT (15.5908°C) is obtained at $\delta = 0.50$ and $\alpha = 0^{\circ}$. Thus the optimum values of δ and α are 0.17 and 90° respectively, which are further verified by exploiting the optimization facility of Design Expert 6.

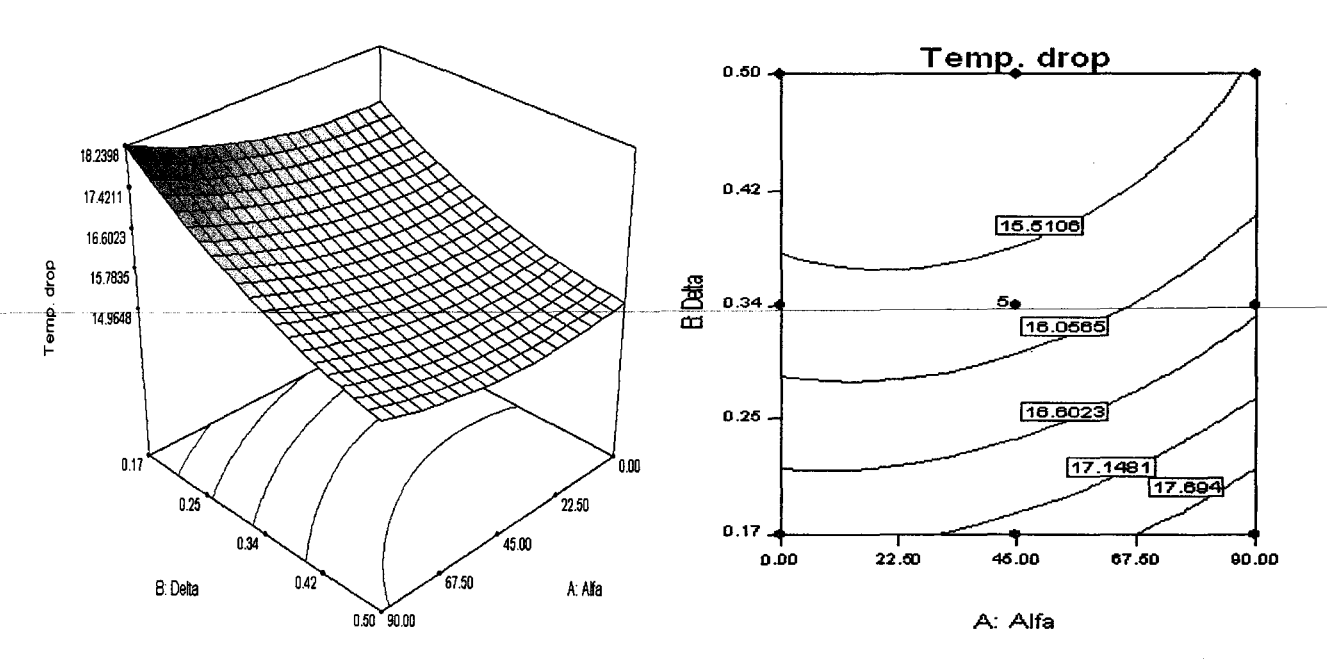


Figure 5.4 (a) Response surface and (b) contour plots for ΔT as functions of δ and α .

5.1.3 Heat transfer coefficient

The experimental convective heat transfer coefficient in each case (without and with the fans) was calculated by using an energy balance on a control volume between the power input and the heat removed from the surface of the heat sink by convection, as proposed by Incropera and Dewitt [21]:

$$h_{hs} = \frac{\dot{q}_h t_h}{T_{s-exp} - T_{\infty}} \tag{15}$$

where \dot{q}_h is the uniform heat generation (W/m³⁾ from the heater, t_h is the heater thickness, and T_s and T_∞ are the temperatures of the heat sink surface and the ambient respectively. Accordingly, h_{hs} for three cases namely, best ($\delta = 0.17$ and $\alpha = 90^\circ$), mediocre ($\delta = 0.33$ and $\alpha = 45^\circ$) and worst ($\delta = 0.50$ and $\alpha = 0^\circ$) are compared with that of natural convection, as shown in Fig. 5.5. It is apparent that, compared to the natural convection case, the multi-piezofan with vertical orientation and minimum tip gap contributed for 88.5% enhancement in heat transfer coefficient while the mediocre and worst cases produced 68.8% and 65% respectively.

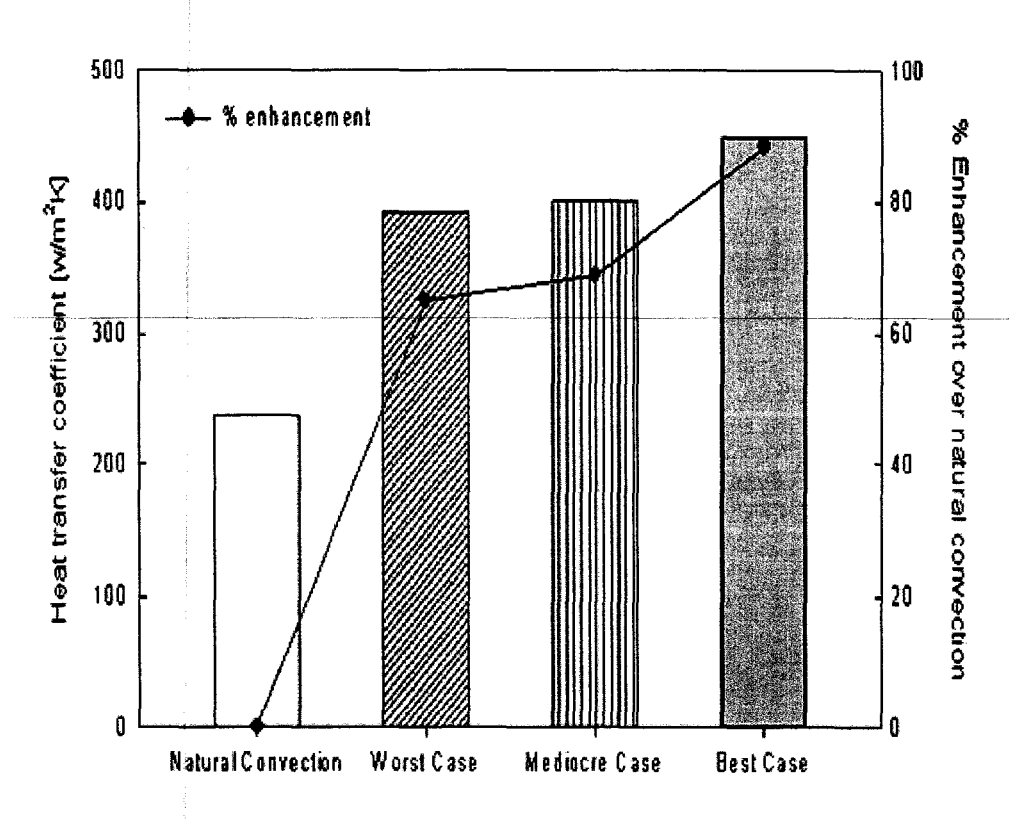


Figure 5.5 Enhancement in heat transfer coefficient for three different cases

5.2 Numerical results

5.2.1 Validation of the Structural model

In the present study, the piezofan was approximated as a clamped-free beam, and equations (10) to (13) were used to define the beam location during vibration. In order to ensure that this mode shape matches the desired amplitude, these equations were programmed in MATLAB software. Fig. 5.6 demonstrates the successful peak-to-peak deflection of the beam (piezoelectric fan) with respect to the phase angle (product of angular velocity and time). The mode equations were then employed into the UDF.

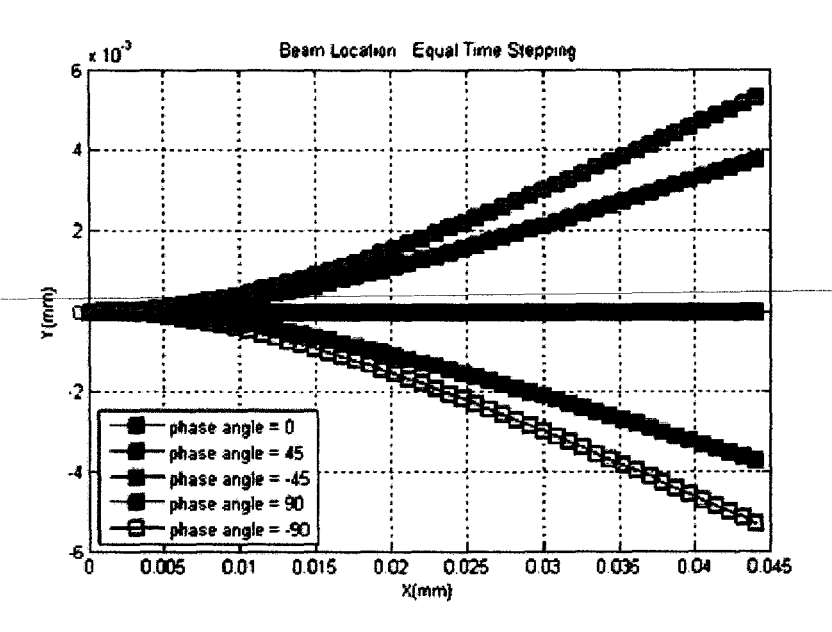


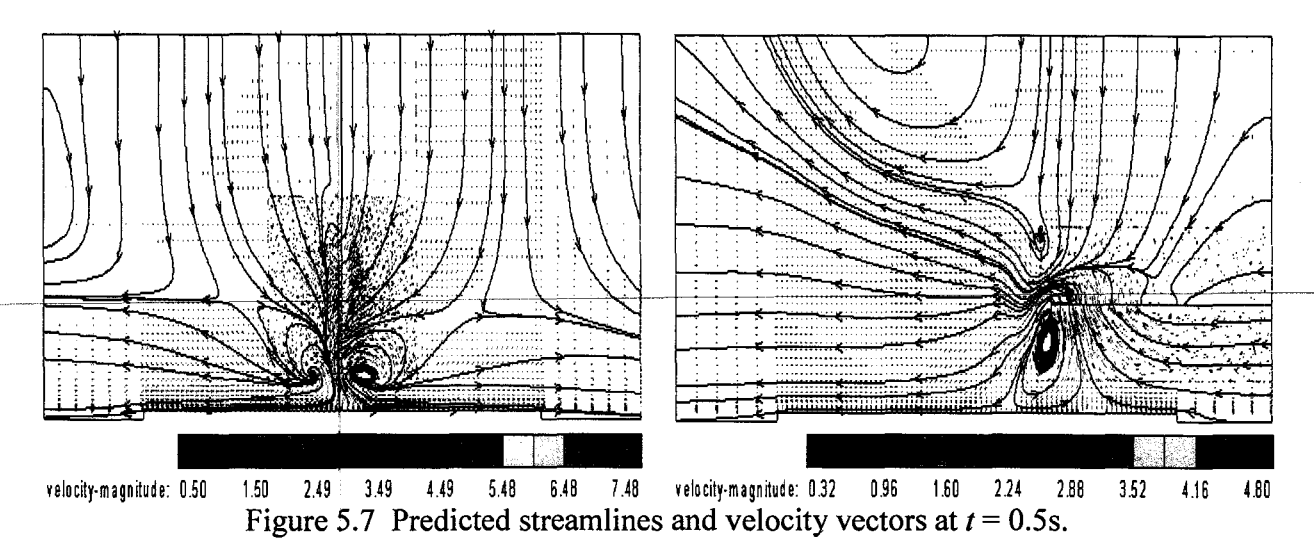
Figure 5.6 Fan location with respect to time

5.2.2 Flow visualization

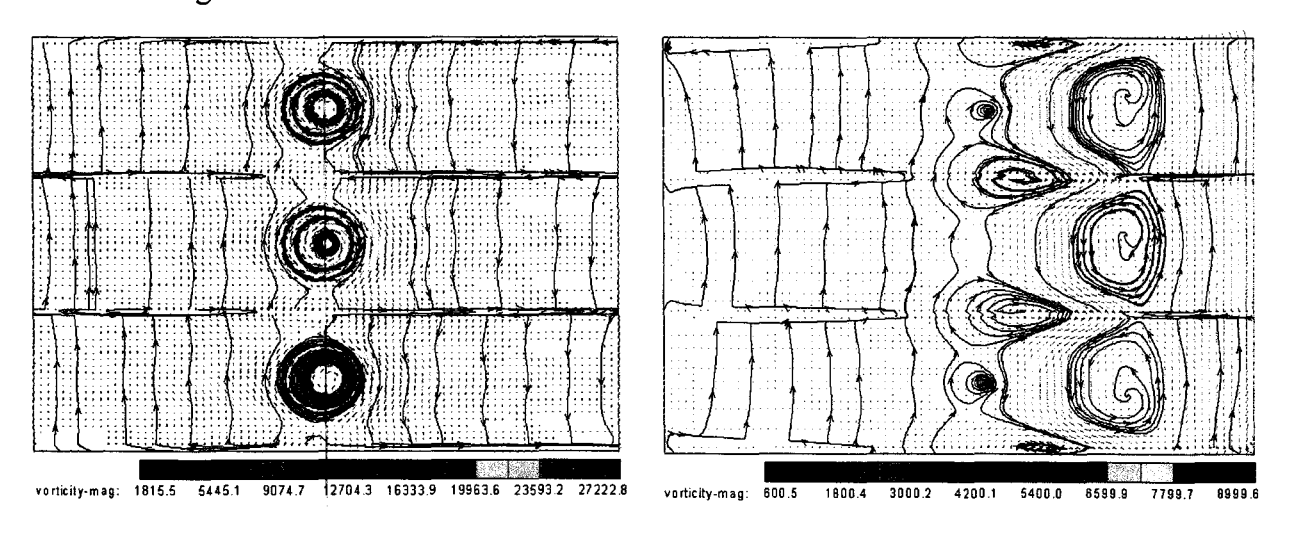
The flow generated by piezoelectric fans can be very complex and needs to be well-understood. The use of high speed camera with particle image velocimetry (PIV) has restrictions in flow visualization because of the presence of solid fins. Therefore, simulation is a practical approach, by which the flow and heat transfer investigation is relatively effective. The transient thermal analysis from FLUENT 6.3.2 was performed to study the flow field and temperature distribution, for the best and the worst cases.

Fig. 5.7a shows the streamlines and velocity vectors for the best case at t = 0.5s. The piezofan produces air streams mainly in the longitudinal and transverse directions (with respect to the piezofan). The first direction is generated by the impinged jet, while the second is generated by the normal force due to the vibration of the beam (Liu et al., 2009). So there is fresh cooling air being entrained into the air flow while the vortices are being formed. Two regions of circulation are formed at the front and rear fan as it vibrates, forcing fluid to displace more rapidly as the beam passes a given position on the heat sink. High velocity regions are found at the front of the moving beam, which then strikes the heat sink surface and flows in the outward direction.

Fig. 5.7b shows the corresponding images for the worst case. Unlike the previous case, the velocity distribution is asymmetric since the states of air on either sides of the vibrating piezofan are different to each other. With respect to the piezofan orientation, the air below the beam is more confined and hotter compared to the other side.



Figures 5.8 shows the top views of streamlines and vortices at t = 0.5s. In the best case (Fig. 5.8a), three vortices are observed exactly at the center of the heat sink surface, while the other case (Fig. 5.8b) shows five vortices located away from the center. As the heater is situated at the bottom center of the heat sink base, the central portion of the heat sink gets hotter, and thus the vortices generated and concentrated centrally in the first case enables efficient heat removal, compared to the second case. Moreover, it is observed that the magnitude of vorticity for the best case is 200% greater than that of the other case.



a) Best case b) Worst case Figure 5.8 Streamlines and vorticity vectors at t = 0.5s

5.2.3 Temperature contours

The temperature contours of the heat sink base, for the best and worst cases are shown in Fig. 5.9 and Fig. 5.10 respectively. For the best case, a rounded rectangular pattern is observed at the heat sink center (due to the middle fan) and this behavior transforms into a lobed pattern towards the locations of side fans. A symmetric growth of the temperature pattern can be observed in all directions. However, a distinctly different distribution of temperature is observed

in the worst case where the temperature distribution is non-uniform. These observations are expected to be genuine according to the velocity and vorticity profiles shown in section 6.2.

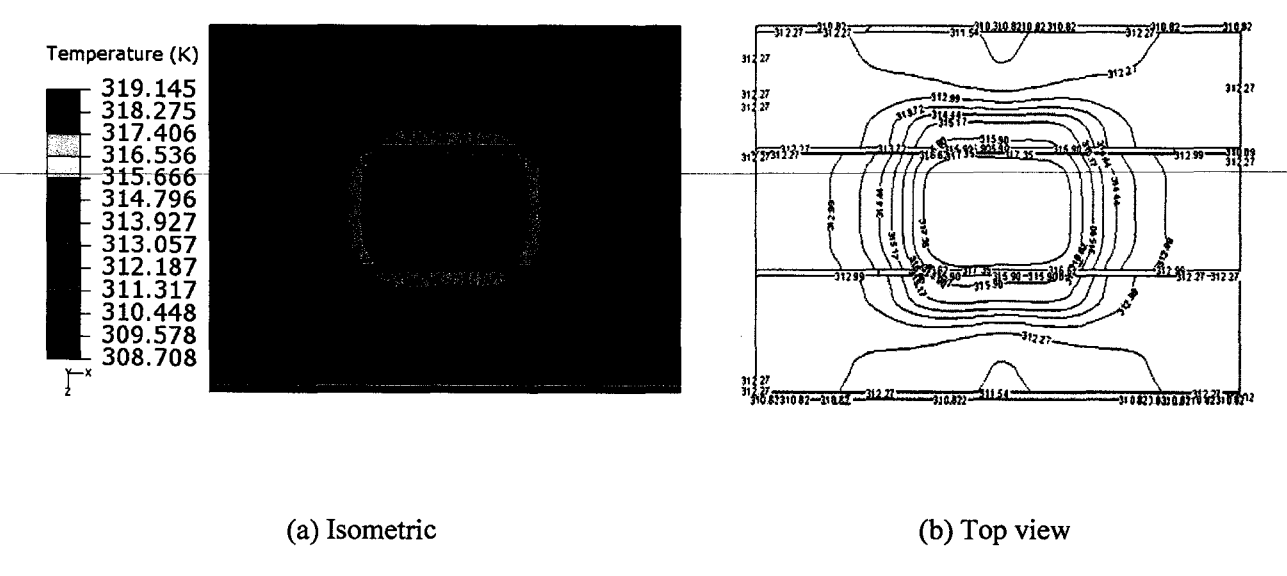


Figure 5.9 Temperature contours and labels for best case at t = 0.5s. At this instant the fan is passing its original position and travelling downward

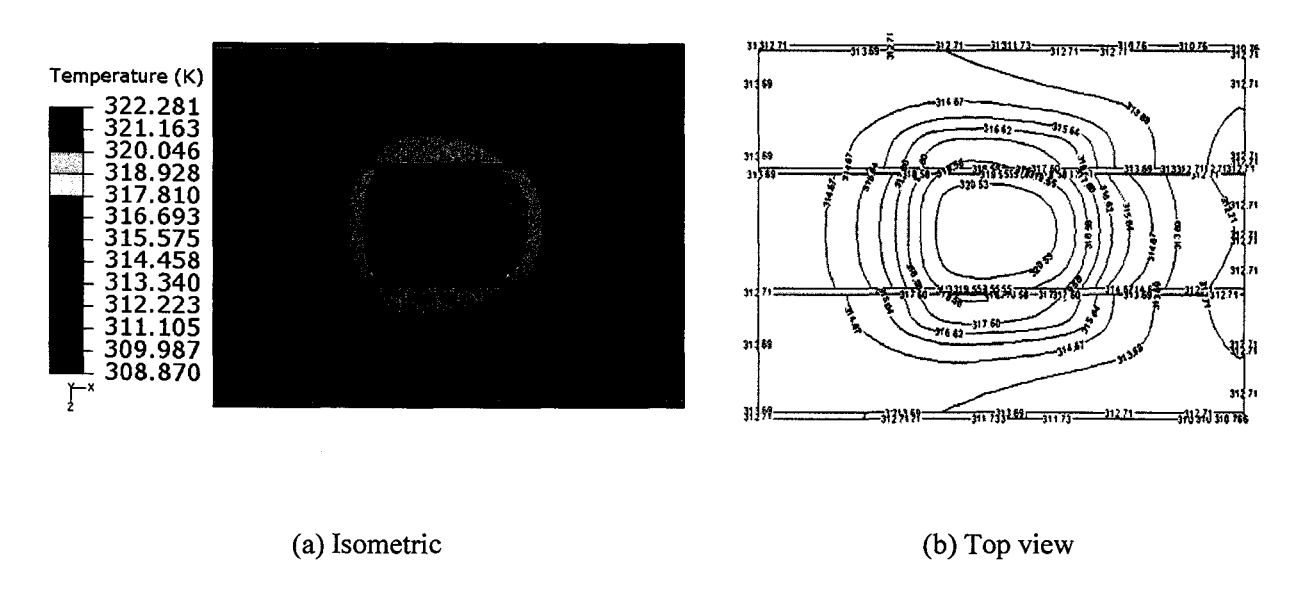


Figure 5.10 Temperature contours and labels for worst case.50 at t = 0.5s. At this instant the fan is passing its original position and travelling downward

Figures 5.11 and 5.12 show the corresponding temperature contours on the fins, at t = 0.5s. For the first case, a droplet cooling zone is observed at the centre of the fins and these droplets appear to be symmetric in the direction of piezofan vibration. The droplet zones widen laterally due to the induced swirling flow on both sides of the fan. However, for the other case, asymmetric cooling zone is observed at one end of the heat sink surface, as the induced flow freely goes outward. Both profiles agree that this droplet cooling zone is prominent at the central

fins compared to the side fins; this is attributed to the enhanced cooling of the central fins due to the presence of piezofans on both sides.

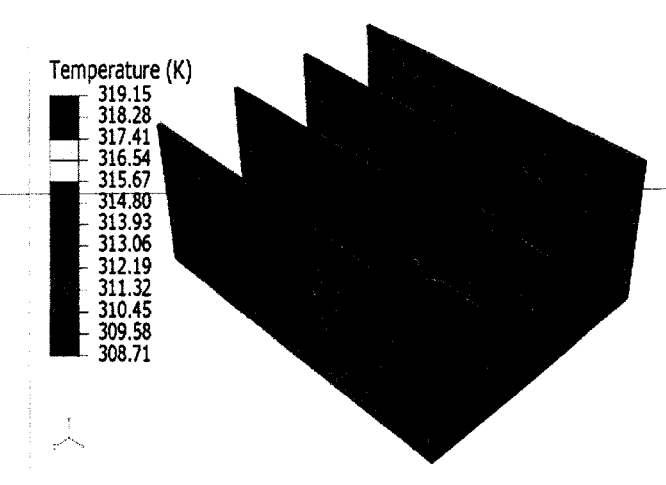


Figure 5.11 Temperature contours of the fins for the best case at t = 0.5s.

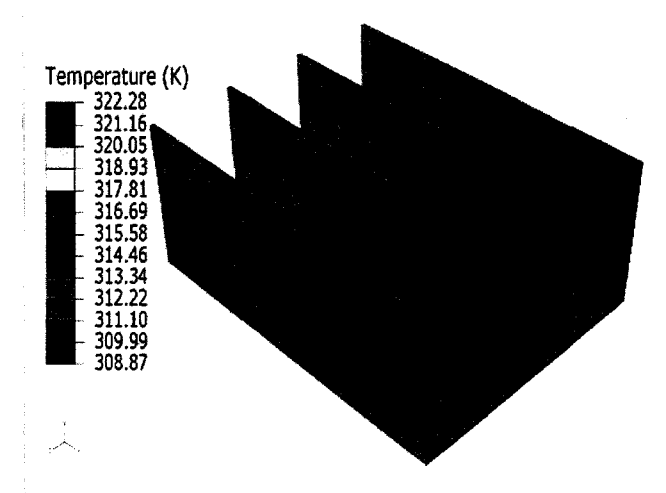


Figure 5.12 Temperature contours of the fins for the worst case at t = 0.5s.

Figure 5.13 illustrates the comparison of temperature distributions for the best and worst cases, along the centre line of the heat sink surface in the x-direction. The significant difference between the trends indicates the critical influence of δ and α on the cooling performance. The temperatures at the leading edge $(l_{hs}/l_h=2.76)$ are almost the same because at this location, the induced flows have similar influences for both the cases. However, temperatures at the center and at the trailing edge are tremendously different (the best case shows lower temperatures); this behavior is expected according to the respective flow and vortex profiles.

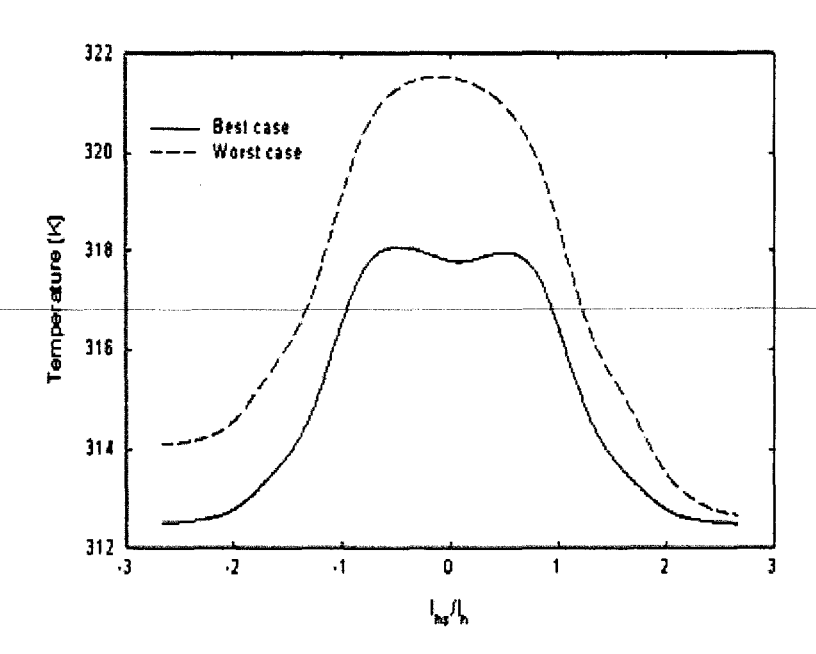


Figure 5.13 Temperature plots on the reference line for the comparison of the cases

5.3 Heat transfer coefficient

Fig. 5.14 shows the heat transfer coefficient (h_{hs}) for the best and worst cases. In each case, the heat transfer coefficient decreases as it moves to the heat sink's center which is the hottest zone. The increase in heat transfer coefficient of the best case compared to the worst case is around 1% at the leading edge, increases dramatically to 16% at the centre and then decreases to 10% at the trailing edge. This trend demonstrates that α and δ have significant role on the heat removal performance.

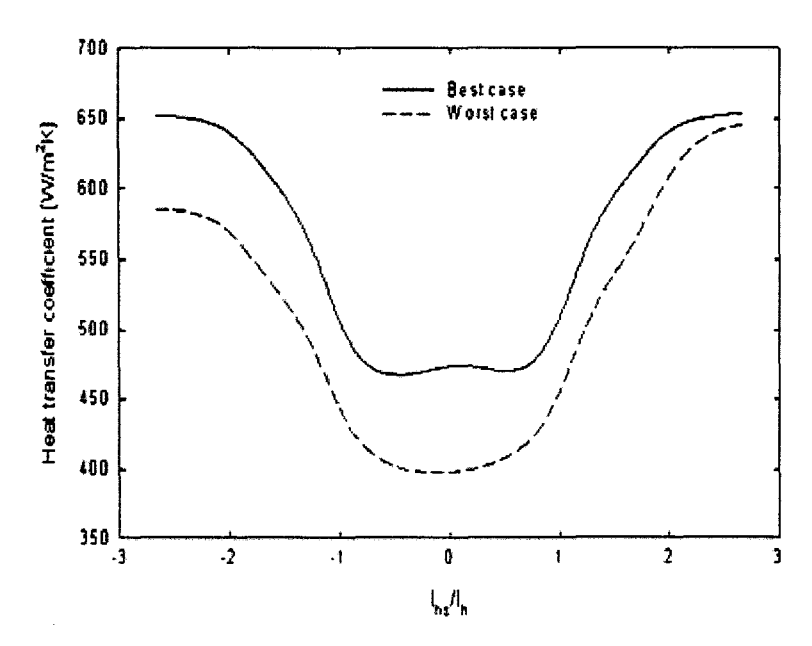


Figure 5.14 Heat transfer coefficient plots on the reference line for the comparison of the cases

5.4 Comparison of simulation and experimental results

The predicted and measured temperatures at the locations shown in Figure 2 (b) are compared for the best and worst cases as summarized in Table 4 and Table 5 respectively. It can be observed that there is good agreement between simulation and experiment, with a maximum discrepancy of only 1%.

Table 4 Comparison of experimental and simulation temperatures (best case)

Tempera Point		T_s	1	2	3	4	5	6	7
Exp.	(K)	317.48	312.34	310.64	312.06	306.46	306.98	306.83	306.33
$\alpha = 90$	(K)	317.80	312.82	311.66	312.44	310.76	311.55	311.29	309.39
$\Delta T_{\text{exp-sim}}$	(K)	0.32	0.48	1.02	0.38	4.3	4.57	4.46	3.06
$\%\Delta T_{\text{exp-sim}}$	` ,	0.1	0.15	0.33	0.12	1.4	1.49	1.45	1.0
% Average 4	$\Delta T_{\text{exp-sim}}$				0.	76			

Table 5 Comparison of experimental and simulation temperatures (worst case)

Temperat Points		T _s	1	2	3	4	5	6	7
Exp.	(K)	320.39	312.76	312.82	311.89	306.08	310.64	305.31	308.06
$\alpha = 0$	(K)	321.52	314.44	313.94	314.02	311.94	313.01	310.79	313.09
$\Delta T_{\text{exp-sim}}$	(K)	1.13	1.68	1.12	2.13	5.86	2.37	5.48	5.03
$\Delta T_{\text{exp-sim}}$	` ,	0.35	0.54	0.36	0.68	1.91	0.76	1.79	1.63
% Average Δ	$\Gamma_{ ext{exp-sim}}$				1.	.0			

Similarly, Fig. 5.15 shows the comparison of convective heat transfer coefficient at the location $\frac{l_{hs}}{l_h} = 0$ of the heat sink. A maximum of 5% under-prediction is observed in the simulation, which is attributed to the omission of radiation effect in the numerical model; this presumption was confirmed by deducting the experimentally determined radiative contribution, from the predicted value.

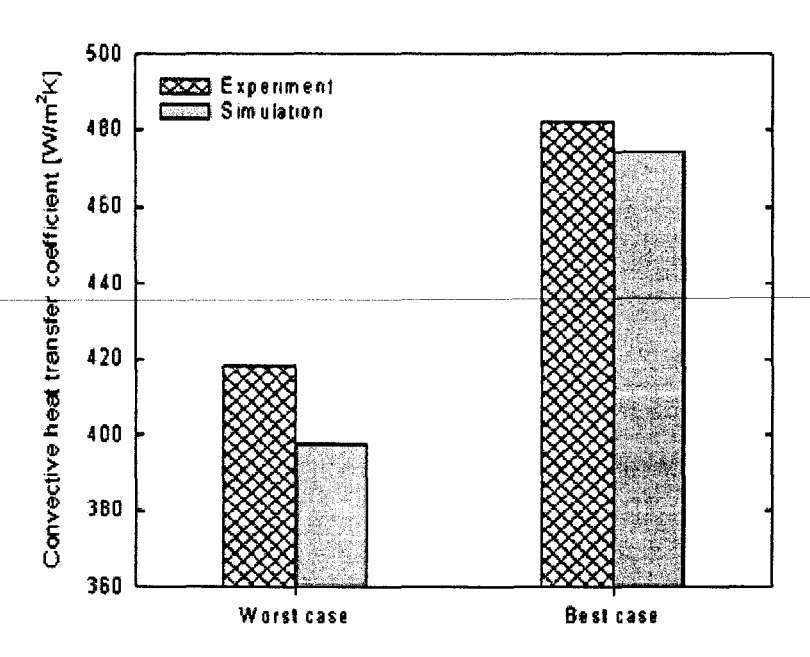


Figure 5.15 Comparison of predicted and experimental heat transfer coefficients.

In addition, the thickness of the thermal compound in the simulation was treated as uniform in all the cases; the real thickness was not necessarily so, as the compound was manually applied. Furthermore, the ambient temperature in the experiments was measured with a single thermocouple, whereas the average fluid temperature inside the domain was used in the simulation.

6. Conclusion

Optimization of tip gap and orientation of piezoelectric fans was performed by using the DOE approach, to maximize the heat removal performance of finned heat sink. A 3D simulation using FLUENT 6.3.2 was carried out to better understand the induced flow and the resulting heat transfer. The turbulence was incorporated by the shear stress transport (SST) k- ω model. The experimental results are well matched with the predictions. By the use of DOE, significant savings in effort and time were achieved to conduct the required experiments and the coupled influence of tip gap and piezofan orientation could be analyzed effectively. It was observed that piezofan with vertical orientation and a tip gap of 5mm could yield 88% enhancement in the convective heat transfer coefficient compared to natural convection. The present finding is expected to be a valuable input in the application of finned heat sink with multi- peizofan in microelectronic cooling. This study may be extended for lesser tip gaps, and with various piezofan-heat sink configurations.

Acknowledgement

This work is supported by the Research University Grant Scheme (RUG-USM), under contract 1001/PMEKANIK/811076. The authors thank to S. F. Shaker, T.Y. Chong, and W.

Amri for their contributions in fabrication of the test apparatus and in the conduct of the noise and vibration experiments, and M. Hashim for help in conducting the control and instrumentation experiment.

References

- [1] T. Acikalin, S.V. Garimella, Analysis and prediction of the thermal performance of piezoelectrically actuated fans, Heat Transfer Engineering, 30(6) (2009) 487–498.
- [2] M. Toda, Theory of air flow generation by a resonant type PVF2 Bimorph cantilever vibrator, Ferroelectrics 22 (1979) 911–918.
- [3] M. Toda, Voltage-induced large amplitude bending device-PVF₂ Bimorph—Its properties and applications, Ferroelectrics 32 (1981) 127–133.
- [4] A. Ihara, H. Watanabe, On the flow around flexible plates, oscillating with large amplitude, Journal of Fluids Structures 8 (1994) 601–619.
- [5] T. Acıkalın, A. Raman, S.V. Garimella, Two-dimensional streaming flows induced by resonating thin beams, J. Acoust. Soc. Am. 114 (No. 4-Pt. 1) (2003) 1785–1795.
- [6] M.K. Abdullah, M.Z. Abdullah, M.V. Ramana, C.Y. Khor, K.A. Ahmad, M.A. Mujeebu, Y. Ooi, Z. Mohd Ripin, Numerical and experimental investigations on effect of fan height on the performance of piezoelectric fan in microelectronic cooling, International Communications in Heat And Mass Transfer 36 (2009) 51–58.
- [7] M.K. Abdullah, M.Z. Abdullah, M.V. Ramana, C.Y. Khor, K.A. Ahmad, M.A. Mujeebu, Y. Ooi, Z. Mohd Ripin, Effect of piezoelectric fan height on flow and heat transfer for electronics cooling applications, International Conference on Electronic Materials and Packaging, EMAP 2008, Taipei, Taiwan, 2008, pp. 165-170.
- [8] R.R. Schmidt, Local and average transfer coefficients on a vertical surface due to convection from a piezoelectric fan. InterSociety Conference on Thermal Phenomena in Electronic Systems, I-THERM IV, Washington, 1994, pp. 41–49.
- [9] T. Acıkalın, S.M. Wait, S.V. Garimella, A. Raman, Experimental investigation of the thermal performance of piezoelectric fans. Heat Transfer Engineering 25 (1) (2004) 4–14.
- [10] J.H. Yoo, J.I. Hong, W. Cao, Piezoelectric ceramic bimorph coupled to thin metal plate as cooling fan for electronic devices. Sensors and Actuators 79 (2000) 8–12.
- [11] T. Acıkalın, I. Sauciuc, S.V. Garimella, Piezoelectric actuators for low-form factor electronics cooling, Proceedings of IPACK2005-ASME InterPACK Conference, San Fransisco, CA, 2005, pp. 939-943.
- [12] H. Hosaka, K. Itao, Coupled vibration of microcantilever array induced by airflow force, ASME Journal of Vibration and Acoustics, 124 (2002) 26–32.
- [13] S. Basak, A. Raman, Hydrodynamic Coupling Between Micromechanical Beams Oscillating in Viscous Fluids, Phys. Fluids, 19(1017105) (2007) 1-13.
- [14] M. Kimber, S.V. Garimella, A. Raman, An experimental study of fluidic coupling between multiple piezoelectric fans, International Society Conference on Thermal Phenomena, San Diego, CA, 2006, pp. 333–340.
- [15] M. Kimber, S.V. Garimella, Cooling Performance of Arrays of Vibrating Cantilevers, Journal of Heat Transfer, 131 (2009) 1-8.
- [16] T. Acikalin, S.V. Garimella, A. Raman, J. Petroski, Characterization and optimization of the thermal performance of miniature piezoelectric fans, International Journal of Heat and Fluid Flow 28 (2007) 806–820.

- [17] J. Petroski, M. Arik, M. Gursoy, Optimization of Piezoelectric Oscillating Fan-Cooled Heat Sinks for Electronics Cooling, IEEE Transactions on Components and Packaging Technology, 33(1) (2010) 25-31.
- [18] Mohamed H A Elnaggar, M. Z. Abdullah and M. Abdul Mujeebu. Experimental investigation and optimization of heat input and coolant velocity of finned twin U-shaped heat pipe for CPU cooling. Experimental Techniques (corrected proof available online).
- [19] Modeling Flows Using Sliding and Deforming Meshes, FLUENT 6.3.26, FLUENT Inc. Lebanon, New Hampshire, 2006, Chapter 11.3.
- [20] Meirovitch, L. Principle and techniques of vibration, Englewood Cliffs: Prentice Hall, Singapore, 1997, pp. 400-403.
- [21] F.P. Incropera, D.P. Dewitt, Fundamentals of Heat and Mass Transfer; 4th Edition, John Wiley & Sons, Singapore, 1996, pp. 103-105.

Effects of tip gap and amplitude of piezoelectric fans on the performance of heat sinks in microelectronic cooling

M. K. Abdullah · N. C. Ismail · M. Z. Abdullah · M. Abdul Mujeebu · K. A. Ahmad · Z. Mohd Ripin

Received: 22 June 2010/Accepted: 14 November 2011 © Springer-Verlag 2011

Abstract Piezoelectric fan is a promising option for cooling microelectronic devices owing to its unique features such as no electromagnetic noise, low power consumption and minimum space requirement. The recent interest is to integrate the piezoelectric fans (piezofans) with heat sink; this idea is widely accepted and researches are still underway. This article presents experimental analysis on the effects of tip gap (δ) and amplitude of piezofan vibration (α) on the heat transfer characteristics of finned heat sinks. Two heat sink configurations, namely A and B (with two and four fins respectively) each of which is arranged with three piezofans, are considered for the study. The transient temperature distributions for cases with and without piezofans are obtained for both the configurations, and compared. The heat transfer coefficient, thermal impedance, Nusselt number and Reynolds number are investigated as functions of δ and α . The effect of α on the fan effectiveness is also analyzed. It is observed that the configuration B has better cooling performance compared to A. Among the tested ranges of δ and α , the case with least tip gap ($\delta = 0.03$) and highest amplitude ($\alpha = 5.29$) is found to be the best; at this setting, the fan effectiveness

is increased to almost 4 times compared to the case without piezofans.

List of symbols

 D_{pz} Piezoelectric fan width (mm)

 h_{hs} Average of heat sink convection coefficient (W/m²K)

k Fluid thermal conductivity (W/mK)

Q Power input (W)

T_{base} Average heat sink base temperature (K)

 T_i Junction chip temperature (K)

t Time (s)

Gap between piezofan and heat sink surface (mm)

 h_{ncn} Average of plate convection coefficient (W/m²K)

Nu Mean Nusselt number

q Heat flux (W/m^2)

 T_n Temperature at a n-point (K)

 T_{∞} Ambient temperature (K)

X 1/2 of peak to peak amplitude (mm)

Greek symbols

α Normalized amplitude

v Kinematic viscosity of air (m^2/s)

 ω Angular velocity (rad/s)

 δ Normalized tip gap

 ε_{fan} Piezofan effectiveness

Thermal impedance (K/W)

M. K. Abdullah (☑) · N. C. Ismail · M. Z. Abdullah · M. A. Mujeebu · K. A. Ahmad · Z. M. Ripin Aerodynamic and Advanced Cooling Laboratory, School of Mechanical and Aerospace Engineering, Universiti Sains Malaysia, Engineering Campus,

14300 Nibong Tebal, Penang, Malaysia e-mail: mkhalil@eng.usm.my

M. A. Mujeebu

Department of Mechanical Engineering, Anjuman Institute of Technology and Management (Visvesvaraya Technological University, Belgaum), Bhatkal, Karnataka 58320, India

Subscripts

1...8 Temperature location at n-point

j Junction chip

pf Piezofan

∞ Ambient

ncp Natural convection of flat plate

pz Forced convection under piezofan actuation

1 Introduction

Thermal management has been an essential requirement for the rapid growth of electronic industry. As the circuit density and power dissipation of integrated circuit (IC) chips are increasing, the associated heat flux levels become crucial. The large amount of heat flux can create unusual heat stress on chips, substrate, and its package. The performance of the electronic devices is directly related to the temperature; therefore it is important to maintain them within the acceptable temperature levels. Decreasing the temperature of a component increases its performance as well as its reliability [1].

Natural convection cooling is obviously advantageous for low power dissipating devices since it offers low-cost, energy-free, and noise-free operation [2, 3]. An additional means of passive cooling namely heat sink has been adapted to natural convection, for maintaining the operating temperature of electronic components at a satisfactory level [4]. The most common method for cooling electronic devices is to use finned heat sinks usually made of aluminum; it provides a large surface area for the dissipation of heat and effectively reduces the thermal resistance [5]. Heat sinks are commonly attached to the surface of the spreader to provide additional surface area. Unfortunately, due to surface roughness the physical contact at the interface of the electronic component and the heat spreader is only around 5% of the total contact area [6]. This lack of contact could significantly limit the heat transfer from the component to the heat sink; however, the recently introduced thermal gap pad could increase the contact surface thereby reducing the contact resistance [7].

Nevertheless, the rising demand for high performance and multi functionality in electronic devices poses thermal challenges that may not be tackled by passive cooling techniques; this situation calls for active cooling techniques [8]. Combination of rotary fans and heat sinks has been a relatively feasible option, as it requires no special packaging considerations. On the other hand, even applications with lower heat dissipation levels could pose severe challenges due to space, weight, power consumption, noise level, or other constraints [9]; for instance, the more the heat generated the larger, faster and noisier is the fan needed to remove it. One of the techniques proposed over the last decade to cope up with this issue is piezoelectric fan [10–13].

Piezoelectric fan (hereafter named as piezofan) is a cantilever beam whose vibration is actuated by means of a piezoelectric element and it is typically bonded near the clamped end of the beam. A bending moment is induced at the interface of the cantilever beam and the piezoelectric element when a voltage is applied [14, 15]. The beam is set into an oscillatory motion if an alternating voltage is

applied, which then creates motion in the surrounding fluid; this motion has proved to provide heat transfer enhancements with minimal power consumption [16]. Moreover, it can be configured to meet the geometric constraints of applications where the limited available volume might preclude the use of traditional cooling techniques. The piezofan can be tailored to operate at certain frequencies which are inaudible to the human ear [17]. A few studies on the use of single piezofan without heat sink were reported, as outlined by Acikalin and Garimella [18]. Fluidic coupling between piezofans was studied numerically and experimentally by Kimber et al. [19, 20]. Their study was extended recently to analyze the performance of piezofans which were eventually recommended for microelectronic cooling [21]. The heat transfer performance was quantified over vibration amplitude, distance from heat source and pitch between piezofans. They found that piezofans could enhance the heat transfer compared to the conventional fans.

However, the use of piezofans substantially increases the complexity in describing the structural, fluidic, and heat transfer behavior [22]. Recent studies by Acikalin et al. [18] and Petroski et al. [23] investigated the possibilities of coupling single piezofan with the heat sink for enhancing the cooling performance. Moving one step ahead, Sauciuc et al. [24] and Mochizuki et al. [25] performed a preliminary study on the use of piezofans with heat sink, yet this promising option needs further exploration. Accordingly, in the present work, a detailed experimental analysis is performed on piezofans with heat sink, in order to observe the effects of tip gap (δ) and piezofan amplitude (a) on the heat transfer performance. Two piezofan-heat sink configurations namely Configuration A (heat sink with two fins) and Configuration B (heat sink with four fins) are tested. The local transient temperature distributions on the chip and heat sink, and the thermal impedance, heat transfer coefficient and Nusselt number of the chip, are analyzed for both the configurations.

2 Materials and methods

2.1 Experimental setup and procedure

In the present experiments, the electronic device (chip) is mimicked as a heater connected to a constant heat flux source. The constant heat flux of $9.1667 \times 10^3 \text{ W/m}^2$ is controlled by one of the direct current (DC) outputs of a digital dual power supply (GW-instek GPS-2303 with accuracy $\pm 0.5\%$); the other terminal is fed to the piezofans. The heater is made from stainless steel with dimensions of $30 \text{ mm} \times 30 \text{ mm} \times 3 \text{ mm}$, pasted with RS[®] heat sink compound and embedded on a wooden



platform which also serves as thermal insulator. The aluminum heat sinks of size $80 \text{ mm} \times 60 \text{ mm} \times 1 \text{ mm}$, are fixed over the heater. Fins of 1 mm thick and 30 mm high extend over the entire length of the heat sink base (80 mm). Figure 1 shows the two heat sink configurations namely A and B with two and four fins respectively, and the thermocouple locations (shown as coordinate points with dimensions in mm).

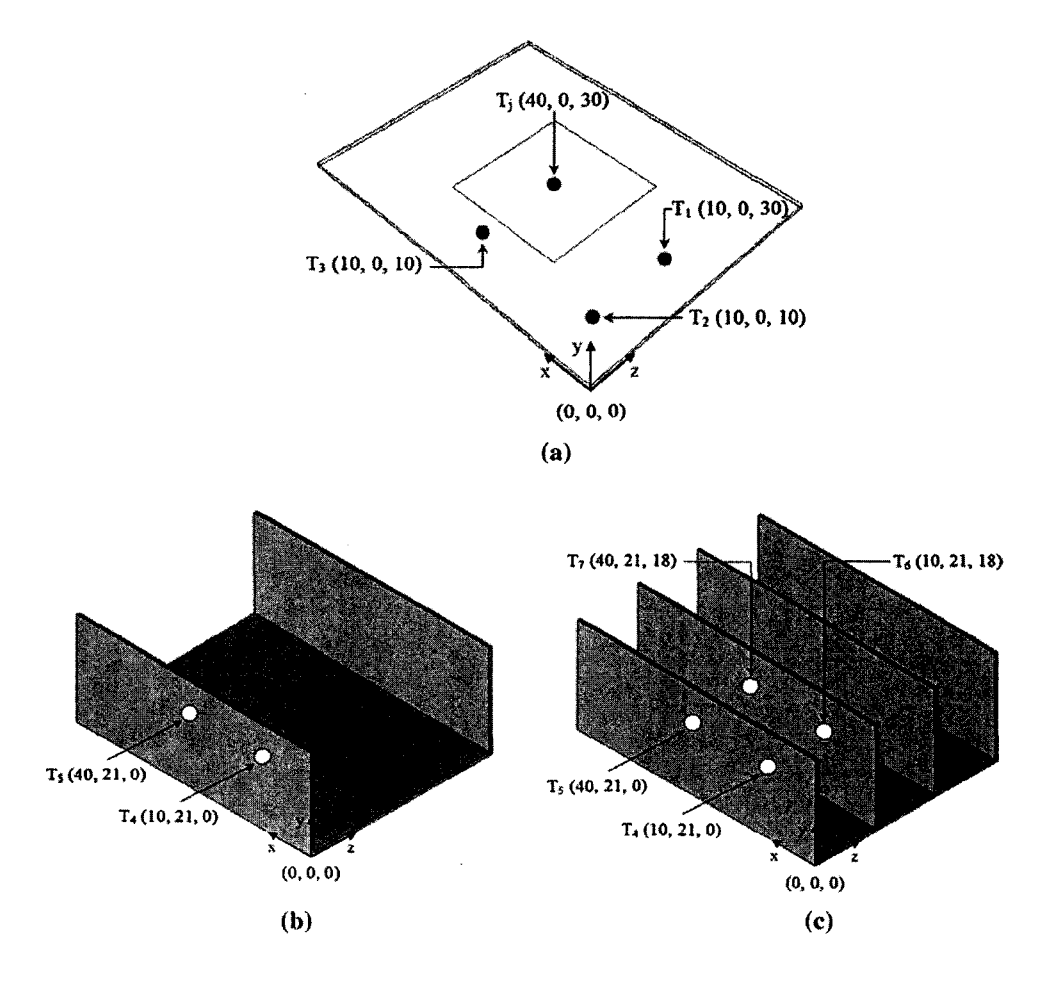
The piezofans are positioned vertically at right angles (Fig. 2) on a special stand and held rigidly at one end; this position was demonstrated to yield significant temperature drop [18]. The term tip gap (δ) used in this article is defined as the ratio of gap height (G, as illustrated in Fig. 2) to the fin height. The total heat transfer areas of the heat sink and fins for configurations A and B are 95.76 \times 10⁻⁴ m² and 190.16 \times 10⁻⁴ m² respectively. The piezofan specifications are given in Table 1. The oscillating drive signal to match the resonance frequency of piezofans is facilitated by a DC to AC inverter circuit.

Figure 3 shows the experimental setup used in the present study, which consists of a glass tunnel of size $250 \text{ mm} \times 120 \text{ mm} \times 800 \text{ mm}$. The chip and heat sinks

along with the piezofans are housed in the glass tunnel to minimize the ambient effects. The thermocouples are connected to the locations shown in Fig. 1; an additional thermocouple is used to monitor the ambient air temperature in the enclosure. The temperatures are displayed and recorded in the computer by means of the data logger (ADVANTECH DAQ System) for every minute during the experiment. Steady state condition is reached after 80 min of heating and 30 min after the piezofans are turned on. The tip displacement of the piezofans is measured by a laser displacement sensor (Keyence LK-G152) with a resolution of 1 ms. An oscilloscope (Agilent Technologies DSO3062-60 MHz) is used to measure the applied voltage and the resonance frequency. For the best performance, the piezofans are excited at the resonance frequency of at 115 Hz and 15 V, as prescribed by the manufacturer. The maximum deflection of each piezofan is 4.75 mm, which is symmetric in both directions. The ambient air temperature is always controlled at 25°C.

There are several important factors that affect the cooling effects of the piezofans, such as piezofans frequency, number of fins, electric signal applied to the

Fig. 1 Schematic of the heat sink configurations with thermocouple locations. a Heat sink base. b Configuration A. c Configuration B





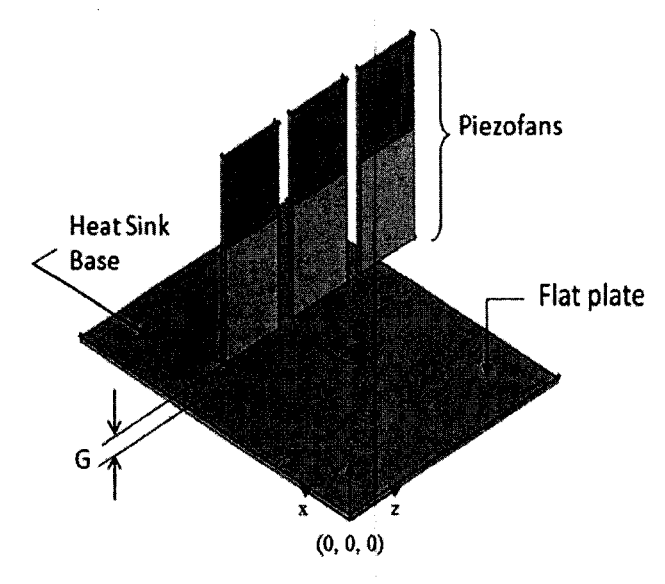


Fig. 2 Orientation of piezofans over the heat sink (fins not shown)

piezoelectric elements and the fan tip gap. In the current experiments, the activation frequency of the bimorph is set at the first resonance frequency, and the power supply is fixed at a certain value. Therefore the electric field, the tip

Fig. 3 Schematic of the experimental setup

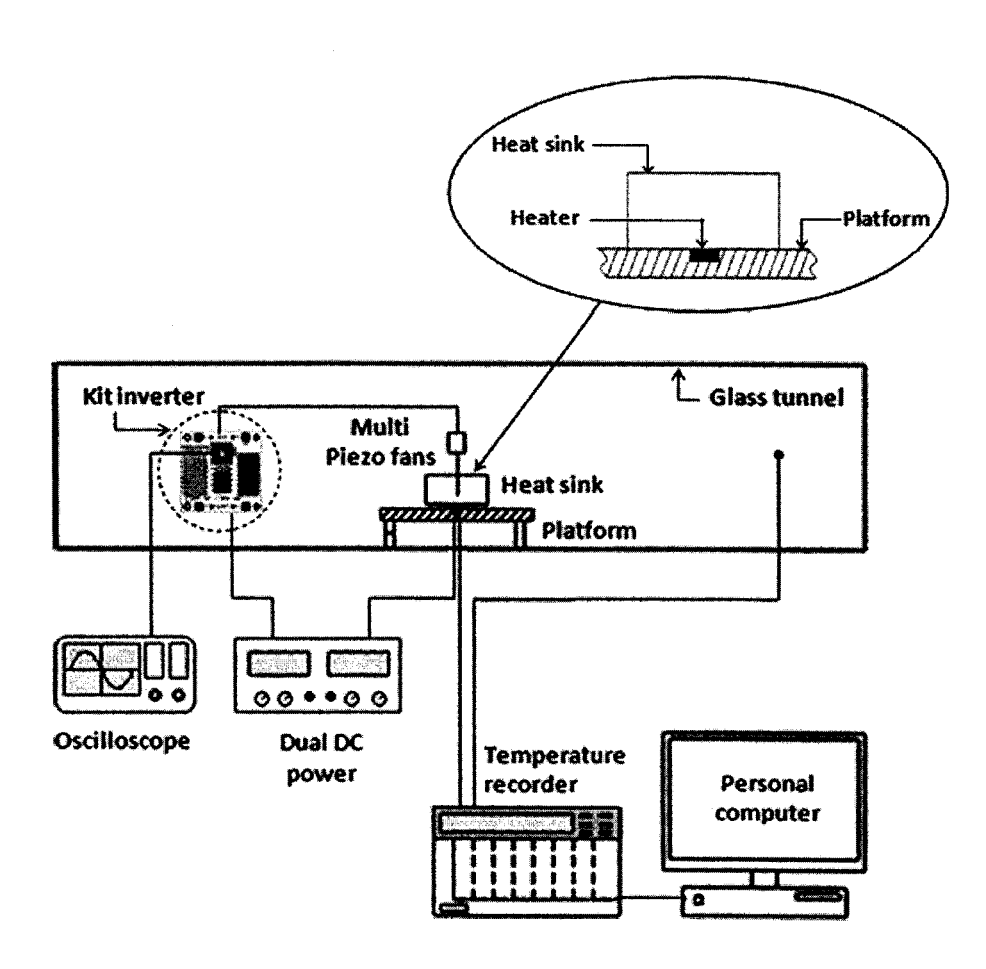


Table 1 Piezofan specifications (PiezoSystem Inc)

Specification	Value		
Material	Stainless steel		
Fan size (mm)	$47 \times 12 \times 0.4$		
Resonant frequency (Hz)	115		
Power consumption of fan and circuit (mW)	42		
Fan weight (kg)	2.0×10^{-3}		

gap and the number of fins are the three variables that influence the cooling.

2.2 Performance parameters

The main focus of the present study is to assess the extent of cooling achieved by the chip (heat source), according to the changes in tip gap and amplitude. Hence, apart from observing the local temperature distributions on the heat sink and the chip, the convective heat transfer coefficient (h), thermal impedance (Θ) [5] and Nusselt number (Nu) for the chip, are evaluated. The Reynolds number (Re) [26] related to the fluid motion over the heat sink base, due to the piezofan vibration, is also estimated. The various expressions are as follows.

$$h_{hs} = \frac{q}{\left(T_j - T_{\infty}\right)} \tag{1}$$

where q and T_j are the heat flux, and the temperature respectively, of the chip, and T_{∞} is the average ambient temperature. In this study, h_{hs} is calculated for both natural (no piezofan) and forced (with piezofan) convection modes, in order to observe the impact of piezofan.

$$\Theta = \frac{T_{base} - T_{\infty}}{O} \tag{2}$$

$$Nu = \frac{h_{hs}D_{pz}}{k} \tag{3}$$

where Q is power input, T_{base} is average heat sink base temperature, D_{pz} is the piezofan width, and k is the thermal conductivity of air.

$$Re = \frac{\omega X D_{pz}}{v} \tag{4}$$

where ω is the vibration frequency, X is the amplitude, and v is kinematic viscosity of air.

The influence of piezofan on the heat sink performance is also evaluated in terms of 'fan effectiveness' (ε_{fan}) which represents the convective heat transfer coefficient divided by that under natural convection of flat plate and it is shown as:

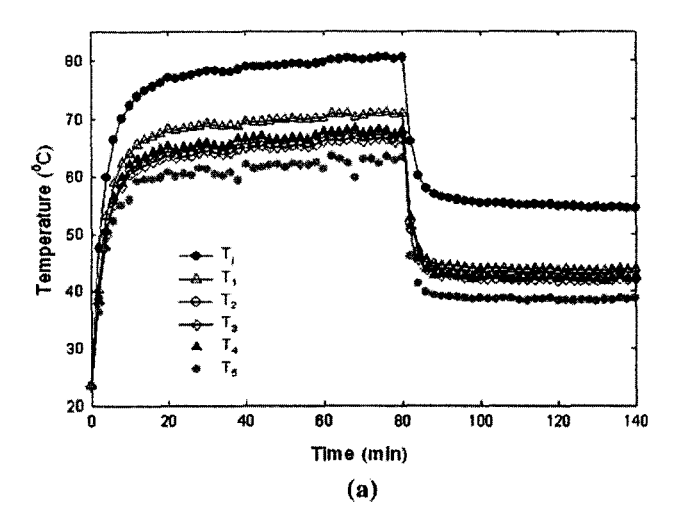
$$\varepsilon_{fan} = \frac{h_{hs}}{h_{ncp}} \tag{5}$$

3 Results and discussion

3.1 Temperature distribution

Figure 4 shows the effect of piezofans on the transient temperature distributions for configurations A and B. At t=0 the heater is turned on and the temperatures are first observed under natural convection condition, until steady state is reached; at t = 80 min, the piezofans are turned on and a new steady state is reached at t = 100 min. As shown in Fig. 4a, for Configuration A, when the piezofans are off (natural convection), the chip temperature is around 80.49°C and heat sink temperatures ranges from 63.33 to 70.88°C. When fans are turned on, these temperatures drop drastically to 54.47°C and 42.48–43.47°C respectively. It is observed from Fig. 4b that the configuration B could yield a temperature drop of 10°C compared to Configuration A, due to the increase of heat transfer area; the piezofans are seen to cause a reduction in the chip temperature from approximately 57.99-69.05°C in natural convection to 49.82-34.03°C.

In order to find the tip gap which brings the maximum temperature drop, the piezofans are actuated at 115 Hz for



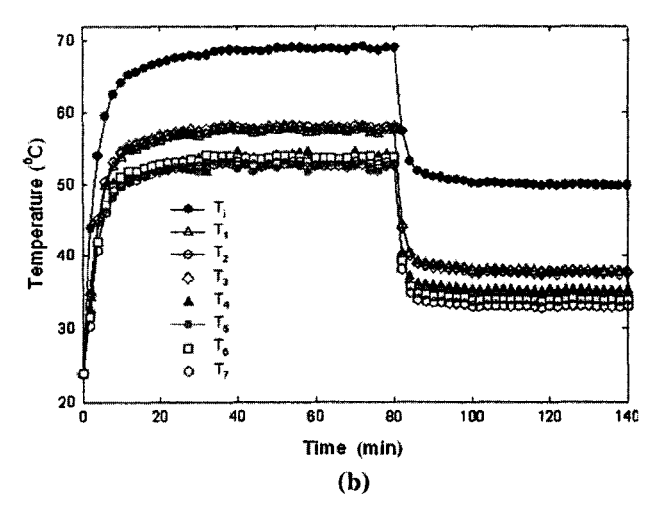


Fig. 4 Effect of piezofans on the transient temperature distributions. a Configuration A. b Configuration B

four distinct values of δ varying from 0.03 to 0.5. Figure 5 shows the corresponding temperature distributions for both the configurations; the best performance is observed at $\delta=0.03$, followed by the increasing order of δ . However, it is worth noting that the effect of chip temperature on the tip gap is more crucial for Configuration B compared to A. For Configuration A, $\delta=0.17$ may be regarded as the optimum, as there is no significant change in temperatures on further reduction. However, for Configuration B, the appreciable reduction in temperature with the reduction of gap calls for further analysis with smaller tip gaps. It can also be seen that the temperature drops rapidly in 10 min after activating the piezofans and the temperature of the chip is nearly stable after 30 min.

The effect of amplitude on the temperature distribution for configurations A and B is shown in Fig. 6. Keeping $\delta = 0.03$ which is found to be the best, the normalized amplitude ($\alpha = X/G$) is varied from 5.29 to 2.76. The frequency is maintained at the resonance value of 115 Hz



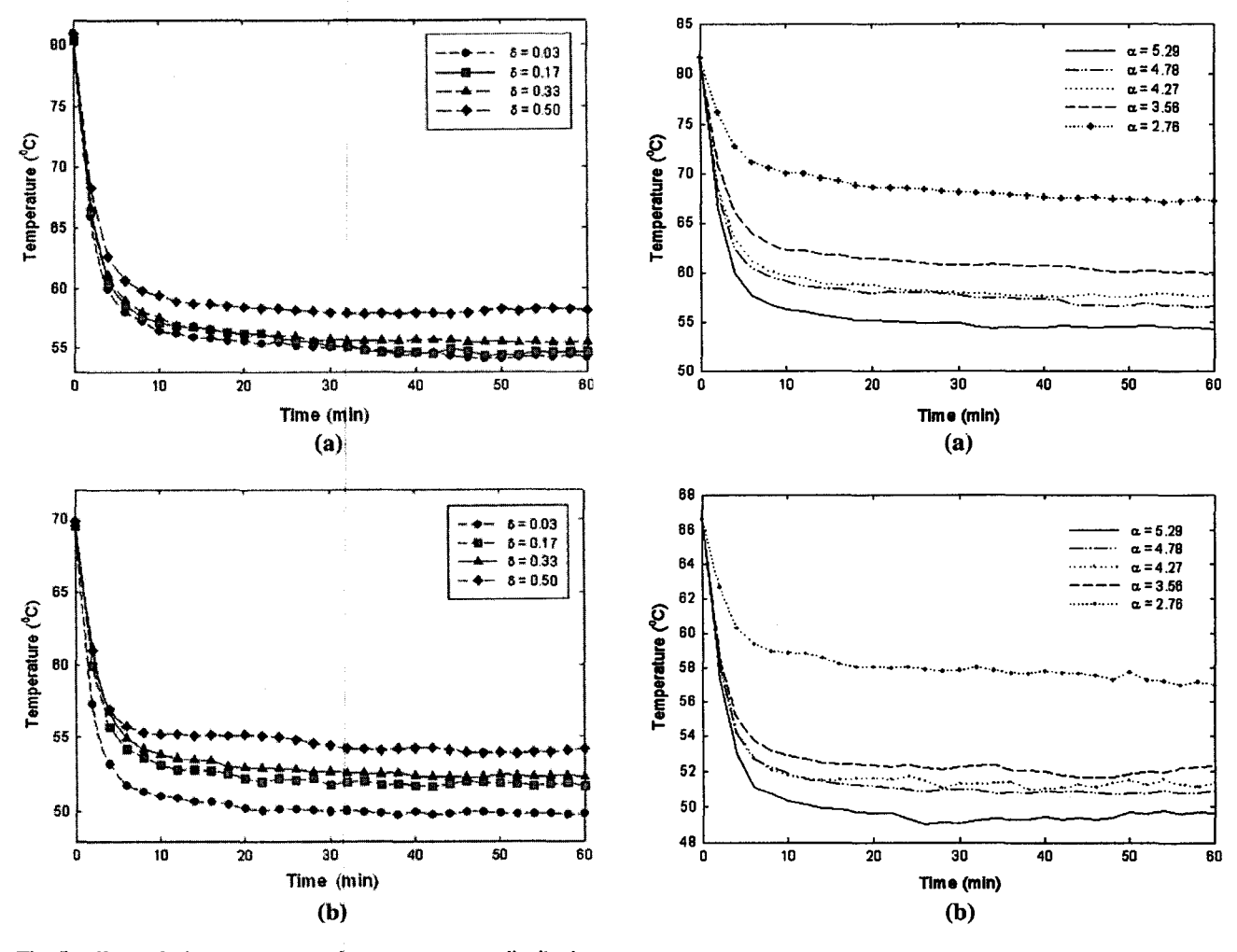


Fig. 5 Effect of tip gap on transient temperature distribution. a Configuration A. b Configuration B

Fig. 6 Effect of amplitude on transient temperature distribution. a Configuration A. b Configuration B

and the voltage is varied for varying the amplitude. The temperature distributions are plotted for different values of α as shown. It is observed that the cooling performance is the best for $\alpha = 5.29$. Hence by correlating this finding with the best gap, it can be concluded that a lower tip gap with higher amplitude is preferable for better cooling.

3.2 Heat transfer analysis

The initial values of average heat transfer coefficients under natural convection when the piezofans fan are not functioning, are 166.4 and 207.9 W/m²K for configuration A and B respectively. The heat transfer coefficient for the Configuration A varies from 247.3 to 316.1 W/m²K (48.62–89.96%), while for the Configuration B it varies from 318.4 to 371.9 W/m²K (53.15–78.88%). The heat transfer coefficients for four different values of δ for configurations A and B are plotted as shown in Fig. 7. The

solid and dashed lines indicate the regression of the heat transfer coefficient for configurations A and B respectively.

It is noticeable that the largest heat transfer coefficients are obtained when the piezofans are close to the heat sinks, i.e., $\delta=0.03$. In this position, compared to natural convection, there is more than 78% increase in heat transfer coefficients for configurations A and B, due to the presence of piezofans. It is also clear that, as δ increases, the heat transfer coefficient decreases. This phenomenon indicates that the tip gap has significant role in the heat transfer performance, and at smaller gaps, the excited fluid is expected to have better physical contact over the heat sink surface, resulting in enhanced heat removal, as also observed by Kimber et al. [20–22].

In the context of the experiments performed here, the configuration B always performs better than the configuration A. The two heat sinks of different fins have different total surface areas. This difference in conjunction with the difference in δ , results in lowering the temperature



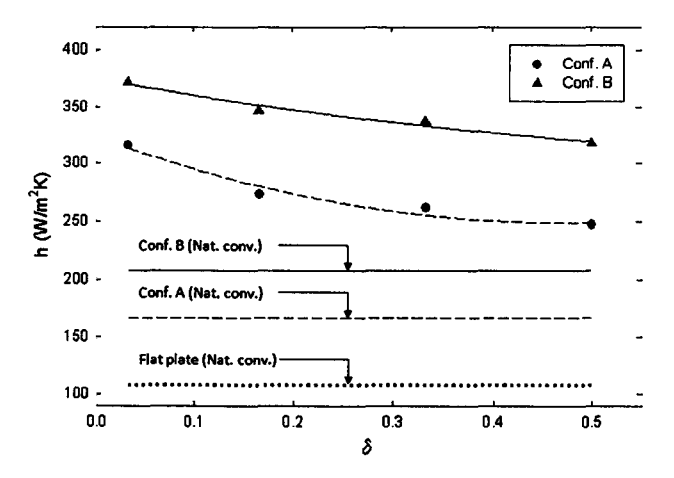


Fig. 7 Effect of piezofans and tip gap on heat transfer coefficient

difference between the chip and the ambient. Figure 8 illustrates the effect of Reynolds number, on the thermal impedance for the configurations A and B respectively; Θ decreases when Re increases. However, Θ of Configuration B is lower compared to that for Configuration A. Thus, it can be concluded that the total surface area with the aid of piezofans mainly contributes to a better performance even if the Reynolds number is increased.

Figure 9 shows the effect of amplitude on the heat transfer coefficient for both the configurations at $\delta=0.17$ and $\delta=0.03$. The extreme positions of the piezofans caused a difference in the heat transfer coefficient approximately 42.8 W/m²K for configuration A and 52.7 W/m²K for configuration B. In both the cases, the heat transfer coefficient increases linearly with the vibration amplitude, due to the fact that the acoustic streaming velocity is proportional to the sound wave intensity, i.e., the vibration amplitude.

Figure 10 shows the Nusselt number as a function of the streaming Reynolds number. It can be observed that the

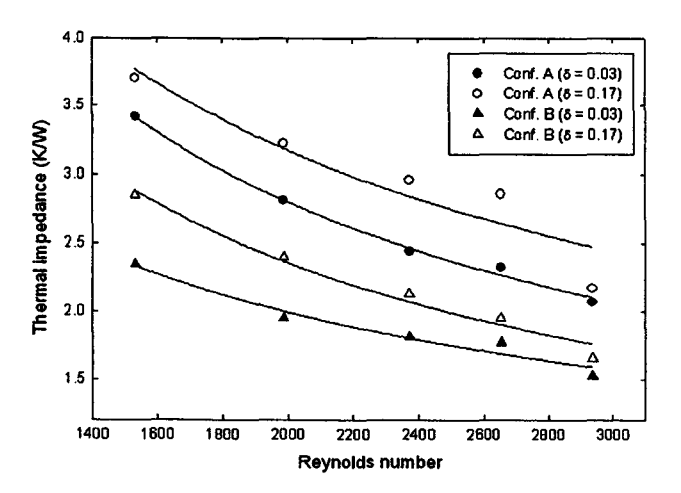
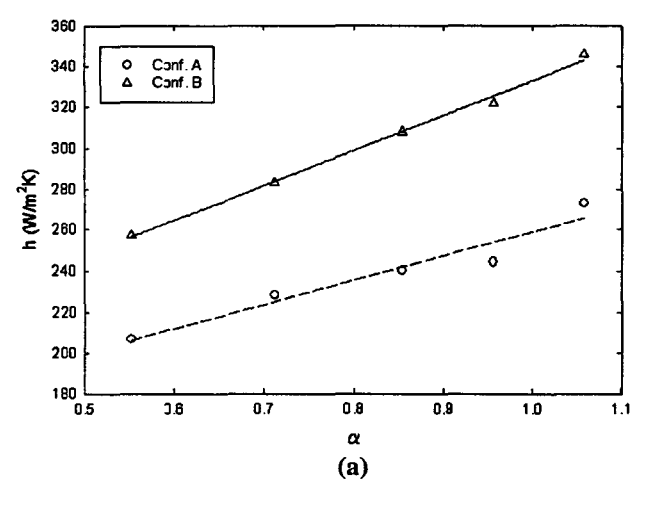


Fig. 8 Effect of Reynolds number on thermal impedance

Nusselt number increases as the Reynolds number increases for both the configurations, and the configuration B with $\delta=0.03$ offers the highest Nusselt number irrespective of change in Reynolds number. In general, it is deduced that, the cooling performance of the 'piezofan-heat sink' assembly increases with decrease in δ and increase in displacement amplitude, as the fluid stream interactions become more vigorous. An increase in amplitude increases the fluid inertia, thereby promoting the development of circulations and the related mingling of flow streams.

3.3 Effects of number of fins and amplitude on fin effectiveness

Interestingly, significant improvement in ε_{fan} is achieved by the use of piezofans in both the configurations. Further, the effect of amplitude on ε_{fan} is also analyzed for configurations A and B keeping δ the minimum, and the results are plotted as shown in Fig. 11. It is worth noting that, the ε_{fan}



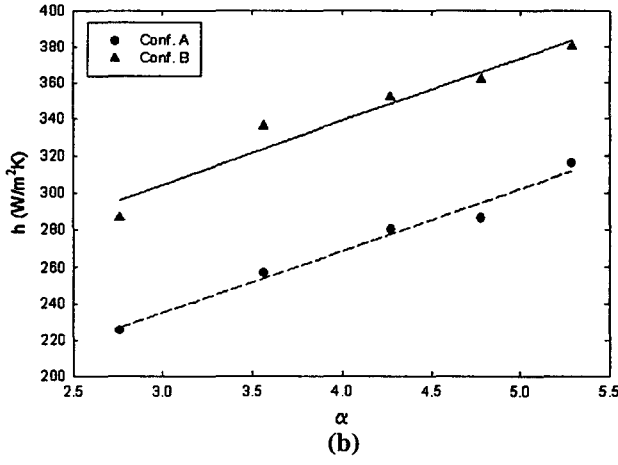


Fig. 9 Effect of amplitude on heat transfer coefficient. a $\delta=0.17.$ b $\delta=0.03$



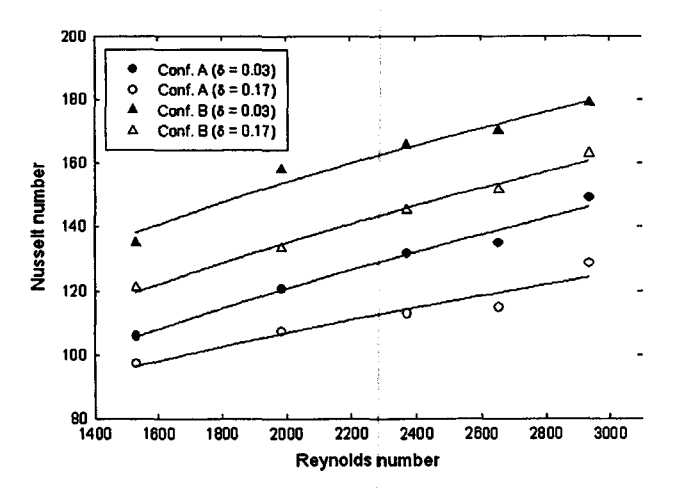


Fig. 10 Relationship between Reynolds number and Nusselt number

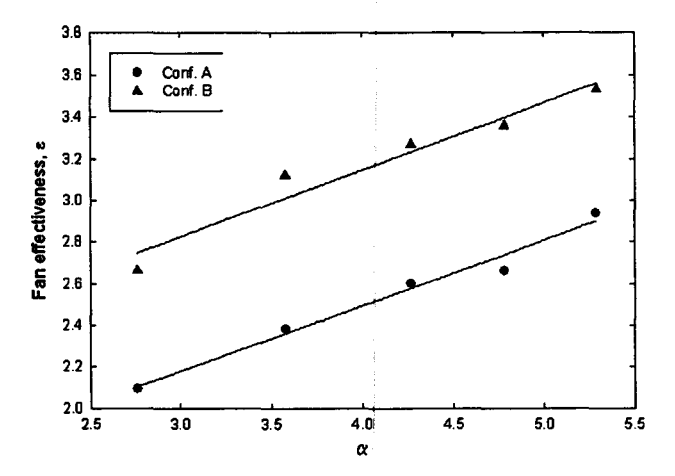


Fig. 11 Effects of number of fins and piezofan amplitude on fan effectiveness

is increasing with the increase of amplitude, as well as with the number of fins. The highest value of ε_{fan} is 3.53 (for configuration B), which indicates that for a given heat sink, use of maximum number of fins in conjunction with piezofans could yield the best cooling effect. For configuration A, there are only two fins at the extreme ends, leaving the spaces between the piezofans unfinned. However, by adding fins at the vacant intermediate spaces of piezofans, enhanced heat removal can be achieved as demonstrated by the configuration B. Therefore it can be concluded that the use of piezofans in combination with multi-finned heat sink can maximize the heat removal rate, if the fans are arranged such that no vacant space is left between the fins.

3.4 Uncertainty analysis

The experimental uncertainties for the aforementioned parameters are estimated from 5 sets of readings, by the

Table 2 Summary of experimental uncertainties

Parameter	Maximum uncertainty (%)					
	Configuration A	Configuration B				
Temperature	±2.20	±1.72				
Heat transfer coefficient	±2.32	±1.88				
Thermal impedance	±2.26	±1.79				

statistical procedure proposed by Taylor [27]. The results so obtained are summarized in Table 2 which indicates that the experimental errors are within the acceptable limits.

4 Conclusion

The effects of tip gap and amplitude of three piezofans, and the number of fins, on the performance of heat sink are experimentally studied. Detailed analysis on the combination of piezofans with heat sink is the contribution in the present study. Investigations on different tip gaps and amplitudes reveal that these parameters have critical effects on the cooling performance. In general, the piezofans give the best result at higher amplitudes and minimum tip gap. It is also shown that the piezofans significantly improve the heat sink performance, and the total surface area and the 'fan-fin' arrangement are crucial factors. Best cooling is achieved by the heat sink with four fins when piezofans vibrate with the highest amplitude and minimum tip gap. Further investigations may be performed on the effects of further reduction in the tip gap especially for Configuration B, and change in side gap. Another potential extension is to perform similar analysis with fans of very narrow width, to study the feasibility of incorporating piezofans to the commercially available multi-finned heat sinks.

Acknowledgments This work is supported by the Fundamental Research Grant Scheme (FRGS), under contract 1001/PMEKANIK/811076. The authors thank to T. Y. Chong, W. Amri and M. Najib for their contributions in fabrication of the test apparatus and in the conduct of the noise and vibration experiments, and M. Hashim for help in conducting the control and instrumentation experiment.

References

- Ohadi M, Qi J (2005) Thermal management of harsh-environment electronics. Microscale Heat Transf 193:479

 –498
- Tou SKW, Tso CP, Zhang X (1999) 3-D Numerical analysis of natural convective liquid cooling of a 3 x 3 heater array in rectangular enclosures. Int J Heat Mass Transf 42:3231–3244
- Adams VH, Joshi Y, Blackburn DL (1999) Three-dimensional study of combined conduction, radiation, and natural convection from discrete heat sources in a horizontal narrow-aspect-ratio enclosure. J Heat Transf 121:992–1001



- Ledezma G, Bejan A (1995) Heat sinks with sloped fins in natural and forced convection. Int J Heat Mass Transf 39(9):1773–1783
- Ismail MA, Abdullah MZ, Mujeebu MA (2008) A CFD-based experimental analysis on the effect of free stream cooling on the performance of micro processor heat sinks. Int J Heat Mass Transf 35:771-778
- Bailey C (2008) Thermal management technologies for electronic packaging: current capabilities and future challenges for modelling tools. In: Proceedings of the EPTC' 08 Conference, 2008, pp 527–532
- Lee YJ (2010) Thermo-mechanical properties of high performance thermal interface gap filler pads. In: Proceedings of the ITherm Conference, 2010, pp 1–8
- Arularasan R, Velraj R (2008) CFD analysis in a heat sink for cooling of electronic devices. Int J Comput Internet Manag 16(3):1-11
- Garimella SV (2006) Advances in mesoscale thermal management technologies for microelectronics. Microelectronics J 37:1165–1185
- Toda M, Osaka S (1979) Vibrational fan using the piezoelectric polymer PVF₂. Proc IEEE 67(8):1171–1173
- Acikalin T, Wait SM, Garimella SV, Raman A (2004) Experimental investigation of the thermal performance of piezoelectric fans. Heat Transf Eng 25:4–14
- Abdullah MK, Abdullah MZ, Wong SF, Khor CY, Ooi Y, Ahmad KA, Mohd Ripin Z, Mujeebu MA (2008) Effect of piezoelectric fan height on flow and heat transfer for electronics cooling applications. In: Proceedings of the EMAP Conference, 2008, pp 165–170
- Abdullah MK, Abdullah MZ, Ramana MV, Khor CY, Ahmad KA, Mujeebu MA, Ooi Y, Mohd Ripin Z (2009) Numerical and experimental investigations on effect of fan height on the performance of piezoelectric fan in microelectronic cooling. Int J Heat Mass Transf 36:51–58
- Kim BJ, Rho JS, Jung HK (2005) Optimal design of piezoelectric cantilever fan by three-dimensional finite element analysis. KIEE Int Trans Electr Mach Energy Convers Syst 5-B(1):90-94
- 15. Wait SM, Basak S, Garimella SV, Raman A (2007) Piezoelectric fans using higher flexural modes for electronics cooling

- applications. IEEE Trans Compon Packaging Manuf Technol 30(1):119-128
- Florio LA, Harnoy A (2006) Analysis of dynamic enhancement of natural convection cooling by a discrete vibrating plate. Heat Mass Transf 43:149–163
- Acikalin T, Garimella SV (2009) Analysis and prediction of the thermal performance of piezoelectrically actuated fans. Heat Transf Eng 30(6):487-498
- Acikalin T, Garimella SV, Raman A, Petroski J (2007) Characterization and optimization of the thermal performance of miniature piezoelectric fans. Int J Heat Fluid Flow 28:806–820
- Basak S, Raman A (2007) Hydrodynamic coupling between micromechanical beams oscillating in viscous fluids. Phys Fluids 19(017105):1–13
- Kimber M, Garimella SV, Raman A (2006) An experimental study of fluidic coupling between multiple piezoelectric fans. In: Proceedings of the ITherm Conference, 2006, pp 333–340
- Kimber M, Garimella SV (2009) Cooling performance of arrays of vibrating cantilevers. J Heat Transf 131:1–8
- Kimber M, Garimella SV, Raman A (2007) Local heat transfer coefficients induced by piezoelectrically actuated vibrating cantilevers. J Heat Transf 129:1168–1176
- Petroski J, Arik M, Gursoy M (2010) Optimization of piezoelectric oscillating fan-cooled heat sinks for electronics cooling. IEEE Trans Compon Packaging Manuf Technol 33(1):25-31
- Sauciuc I, Moon SW, Prstic S, Chiu CP, Chrysler G (2006) Key challenges for the piezo technology with application to low form factor thermal solutions. In: Proceedings of the ITherm Conference, 2006, pp 781–785
- Mochizuki M, Mashiko K, Saito S, Nguyen T, Wu XP, Nguyen T, Wuttijumnong V (2008) Thermal management in high performance computers. In: Proceedings of the International Heat Pipe Symposium, 2008, pp 39–48
- Kimber M, Suzuki K, Kitsunai N, Seki K, Garimella SV (2009)
 Pressure and flow rate performance of piezoelectric fans. IEEE
 Trans Compon Packaging Manuf Technol 32(4):766-775
- Taylor JR (1997) An introduction to error analysis: the study of uncertainties in physical measurements, 2nd edn. University Science Books, Sausalito, CA 94965, pp 94–104



Contents lists available at ScienceDirect

International Communications in Heat and Mass Transfer

journal homepage: www.elsevier.com/locate/ichmt



Numerical and experimental investigations on effect of fan height on the performance of piezoelectric fan in microelectronic cooling

M.K. Abdullah *, M.Z. Abdullah, M.V. Ramana, C.Y. Khor, K.A. Ahmad, M.A. Mujeebu, Y. Ooi, Z. Mohd Ripin

Aerodynamic and Advanced Cooling Laboratory, School of Mechanical and Aerospace Engineering, Engineering Campus, Universiti Sains Malaysia, 14300 Nibong Tebal, Penang, Malaysia

ARTICLE INFO

Available online 18 October 2008

Keywords: Microelectronic cooling Piezoelectric fan Heat transfer coefficient Particle image velocimetry

ABSTRACT

A piezoelectric fan is an attractive device to remove heat from microelectronic systems due to its low power consumption, minimal noise and compactness. In the present study, a piezoelectric fan is investigated to analyze the cooling capability for possible use in electronic devices. Both numerical and experimental analyses are carried out on the piezoelectric fan which was oriented horizontally. The FLUENT 6.3 software is used in the 2D simulation to predict the heat transfer coefficient and the flow fields using a dynamic mesh option to observe the fan swinging phenomena. Two heat sources in in-line arrangement are used in the experiment. The flow measurements are carried out at different piezoelectric fan heights by using a particle image velocimetry (PIV) system. The result shows that the piezofan height of $h_p l l_p = 0.23$ can reduce the temperature of the heat source surface as much as 68.9 °C. The numerical and experimental values of heat transfer coefficients are plotted and found in good agreement.

© 2008 Elsevier Ltd. All rights reserved.

1. Introduction

The rapid growth in science and technology has driven the electronic industry to develop efficient microelectronic products with high functionality. The resulting shrinkage in size and weight of electronic systems has increased the volumetric heat generation rates and surface heat fluxes over their components. As the size of electronic components decreases, cooling by conventional fans would restrict the components' miniaturization. Hence the need for developing advanced cooling techniques to improve performance of microelectronic components is increasingly significant, which has motivated the usage of a cantilever-type piezoelectric bimorph structure as a miniature fan. This is achieved by using a bimorphtype bending actuator, which consists of one or two thin piezoelectric ceramic layers bonded together. These piezoelectric bimorph structures have been introduced as an alternative cooling mechanism for microelectronic components.

A lot of researches have been done and are still underway in the area of electronic cooling. However, quite a few works have been reported on the application of the piezoelectric fan in this area. A number of numerical and experimental works have been carried out by using flexural waves by Roh and Loh [1]. The application of piezoelectric materials in sensors and actuators for actuating and controlling the smart structures were extensively studied by Crawly and Luis [2]. The potential convective heat transfer capability of a UFW

generated by direct and inverse piezoelectric effect was experimentally investigated by Wu et al. [3] and Loh et al. [4]. Yoo et al. [5] developed several types of piezoelectric fans using PZT, one of which resulted in a fan tip deflection of 3.55 cm and air velocity of 3.1 m/s measured 0.1 cm away from the tip. Schmidt [6] used the naphthalene sublimation technique in experiments to determine the local and average transfer coefficients on a vertical surface cooled by two piezoelectric fans resonating out of phase. Changing the distance between fans, was found to noticeably change the heat transfer coefficients for the system. Acikalin et al. [7] developed a closed-form analytical solution to predict the two-dimensional streaming flow from an infinite vibrating beam. The solution was used to develop a computational flow model for a baffled piezoelectric fan vibrating at its first mode of resonance in an infinite medium. Experimentally mapped flow patterns were found that closely matched those predicted by the model for the baffled fan. The feasibility of using piezoelectric fans in small scale electronic cooling applications was investigated by Wait et al. [8] and Acikalin et al. [9]. The visualization experiments were conducted to observe the flow induced by the piezofans. They also investigated the thermal performance in two different arrangements and found the use of piezofans have enhanced the convective heat transfer coefficients.

Ramana et al. [10] has presented a numerical study on cantilever piezoelectric fans to understand their mechanical behavior and to aid in design-optimization studies. Three-dimensional analysis was carried out by using the finite element analysis software package, ANSYS. The effects of various parameters like length, thickness, location of the piezoelectric metal layer, temperature, damping ratio, and electric field on the vibration characteristics are investigated and

Communicated by W.J. Minkowycz.

^{*} Corresponding author.

E-mail address: mezul@eng.usm.my (M.K. Abdullah).

Nomenclature

F	Body	force
---	------	-------

H Height of test section

h Static enthalpy

 h_p Height of piezofan from heat source

G Gravitational acceleration

HS Heat source

*h*_{ave} Average of convection coefficient

k Fluid thermal conductivity

L Length of test section

l_P Length of piezofan

P Pressure

PZT Lead Zirconate Titanate

q Heat fluxS Source term

T Temperature

*T*_{ave} Average temperature

*T*_∞ Ambient temperature

T Time

t_P Piezofan thickness

u, *v*, *w* Velocity component*u*_i Velocity component

Velocity componer

Volume

W Width of test section

 w_P Width of piezofan x, y Coordinate

Greek symbols

au Shear stress

ρ Fluid density

Φ General scalar for transport equation

Γ Diffusion coefficient

consolidated through artificial neural networks. Feed-forward single hidden layer perceptron neural networks and Levenberg-Marquardt back-propagation (LMBP) algorithms are used to train the neural network. Optimal geometrical dimensions for maximum performance are then obtained using genetic algorithm.

In the present study, the effect of piezoelectric fan height on the flow and heat transfer coefficient is investigated numerically and experimentally. The numerical simulation is done by using FLUENT 6.3. Particle image velocimetry (PIV) technique is used to make flow measurements. The piezoelectric fan is applied to cool two in-line heat sources horizontally mounted with no gap between them. The fan was arranged at different heights above the heat sources in order to obtain the effectiveness of cooling by the fan. It has been found that the fan height of $h_{\rm p}/l_{\rm p}$ =0.23 gives the best cooling.

2. Modeling

The governing equations describing the fluid flow are conservation of mass, conservation of momentum and conservation of energy. The equations are detailed below. FLUENT normally solves the governing equations using Cartesian spatial coordinates and velocity components.

The conservation of mass or continuity equation is:

$$\frac{\partial \rho}{\partial t} + \frac{\partial}{\partial x_i} (\rho u_i) = 0 \tag{1}$$

Eq. (1) is the general form of the mass conservation equation and is valid for incompressible and compressible flows.

Conservation of momentum in i-th direction in an inertial (non-accelerating) reference frame is described by:

$$\frac{\partial}{\partial t}(\rho u_i) + \frac{\partial}{\partial x_i}(\rho u_i u_j) = -\frac{\partial P}{\partial x_i} + \frac{\partial \tau_{ij}}{\partial x_i} + \rho g_i + F_i$$
 (2)

Where, P is the static pressure, τ_{ij} is the viscous stress tensor and g_i and F_i are the gravitational acceleration and external body force in the i direction, respectively.

The energy equation cast in terms of h (static enthalpy) can be written as

$$\frac{\partial}{\partial t}(\rho h) + \frac{\partial}{\partial x_i}(\rho u_i h) = \frac{\partial}{\partial x_i} \left(k \frac{\partial T}{\partial x_i} \right)$$
(3)

Where T is the temperature and k is the thermal conductivity.

Fluent 6.3 also provides the users with ability to simulate moving and deforming domains through the use of dynamic meshes. Dynamic meshes can be used to model flow where the shape of the domain is changing with time due to motion of the domain boundaries. The changing motion can be a prescribed motion or an unprescribed motion where subsequent motion is determined based on the solution at the current time.

The integral form of the transport equation for a general scalar Φ , on an arbitrary control volume, V, on a moving mesh is written as,

$$\frac{d}{dt} \int_{V} \rho \Phi dV + \int_{\partial V} \rho \Phi \left(\overrightarrow{\mathbf{u}} - \overrightarrow{\mathbf{u}}_{\mathbf{g}} \right) d\mathbf{A} = \int_{\partial V} \Gamma \nabla \Phi d\mathbf{A} + \int_{V} S_{\Phi} dV$$
 (4)

Where $\overrightarrow{\mathbf{u}}$ is the flow velocity vector and $\overrightarrow{\mathbf{u}_g}$ is the grid velocity of the moving meshes. The first and second terms on the left are the time derivative term and the convective terms. The terms on the right are the diffusive terms and the source terms. The term Γ represents the diffusion coefficient and $S_{\mathcal{O}}$ represents the source term of Φ . The term ∂V is used to represent the boundary of the control volume V and $\mathrm{d} A$ is the area movement.

All surfaces of the enclosure are isothermal and non-slip boundary conditions are applied at all solid surfaces. Thus, for top and bottom faces:

$$0 < x < L; y = 0; u = v = 0; \partial T/\partial x = 0$$

 $0 < x < L; y = H; u = v = 0; \partial T/\partial x = 0$

And, for front and back faces,

$$0 < y < H$$
; $x = 0$; $u = v = 0$; $T = T_{ambient}$ for inlet conditon $0 < y < H$; $x = L$; $P = 0$ for outlet condition.

As for the platform and heat sources, similar no-slip boundary conditions are also applied at the surfaces and detail descriptions are explained in Section 3. Thus, all the basic equations along with the necessary boundary conditions related to the flow domain given above are used in the present study.

3. Description of the model and computational technique

The model used in this simulation consists of an air chamber with the nozzle to a glass tunnel (test Section). The size of a heat source used is $2.72 \text{ cm} \times 2.72 \text{ cm}$. The tetrahedral elements are used in the present 2D analysis (see Fig. 1). Both heat sources are supplied with a heat flux of 4700 W/m^2 each for the heat transfer achieved at the heat source. In the model, the actual three-dimensional geometry of the experimental setup is simplified to a two-dimensional one as shown in Fig. 1. The two-dimensional computational model considers the vertical mid-plane through the experimental test section as illustrated

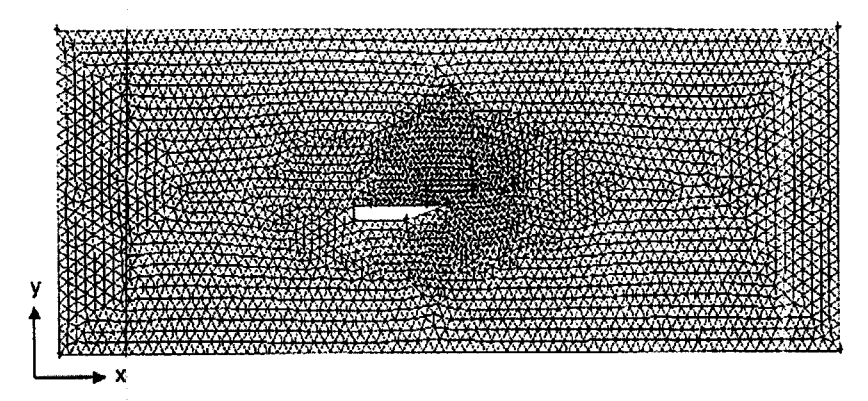


Fig. 1. Mesh generation using tetrahedral elements.

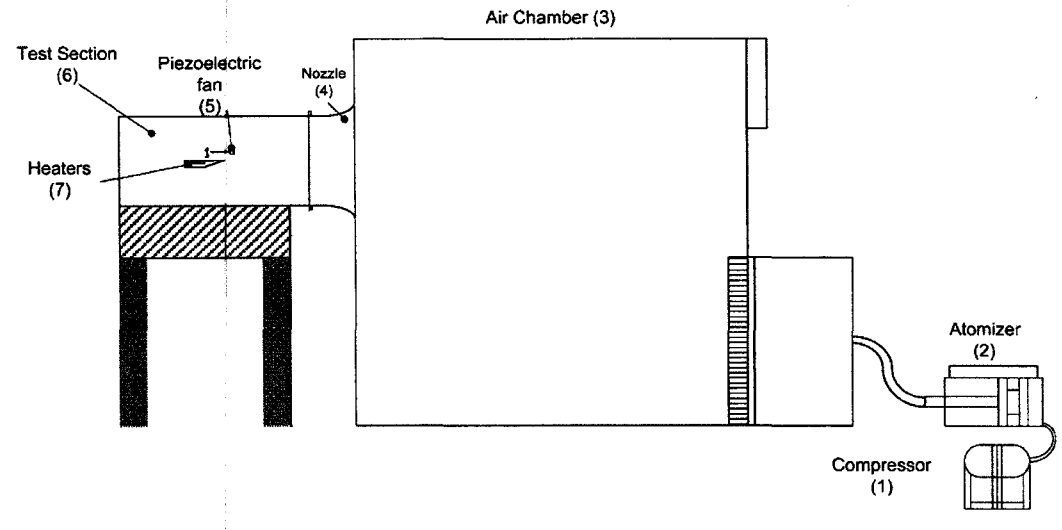


Fig. 2. The experimental setup.

in Fig. 2. Since gravity is normal to this two-dimensional plane, buoyancy effects are negligible and hence need not be included in the model.

The size of the computational domain is similar to those used in the experiments (25 cm×80 cm). The four sides of the enclosure shown in Fig. 1 are set as isothermal walls in the numerical model. The clamp of the piezoelectric fan is neglected and instead replaced by a simple adiabatic wall as shown. The fan boundary is modeled as a moving adiabatic wall whose location in time is set by a user-defined function in FLUENT. The fan is modeled as infinitesimally thin walls with no thermal conduction allowed through them. The left and right boundaries are set as inlet and outlet respectively.

The enclosure includes two in-line heat sources mounted horizontally embedded in the platform, as shown in Fig. 3. Corresponding to the heat dissipation from both heat sources, a uniform heat flux of

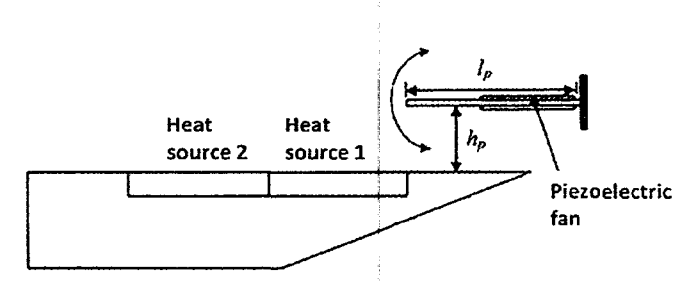


Fig. 3. Schematic of the piezoelectric fan and heat source arrangements.

4700 W/m² is applied to the exposed uninsulated wall of the heat source in the numerical model (as shown in Fig. 1). The other three walls of the heat source are considered to be adiabatic.

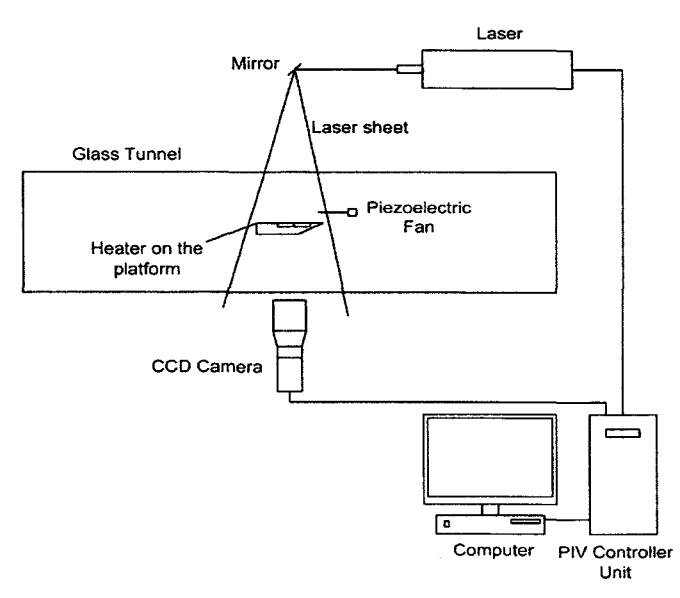


Fig. 4. Set-up of particle image velocimetry (PIV) system.

Table 1 Specifications of the piezoelectric fan under study

Specification	Valu e
Material	Aluminum
Fan size (cm)	$4.7 (l_P) \times 1.2 (w_P) \times 0.04 (t_P)$
Resonant frequency (Hz)	115
Power consumption of fan and circuit (mW)	42
Blade swing, peak to peak (cm)	0.95
Fan weight (gm)	2.0

The assumptions in the two-dimensional computational model include laminar, incompressible flow with no buoyancy or radiation contributions. First-order upwind discretization is used both for momentum and energy, with the SIMPLE scheme used for pressure-velocity coupling. Although a second-order scheme would yield better accuracy, these schemes were not explored due to constraints on computational time. In order to capture the flow field correctly, a very small time step is required. For all the results presented here, a time step of 1.0×10^{-4} s was used. Thus, 100 steps in time were needed for one cycle of fan vibration.

The heat transfer coefficient is calculated based on the average fluid temperature and the average heat source surface temperature. The total duration of the simulation is selected such that the heat transfer coefficient has reached a steady value during this period. This took 4000 time steps, which corresponds to approximately 0.5 h of computation time per each case on a Pentium D processor (each 2.8 GHz) computer with 0.512 GB of memory. In this study, the coarser mesh with 13,189 nodes, and run with timestep size of 0.0001 s has been used for Case A. The results presented are obtained using a finer mesh with 15,575 nodes, with same time step of 0.0001 s (100 time steps per cycle of fan vibration).

4. Experimental apparatus and test section

Fig. 2 shows the experimental apparatus used in the present study. The compressor (1) is used to atomize the corn oil particles in an atomizer (2). This oil particle is used as the seeding for the particle image velocimetry system. The air chamber (3) with the dimension of $1.5 \times 1.5 \times 1.5 \text{ m}^3$ and which has a test section (6) size of 25 cm (H)×6 cm (W)×80 cm (W) made of glass has been fabricated for the study. The oil particles are settled in the air chamber and slowly drawn into the glass tunnel (test Section).

Fig. 3 illustrates the arrangement of heaters. The heat source is supplied by the heater (7) and the piezoelectric fan (5). The platform of heat sources (7) is made from wood which serves as a thermal insulator. Angles of 45° at leading and trailing edges are made to avoid the flow separation. The heat loss through the platform is assumed negligible. The heat source surface temperature is measured by the thermocouple which is soldered underneath the heat source. Steady state condition is reached after 8 h of the heating.

A Dantec 2D particle image velocimetry (PIV) system (Fig. 4) has been used to measure the velocity induced by the piezoelectric fan. The piezoelectric fan under study is obtained from Piezo-System Inc. and its specifications are given in Table 1. The movement of the seeding particle (atomization of corn oil) has been captured by a CCD camera which is synchronized with a double pulse YAG laser and controlled by the computer via a PIV controller unit. The induced velocity is calculated by the software provided by the system.

5. Results and discussion

Fig. 5 shows the velocity vectors for case A, where the piezoelectric fan is located $h_{\rm p}/l_{\rm p}$ =0.13 from the heat source. The vectors are measured at 2 different times when the fan swings downward (Fig. 5a) and upward (Fig. 5b). The piezoelectric fan has been adjusted to the

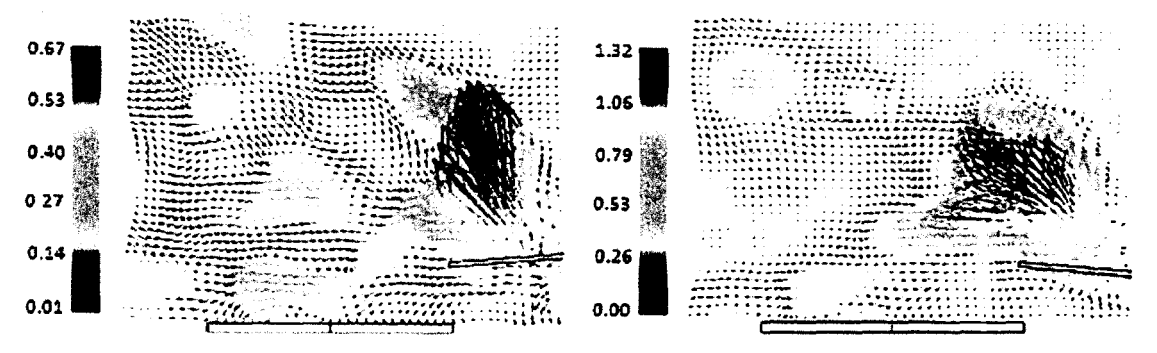


Fig. 5. Velocity vectors for Case A $(h_p/l_p=0.13)$ induced by the piezofan.

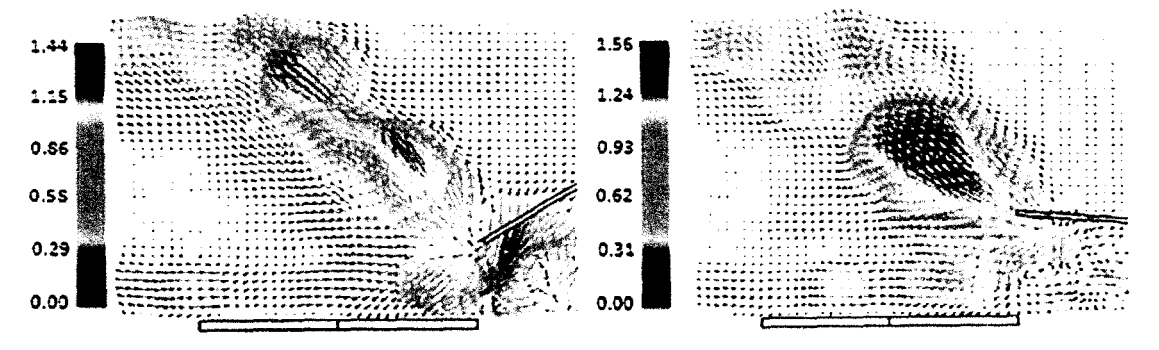


Fig. 6. Velocity vectors for Case B ($h_{\rm p}/l_{\rm p}$ =0.23) induced by the piezofan.

resonance mode, when it operates the velocity is induced very much depending on the movement of the piezofan. There is more induced velocity when the fan swings in an upward direction, and it is observed that there is a higher volume of flow on the top surface of heat sources, where the maximum velocity reaches about 0.8 m/s. Whereas, when the fan swings downward less volume of flow passes through on the top surface of the heat source. The maximum velocity reaches 0.4 m/s.

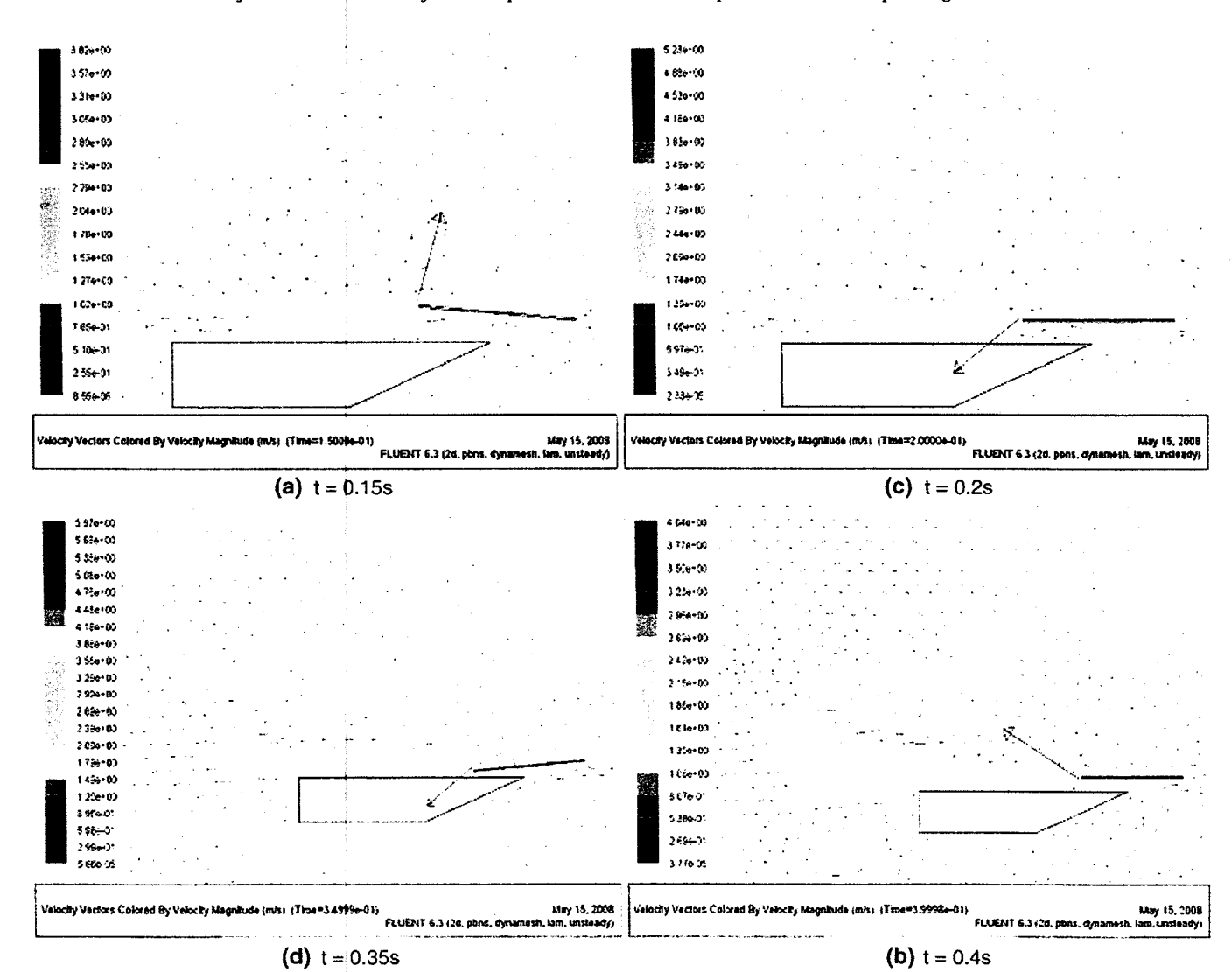
The velocity vectors for case B are shown in Fig. 6 when the location of the piezofan is located slightly higher at h_p/l_p =0.23 from the heat sources. The velocity vectors of higher magnitude are induced on the top surface of heat sources where the maximum velocity reaches up to 1.1 m/s especially for when the piezofan swings upward. For when the piezofan swings downward, the velocity vectors slightly lower where the maximum velocity is about 1.0 m/s. Thus, one can conclude that the heat transfer will be higher for case B compared to case A since the flow velocity increases with h_p/l_p on the heat source.

Fig. 7a through d illustrate the velocity vectors for four different time intervals (e.g. t=0.15 s, 0.2 s, 0.35 s and 0.4 s) for case A. These show that the induced flow by a piezoelectric fan is an unsteady phenomenon. At these time intervals, the position of the fan changes with time when the fan is swinging either in a downward or upward direction. The results also show that the velocity vector induced is very much dependent on

the fan swinging. The induced velocity is higher when the fan swings downward on the heat source's surface. The magnitude of velocity is the highest at t=0.4 s where the velocity is about 2.0 m/s for fan swinging upward compared to the downward swinging, when the maximum velocity is about 1.2 m/s on the heat source surface. Moreover the vortex generated by the induced flow using a piezofan is observed and the vortex is slowly moved forward pushed by air flow at higher time intervals. Double vortices are clearly observed at t=0.35 s and 0.4 s downstream of the platform (see Fig. 7c and d).

Fig. 8a through d are the velocity vectors for case B $(h_p/l_p=0.23)$. Similar results are observed as in Fig. 7a–d, in terms of flow patterns for different positionings of the piezofan. However, the flow velocity induced by the piezofan at this height is very much better in terms of magnitude and flow distribution on the heat source surface compared to $h_p/l_p=0.13$. The maximum velocity increases about 20% compared to case A. The results illustrate that the piezofan with case B will provide better flow performance on the heat source surfaces and will provide a better heat transfer coefficient compared to case A.

Fig. 9a through d show the temperature contour for case A at different time intervals. The heat from the heat source surface is slowly removed to downstream by the air flow that is induced by the piezofan. The temperature on the heat source decreases gradually since the piezoelectric fan is operating. The contours illustrate that the



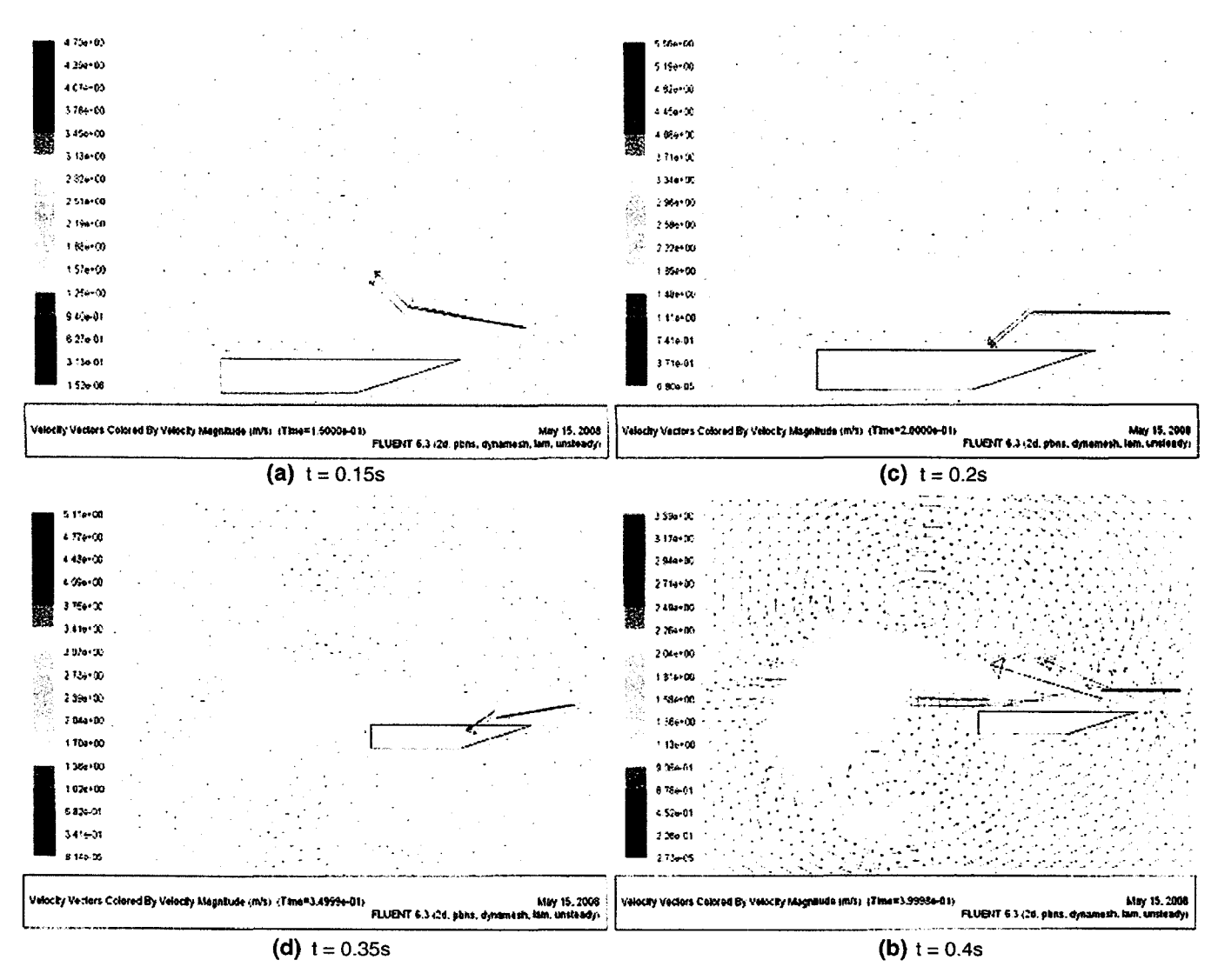


Fig. 8. (a)-(d) Velocity magnitude for Case B at different time intervals.

piezofan reduces the temperature on the heat source surface as much as 23 °C at t=0.4 s. The double vortices of temperature can also be observed in the figures at t=0.35 s and 0.4 s. Furthermore the temperature on the heat source surface reduces and temperature variation is small (less than 10%) for t=0.35 s and t=0.4 s. Thus, in the present study, it is assumed the heat convection has reached a steady state condition at t=0.35 s.

In case B $(h_p/l_p=0.23)$, Fig. 10a through d show a similar pattern with case A $(h_p/l_p=0.13)$. However, the heat transfer from the heat source to the air stream is higher compared to case A. The temperature on the heat source reduces with time, and just after t=0.35 s the temperature is almost constant. The figures show that the heat is slowly removed from the heat sources to downstream of the platform. The contour also shows that the temperature distribution has reached a steady condition at t=0.35 s, since a similar temperature contour at t=0.4 s is observed. The contours illustrate that the piezofan reduces the temperature on the heat source surface as much as 25.1 °C. It can be concluded that the height of the piezofan has influenced the temperature drop on the heat source surface.

Two different heights of the piezoelectric fan are studied in the present work. The velocity vectors indicated comparatively more air flow over the heat sources for case B hence better heat convection performance. The results also show that the location of the piezo-

electric fan with h_p/l_p =0.23 has the bigger profile. Fig. 11 shows that the average heat convection coefficient for case B is 45.14 W/m² K and about 4% higher compared to case A. The heat transfer coefficient is calculated based on the average of heat source surface temperature using the equation:

$$h_{\text{ave}} = \frac{q}{(T_{\text{ave}} - T_{\infty})} \tag{5}$$

The results generally show that the piezoelectric fan height of $h_{\rm p}/l_{\rm p}$ =0.23 above the heat source has a better performance in thermal management. The results predicted by the CFD software are found in good agreement with the experimental values (the difference is about 11% only).

6. Conclusion

The experimental and simulation studies have been made for a piezoelectric fan for two different heights above the heat source. The piezofan manages to reduce the temperature of the heat source by as much as 68.9 °C. The piezoelectric fan operation is modeled using the dynamic meshes coupled with a harmonic motion in FLUENT 6.2.3 software and has predicted the induced flow and heat convection

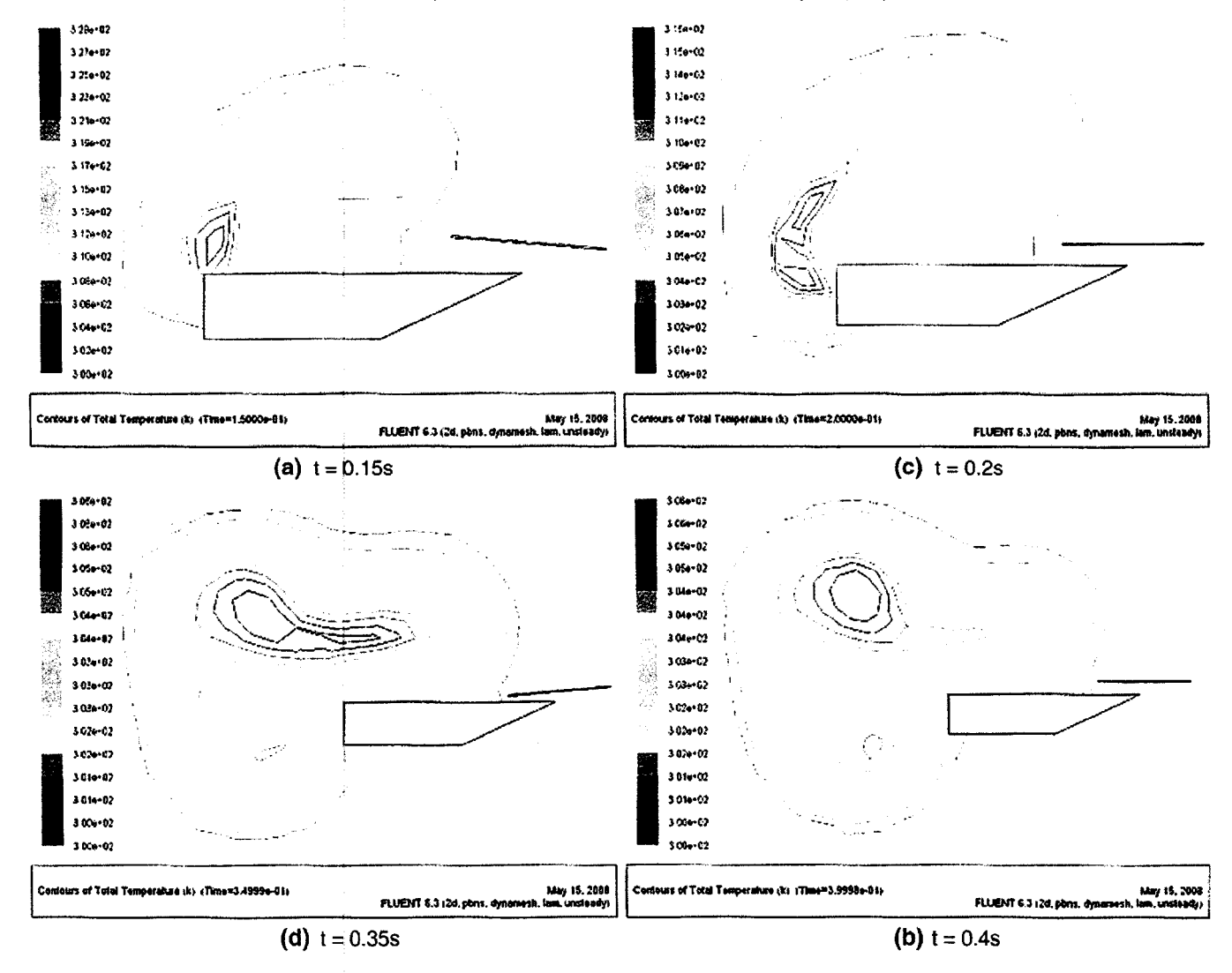


Fig. 9. (a)-(d) Temperature contours for Case A at different time intervals.

involved. The results showed that the height of the piezofan from the heat source has influenced the heat transfer coefficient. A height of h_p/l_p =0.23 has increased about 4% in heat transfer coefficient compared to h_p/l_p =0.13. The piezofan swinging is an unsteady phenomenon and influences flow behavior on the heat source surface. The heat transfer coefficient predicted by CFD simulation has shown good agreement with the experimental data with a difference of 11%.

References

- [1] P.I. Ro, B.G. Loh, Feasibility of using flexure waves as a cooling mechanism, IEEE Transactions on Industrial Electronics 48 (1) (2001) 143–149.
- [2] E.F. Crawly, D.J. Luis, Use of piezoelectric actuator as elements of intelligent structures, AIAA Journal 25 (1987) 1373–1385.
- [3] T. Wu, P.I. Ro, A.I. Kingon, J.F. Mulling, Piezoelectric resonating structures for microelectronic cooling, Smart Materials and Structures 12 (2003) 181–187.
- [4] B.G. Loh, S. Hyun, P.I. Ro, C. Kleinstreuer, Acoustic streaming induced by ultrasonic flexural vibrations and associated enhancement of convective heat transfer, Journal of Acoustics Society of America 111 (2002) 875–883.

- [5] J.H. Yoo, J.J. Hong, W. Cao, Piezoelectric ceramic bimorph coupled to thin metal plate as cooling fan for electronic devices, Sensor and Actuators, A, Physical 79 (2000) 8-12.
- [6] R.R. Schmidt, Local and average transfer coefficients on a vertical surface due to convection from a piezoelectric fan, Proc. ITHERM, Washington, D.C., 1994, pp. 41–49.
- [7] T. Acikalin, A. Raman, S.V. Garimella, A. Raman, Two dimensional streaming flows induced by resonating thin beam, Journal of Acoustics Society of America 114 (2003) 1785–1795.
- [8] S.M. Wait, T. Acikalin, S.V. Garimella, A. Raman, Piezoelectric fans for the thermal management of electronics, Proc. Sixth ISHMT/ASME Heat and Mass Transfer Conference, Kalpakkam, India, January 5-7 2004, pp. 447-452, Paper No. HMT-2004-C76.
- [9] T. Acikalin, S.V. Garimella, A. Raman, J. Petroski, Characterization and optimization of the thermal performance of miniature piezoelectric fans, International Journal of Heat and Fluid Flow 28 (2007) 806–820.
- [10] M.V. Ramana, I.P. Almanar, M.Z. Abdullah, Z. Mohd Ripin, K.N. Seetharamu, Design and optimization of piezoelectric fans for cooling of microelectronic devices, International Journal of Microelectronic and Packaging Society 4 (3) (2007) 121–129.

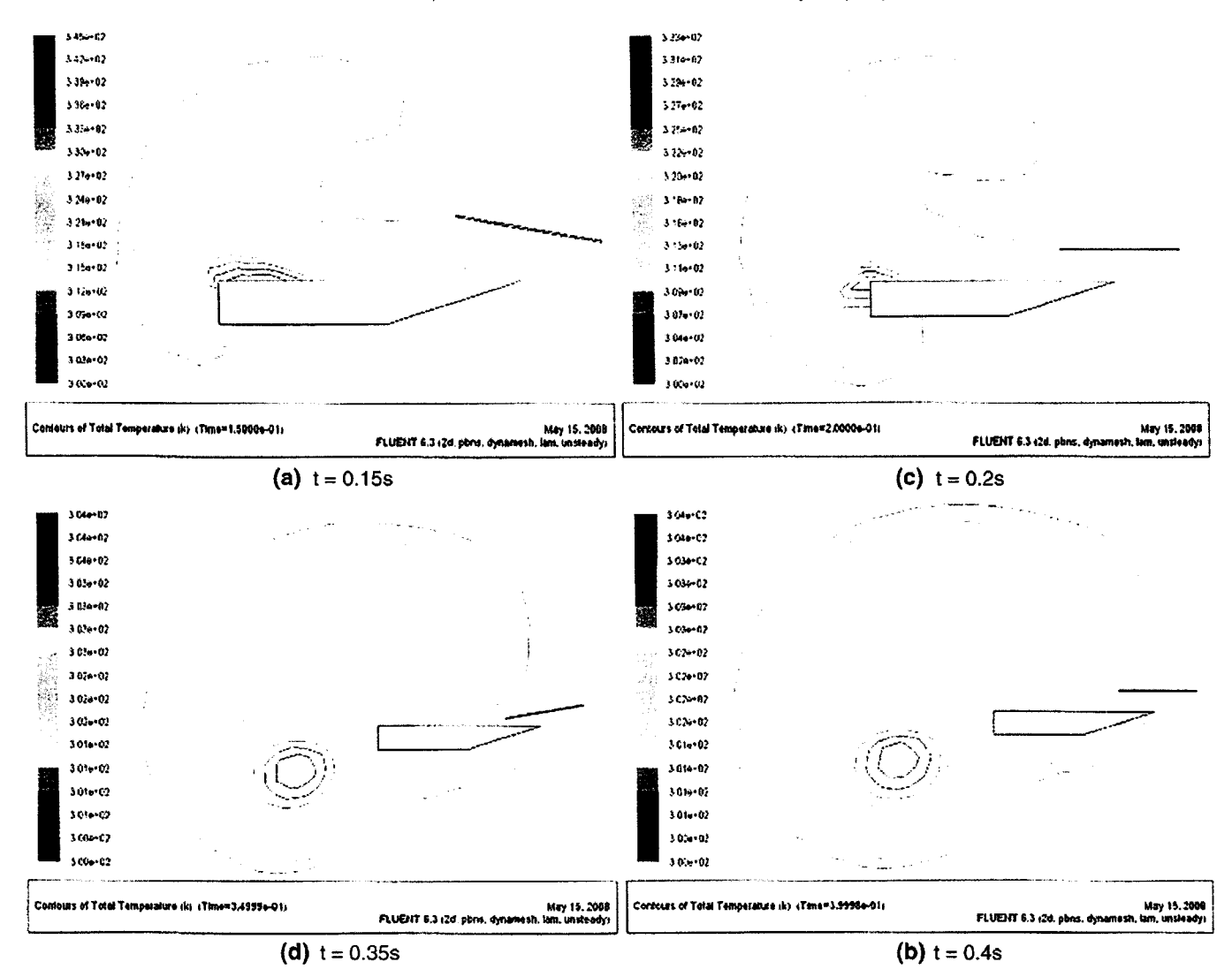


Fig. 10. (a)-(d) Temperature contours for Case B at different time intervals.

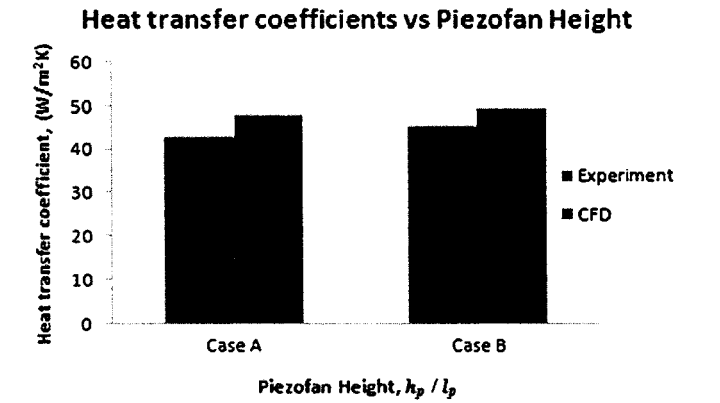


Fig. 11. Heat transfer coefficients for cases A and B.

Acceptance of your manuscript

1 Messages

Acceptance of your manuscript

Fri Nov 12 2010 16:55:36 GMT+0800 (Malay Peninsula Standard Time)

From: nuyucel@gazi.edu.tr
To: mkhalil@eng.usm.my
Attachments: Copyright Form.pdf (12.1KB)

12/11/2010

Dear Abdullah;

Your manuscript titled 'HEAT TRANSFER ENHANCEMENT USING PIEZOELECTRIC FAN IN ELECTRONIC COOLING - EXPERIMENTAL AND NUMERICAL OBSERVATIONS' (Manuscript No:2010_40) has been accepted for publication in Journal of Thermal Science and Technology. Your manuscript will be published in volume 32-1 in April-2012. Please, fill out the attached Copyright Agreement Form and sent it.

Yours Sincerely.

Prof. Dr. Nuri Yucel Editor-in-chief Journal of Thermal Science and Technology

G. Ü. Mühendislik-Mimarlık Fakültesi Makina Mühendisliği Bölümü 06570 Maltepe, Ankara

e-posta: nuyucel@gazi.edu,tr Tel: (312) 582 3422

HEAT TRANSFER ENHANCEMENT USING PIEZOELECTRIC FAN IN ELECTRONIC COOLING - EXPERIMENTAL AND NUMERICAL OBSERVATIONS

M. K. Abdullah^{*}, B. H. Murni, M. Z. Abdullah, M. A. Mujeebu, F. Hussin, H. Yusoff, N.C. Ismail, K. A. Ahmad, and Z. Mohd Ripin

Aerodynamics and Advanced Cooling Laboratory, School of Mechanical and Aerospace Engineering Engineering Campus, Universiti Sains Malaysia 14300 Nibong Tebal, Penang, Malaysia

*Corresponding Author - Email: mkhalil@eng.usm.my Phone: 006045996398 Fax : 006045941025

Abstract

Piezoelectric fan is an innovative design and feasible solution to remove heat from microelectronic systems for portable electronic products. It is small in size, has low power consumption and minimal noise. This paper presents experimental and computational investigations of incompressible three-dimensional streaming flows induced by piezoelectric fan and the associated heat transfer enhancement, on a Plastic Leaded Chip Carrier (PLCC) package. Piezoelectric fan (piezofan) is arranged at two different heights normal to the heat source surface (in each case, the normalized gap $\delta = G/l_p$) and tested for its performance, compared to the base case (natural convection or no fan). The flow field is observed and captured by means of a particle image velocimetry (PIV) system. The heat transfer coefficient in each case is also computed. The finite volume based computational fluid dynamics package, FLUENT 6.3.2 is used to investigate the heat transfer coefficient and the flow fields using a dynamic mesh option. The result shows that the piezofan yields significant improvement in heat transfer, and a normalized gap of 0.106 is offered a better cooling compared to the 0.0604. The experimental results are in good agreement with the predicted results.

Keywords: Electronic cooling; PLCC, piezofan; heat transfer coefficient

Nomenclature

\boldsymbol{A}	Frequency dependent amplitude	Q	Heater power (W)
A_h	Area of heater surface (m ²)	S	Source term
F	Body force (m/s ²)	T	Temperature (K)
g	Gravitational acceleration (m/s²)	T_h	Heater temperature (K)
G	Height of piezofan from heat source (m)	T_a	Ambient temperature (K)
H	Height of test section (m)	u, v, w	Velocity component (m/s)

1 · · · · · · · · · · · · · · · · · · ·	ty vector
h_{ave} Average of convection coefficient u_g Grid v	elocity
(W/m ⁻ K)	•
7.01	ol volume
	t of resolution
	of test section (m)
l_p Length of piezofan (m) w Blade	position (m)
	velocity (rad/s)
P Pressure (Pa) w_P Width	of piezofan (m)
t Time (s) x, y, z Space	coordinates
t_p Piezofan thickness (m)	
Greek symbols	
Γ Diffusion coefficient Φ General equation	
	stress (N/m ²)
ω Angular velocity (rad/s) β Eigen	, ,
δ Normalized gap	
Subscripts	
a Ambient hor Horizon	
ave Average i, j, k Coord	inate indices
	inate indices an

1. Introduction

The continuing increase of power densities in microelectronics and simultaneous drive to reduce the size and weight of electronic products have led to crucial thermal management issues in the industry. Inappropriate thermal management of the electronic device degrades its performance significantly (Sparrow et al. 1982). The conventional cooling devices such as rotary fan and heat sink are popular in the current market. Ironically, they are not so suitable for portable devices such as laptop and mobile phone owing to space and power limitations (Sparrow et al. 1983). Plastic Leaded Chip Carrier (PLCC) arrangement is an alternative that can be used in portable electronic devices to improve thermal performance and hence the electronic performance (Mohamed et al. 2008).

However, a PLCC alone cannot resolve the issue since it also requires a cooling mechanism. One of the viable solutions is piezoelectric fan, hereafter named as piezofan. It is an innovative design which is gaining acceptance as feasible solution for portable electronic products (Buermann et al. 2002). Piezofan generally consists of a patch of piezoelectric material bonded to a flexible cantilever blade. An alternating voltage is applied to the piezoelectric patch; it expands and contracts in the lengthwise direction, causing bending moments at both ends of the patch. These moments drive the attached blade to oscillate at the same frequency (Kim et al., 2005). These piezofans use very little power and can be developed to meet various

geometric constraints for many applications (Kimber and Garimella, 2009). It clearly enhances the heat transfer when compared to natural convection. This technology is desirable because it is noiseless at the frequencies of operation, compact, light in weight and durable (Garimella et al., 2006).

A number of studies on piezofan were reported in the literature. Toda and Osaka (1979) &1981) found that placing a piezoelectric fan on either side of a power transistor panel of a television receiver resulted in temperature reductions of 17°C and 5°C on the panel surface and inner space respectively. A numerical model was developed by Acikalin and Garimella (2009), to analyze the operation of a piezoelectrically actuated cantilever vibrating close to a heated surface. They found that the length as well as the frequency of the piezofan could alter its heat transfer characteristics. Yoo et al. (2000) fabricated various kinds of piezofans and characterized the induced flow for application to electronic cooling apparatus. It was found that the most effective fan was the one made from a phosphor bronze shim and with PZT in a bimorph configuration where it shows a tip displacement of 35.5 mm and a produced wind velocity of 3.1 m/s driven by a 220 V, 60 Hz power source. Kwon et al. (2005) studied the vibration characteristic of piezoelectric vibration actuator. The geometric size of the vibration device has decided the resonance frequency dependency according to the change of length, width, thickness and dummy weight of the vibration device where energy conversion efficiency could become the maximum. The performance of piezofan operating at higher resonance modes was studied in detail by Wait et al. (2007) who showed that certain advantages of piezofan operation at higher resonance modes were offset by increased power consumption and decreased fluid flow. Abdullah et al. (2008, 2009) investigated the effect of piezofan height on the performance of piezofan both numerically and experimentally. They found that, the heat transfer coefficient was significantly affected by the height of piezofan from the heat source. The piezofan swinging was observed to be an unsteady phenomenon and influenced the flow behavior on the heat source surface. Liu et al. (2009) studied the influence of horizontal and vertical arrangements of piezofans, and found that the heat transfer augmentation of the piezofan was resulted from the entrained airflow during each oscillation cycle, and the jet-like air stream at the fan tip. The heat transfer performance for vertical arrangement showed a symmetrical distribution and peaked at the center region whereas the horizontal arrangement possessed an asymmetrical distribution and showed an early peak at x/L = 0.25. It was also found that the heat transfer performance for horizontal arrangement was not necessarily lower than that of vertical one.

In the current study, the potential offered by piezofan for the thermal management of PLCC package is assessed experimentally as well as numerically. As far as the authors are aware, the previous works focused only on two-dimensional simulations, owing to the complexity of displacement of the vibrating blade and the computer-intensive nature of the numerical model. In the present study, a three-dimensional modeling is performed using FLUENT 6.3., in order to have more realistic analysis of fluid and temperature fields during piezofan operation. Two different experimental configurations are set up in order to study the effect of piezofans on the heat transfer from a small, vertically mounted heat source which duplicates the PLCC. Experiments are conducted for two different gaps of piezofan, and the results are compared with the base case (no fan condition). Particle image velocimetry (PIV) technique is used to make the flow measurements.

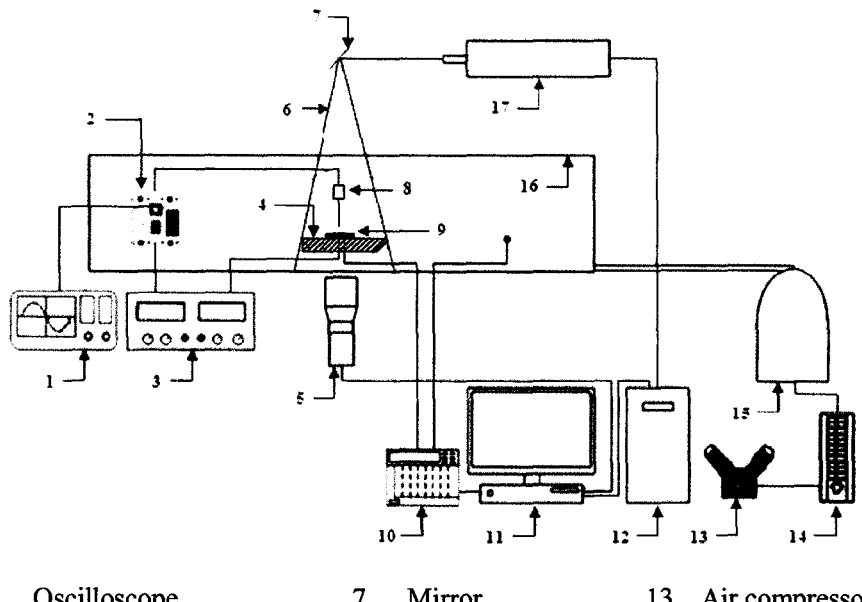
2. Experimental apparatus and procedure

The flow visualization experiments are conducted to gain insight into the flow induced by the piezofan. The schematic of experimental setup used in the present study is shown in Fig. 1. A clear glass tunnel of size 0.25m (H) × 0.06m (W) × 0.8m (L) is constructed to act as the test section. The electronic chip (PLCC) is replicated as a heater with constant heat flux of 4.6 kW/m^2 controlled by a direct current (DC) power supply (GW instek GPS2303). The stainless steel heater of dimension $0.03m \times 0.03m \times 0.003m$, is embedded onto a wooden platform which also serves as thermal insulator. The heater along with the piezofan is housed by the glass tunnel. The heater and ambient air temperatures are measured at one minute interval, by thermocouples linked to computer by means of a data logger (ADVANTECH DAQ System).

Table 1 summarizes the specifications of the piezofan which is arranged vertically at two different normalized gaps (δ) defined by, $\delta = G/l_p$ (G and l_p are shown in Fig.2). The piezofan is operated in the first mode condition and excited at its resonance in order to achieve the maximum vibration amplitude. DC to AC inverter circuit (Kit inverter) is used to facilitate oscillating drive signal according to the resonance frequency of the piezofan; the applied voltage and resonance frequency are measured by an oscilloscope (Agilent Technologies DSO3062-60MHz). Seeding for the PIV system is facilitated by atomized corn oil particles slowly drawn into the glass tunnel. The air flow is supplied by a reciprocating air compressor, and regulated by an air flow-meter. The nominal diameter of the corn oil particle is 1 to 2 μ m in size (Melling, 1997). The leading edge of the wooden platform is made inclined at an angle 45° in order to avoid the flow separation.

Table 1 Specifications of the piezofan (Piezo Systems Inc., USA)

Specification	Value
Material	Stainless steel
Piezofan size (m)	$0.047 (l_P) \times 0.012 (w_P) \times 0.0004 (t_P)$
Piezofan height without patch (m)	$0.023 (l_u)$
Resonant frequency (Hz)	115
Power consumption of piezofan and circuit (mW)	42
Blade swing, peak to peak (m)	0.0098
Piezofan weight (kg)	0.002



1	Oscilloscope	7	Mirror	13	Air compressor
2	Kit inverter	8	Piezofan	14	Air controller
3	Dual digital power supply	9	Heater	15	Atomizer
4	Wood platform	10	Temperature DAQ	16	Glass tunnel
5	CCD camera	11	Personal computer	17	Laser
6	Laser sheet	12	Laser controller		

Fig. 1 Schematic of the experimental setup

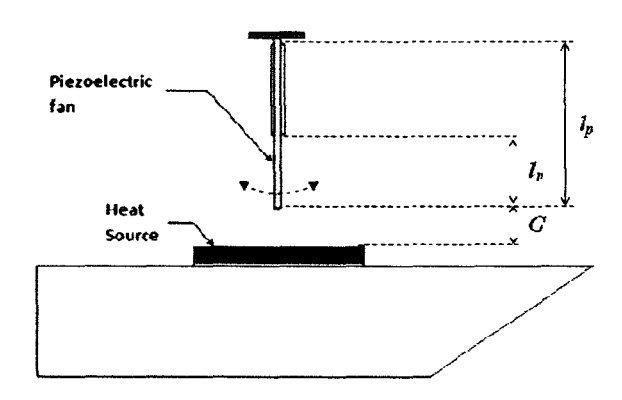


Fig. 2 Illustration of gap G, piezofan height l_p , and un-patched length of piezofan l_u

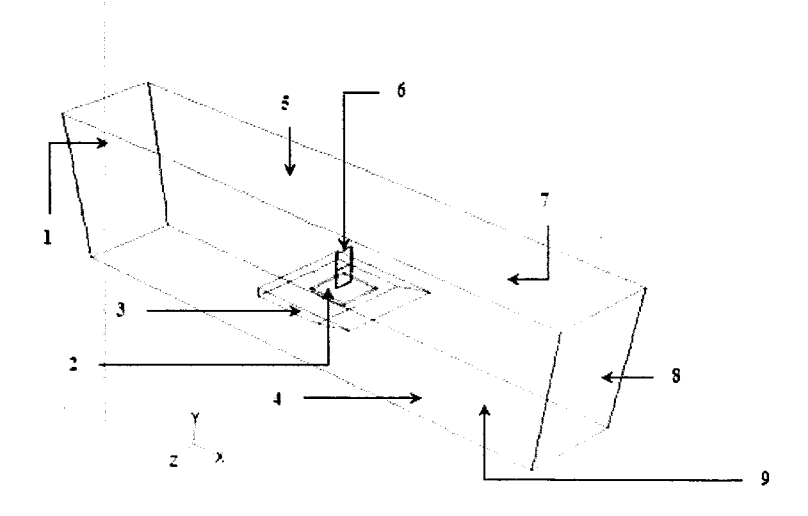
A Dantec 2D particle image velocimetry (PIV) system has been used to measure the velocity induced by the piezofan. The CCD camera in conjunction with a double pulse Nd: YAG laser captures the flow field induced by the piezofan and the images are stored in the computer via a PIV controller unit. A section of the flow was illuminated with long exposure with light sheet generated by a 300mW Argon-ion laser and the beam reflected 90° by a mirror

and the narrow sheet of light that is produced through the convex lens and cylindrical lens. The thickness of the laser sheet illuminating the flow field was approximately 1.0 mm.

A digital video camera (Digital monochrome progressive scan camera; Flowsense M2 8bits) with a resolution of $1600 \ (h_{hor}) \times 1186 \ (v_{ver})$ pixels was used to record of two sequence of frame continuously with 4μ second for each frame. Live feedback of the images was displayed on a screen monitor connected to the video camera. Selected scene or sequence images were stored in the computer by using FlowManager software. It also offered two-frame cross-correlation technique to calculate the raw displacement vector field from the particle image velocity data. In the image processing, 64×64 pixels rectangular effective interrogation windows were used. Velocity vectors of the flow were calculated from this displacement vector field.

3. Simulation setup

The physical model for simulation is in accordance with the experimental setup (but size is reduced to one third), which contains the glass tunnel, heater, wood platform and piezofan as shown in Fig. 3. The four sides of the enclosure and wood platform are set as isothermal walls in the numerical model. A uniform heat flux of 4.6 kW/m^2 is imposed as the heat source. The left and right boundaries are set as pressure outlets, and the clamp of the piezofan is neglected. The blade (piezofan) swinging phenomena is set to move according to the simple harmonic vibration equations (5) - (8) and its position is calculated accordingly, at each time step. This boundary is modeled as a moving adiabatic wall whose location in time is set by a user-defined function (UDF) in C language, with no thermal conduction allowed through it.



- 1 Pressure outlet-1 4 Bottom wall 7 Left wall
- 2 Heater 5 Top wall 8 Pressure outlet-2
- 3 Wood platform 6 Piezofan 9 Right wall

Fig. 3: 3-D view of the simulation set-up

The hybrid elements are used in the present 3-D analysis. The flow is assumed as laminar and incompressible with no radiation contributions. First-order upwind discretization is used both for momentum and energy, and the SIMPLE scheme is used for pressure-velocity coupling. The convergence factors have been set to 1×10^{-3} and 1×10^{-6} for continuity and momentum, and energy respectively. The piezofan is set to vibrate at 115Hz corresponding to a period approximately 0.0087s for each case.

The heat transfer coefficient based on the average fluid and heat source surface temperatures is calculated. The total duration of the simulation is selected such that the heat transfer coefficient has reached a steady value during this period. This took 150,000 time steps, which corresponds to approximately 4 days of computation time per each case on a Pentium Quadcore processor (2.8 GHz) computer with 2 GB of memory.

The effects of time step and mesh size are investigated to verify that the solution is independent of those parameters. Time-step size of 0.0001s is chosen for all the cases to achieve numerical stability, with the mesh size around 180,000 elements (87 time steps per cycle of piezofan vibration). These values are arrived at after three attempts to check the trend and proximity with the profiles investigated. For instance, the trials are done by increasing the mesh elements and decreasing the time steps. However, a problem arose when the mesh elements were increased, due to the negative volume detected in FLUENT during analysis. This problem is typically found in dynamic meshing setup.

4. Numerical model

The flow is assumed as laminar and incompressible with no radiation contribution. The governing equations are chosen accordingly (FLUENT[©], 2006) along with the necessary boundary conditions of the flow domain, as follows.

The conservation of mass is:

$$\frac{\partial \rho}{\partial t} + \frac{\partial}{\partial x_i} (\rho u_i) = 0 \tag{1}$$

The conservation of momentum in *i*-th direction in an inertial (non-accelerating) reference frame is described by:

$$\frac{\partial}{\partial t}(\rho u_i) + \frac{\partial}{\partial x_j}(\rho u_i u_j) = -\frac{\partial P}{\partial x_i} + \frac{\partial \tau_{ij}}{\partial x_j}$$
(2)

where, P is the static pressure, and τ_{ij} is the viscous stress tensor.

The energy equation in terms of h (static enthalpy) can be written as,

$$\frac{\partial}{\partial t}(\rho h) + \frac{\partial}{\partial x_i}(\rho u_i h) = \frac{\partial}{\partial x_j}(k\frac{\partial T}{\partial x_i})$$
(3)

where T is the temperature and k is the thermal conductivity.

The integral form of the transport equation for a general scalar, Φ on an arbitrary control volume, V, on a moving mesh is written as,

$$\frac{d}{dt} \int_{V} \rho \Phi dV + \int_{\partial V} \rho \Phi (\vec{u} - \vec{u}_g) dA = \int_{\partial V} \Gamma \nabla \Phi dA + \int_{V} S_{\Phi} dV$$
(4)

where \vec{u} is the flow velocity vector and \vec{u}_g is the grid velocity of the moving meshes. The first and second terms on the left are the time derivative term and the convective term respectively. The terms on the right are the diffusive and the source terms. The term Γ represents the diffusion coefficient and S_{Φ} represents the source term of Φ . The term ∂V represents the boundary of the control volume V and dA is the area movement.

The resulting mode shapes of a piezofan can be approximated by the mode shape of a clamped-free blade. Assuming a sinusoidal driving, position of the blade is given by Meirovitch (1997):

$$w(x,t) = A \cdot \left[\frac{(\sin(\beta l_u) - \sinh(\beta l_u))(\sin(\beta x) - \sinh(\beta x))}{+(\cos(\beta l_u) + \cosh(\beta l_u))(\cos(\beta x) - \cosh(\beta x))} \cdot \sin(\omega t) \right] \cdot \sin(\omega t)$$
(5)

Differentiating this equation with respect to time gives the velocity of the blade,

$$\dot{w}(x,t) = A \cdot \left[\frac{(\sin(\beta l_u) - \sinh(\beta l_u))(\sin(\beta x) - \sinh(\beta x))}{+(\cos(\beta l_u) + \cosh(\beta l_u))(\cos(\beta x) - \cosh(\beta x))} \right] \cdot \omega \cos(\omega t)$$
(6)

Where β values can be calculated from the frequency equation

$$\cos(\beta l_u) \cdot \cosh(\beta l_u) = -1 \tag{7}$$

This must be solved numerically and yields infinity solutions of β . The β value corresponding to the first mode shape is

$$\beta = \frac{1.875}{l_u} \tag{8}$$

All surfaces of the enclosure, the platform, and the heat source surfaces, are identified as no-slip boundary conditions. Fig. 4 shows the position of the blade with respect to the phase

angle (product of angular velocity and time) for 0.0049m peak to peak deflection. Fig. 5 shows the velocity of the blade at different positions (x) with respect to time, in one cycle.

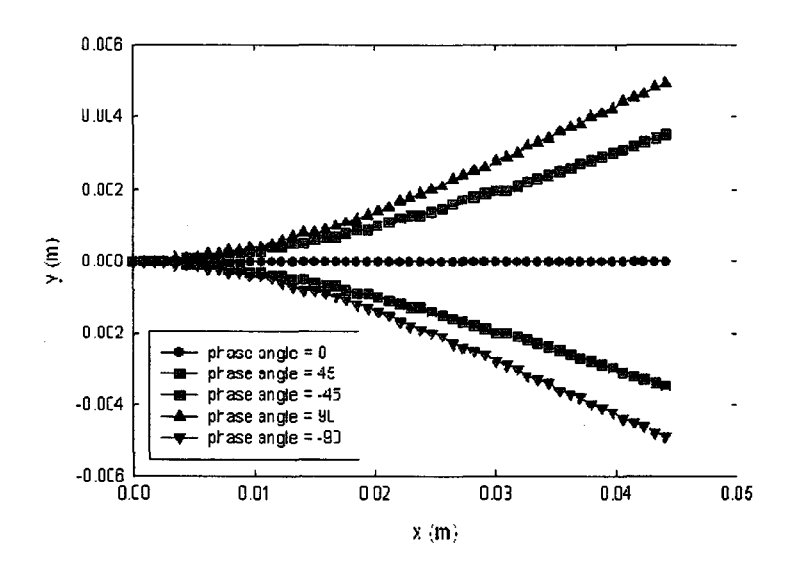


Fig. 4 Blade location with respect to time

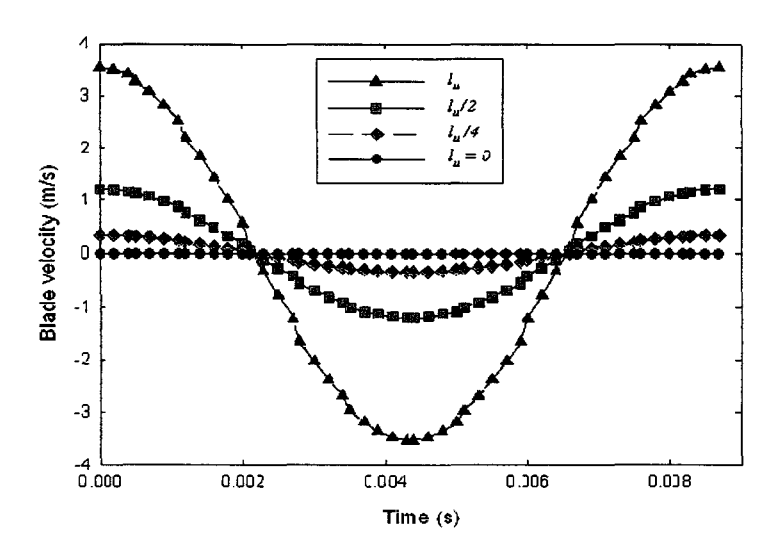


Fig. 5: Blade velocity at different positions of blade

5. Results and discussion

5.1 Flow profiles and velocity vectors

The goal of this study is to analyze the flow and heat transfer enhancement by using piezofan at for two different normalized gaps, $\delta = 0.064$ and $\delta = 0.106$. Fig. 6 shows the transient flow generated by the piezofan at $\delta = 0.106$. Creation of vortices due to piezofan deflection is visualized by the oil smoke particles. The results clearly show the development of vortices according to the swinging of the piezofan. When the piezofan swings left, the vortex is observed at the left side and when swings right, the left side vortex slowly disappears and emerges at the right side of the piezofan. Double vortices are developed on both the sides after the piezofan is moved to the neutral position.

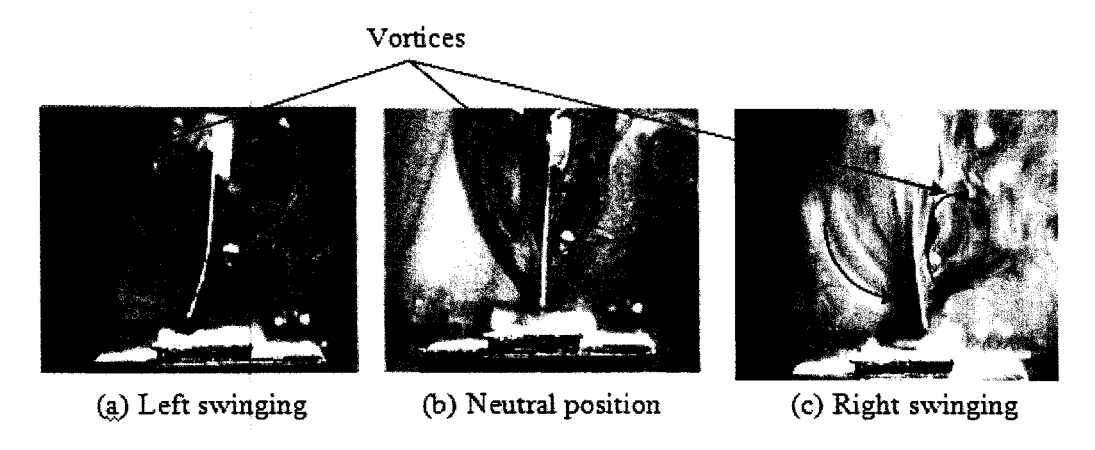


Fig. 6 Vortex formations at different swinging positions of the piezofan (for $\delta = 0.106$)

Fig. 7 shows the velocity vectors for $\delta = 0.0604$, measured at two different times i.e., when the piezofan swings towards right (Fig. 7a) and left (Fig. 7b). The piezofan is first adjusted to the resonance mode but when it operates the velocity is induced very much depending on its direction of movement. It is observed that more velocity is induced when the piezofan swings towards left, as evidenced by a higher volume of flow on the PLCC surface where the maximum velocity reaches about 1.5m/s. As the piezofan swings right less volume of flow is observed, with the velocity reaching to a maximum of 1.0m/s.

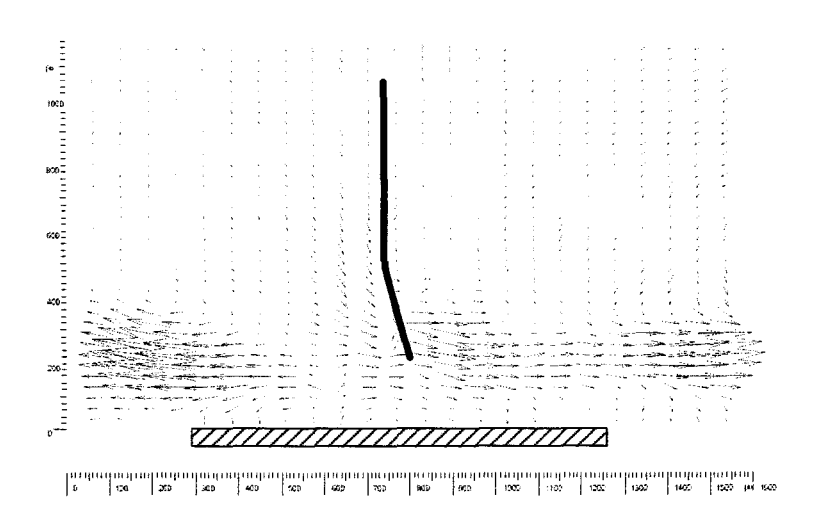


Fig. 7a Velocity vectors when piezofan swings right, at $\delta = 0.064$

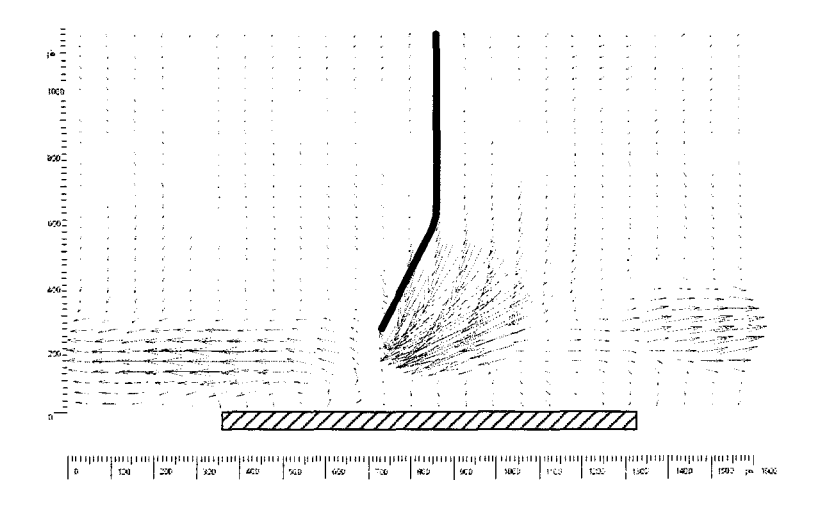


Fig. 7b Velocity vectors when piezofan swings left, at $\delta = 0.064$

Fig. 8a and Fig. 8b respectively show the velocity vectors for right and left swinging when the piezofan is located at $\delta = 0.106$. The velocity vectors of higher magnitude are induced on the top surface of the heat source where the maximum velocity reaches up to 2.0m/s especially when the piezofan swings towards left. For the rightward swing, the velocity is slightly lowered to about 1.7m/s. It is obvious that, as δ increases the induced volume of flow also increases which provide better convective heat transfer.

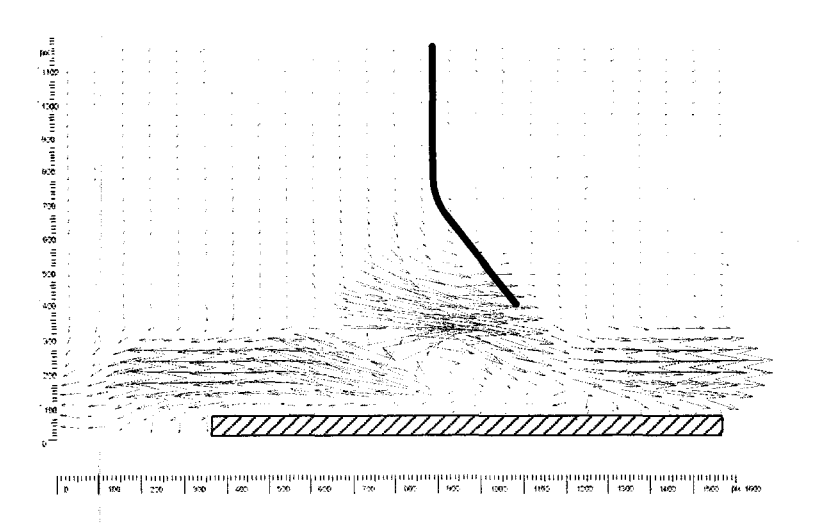


Fig. 8a Velocity vectors when piezofan swings right, at $\delta = 0.106$

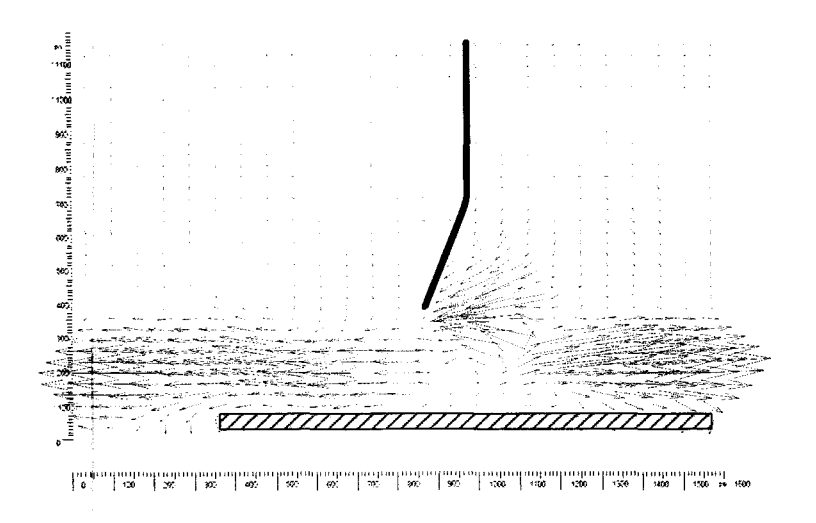


Fig. 8b Velocity vectors when piezofan swings left, at $\delta = 0.106\,$

Fig. 9 shows the velocity vectors when the piezofan is located at $\delta = 0.064$. The vectors are observed at three different piezofan positions namely initial (Fig. 9a), left swing (Fig. 9b) and right swing (Fig. 9c). Two regions of circulation are observed on either side of the vibrating piezofan, owing to its rapid swinging. The maximum velocity when the piezofan swings left is found to be1.52m/s and for right swing, it is 1.1m/s.

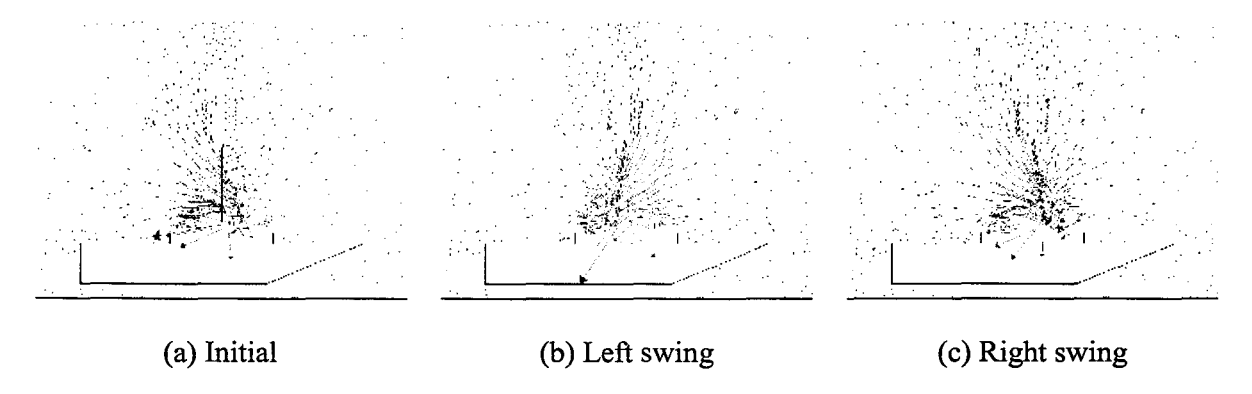


Fig. 9 Velocity vector for $\delta = 0.064$ at different piezofan positions

Figures 10a to 10c illustrate the velocity vectors for three different time intervals at $\delta = 0.106$. Here also, the results show that the velocity vector induced depends on the piezofan swinging. The induced velocity is higher when the piezofan swings left/rightwards on the PLCC surface. The double vortex generated by the induced flow using a piezofan is observed and the vortex moved downward to heat source surface. The maximum velocities during leftward and right ward swings are observed to be $2.05 \, \text{m/s}$ and $1.75 \, \text{m/s}$ respectively. In both the cases, the predicted velocities closely match the experimental results. Fig. 11 shows the comparison of predicted and experimental results of velocities during right and left swings of the piezofan and heat transfer coefficient, for 0.064 and 0.106.

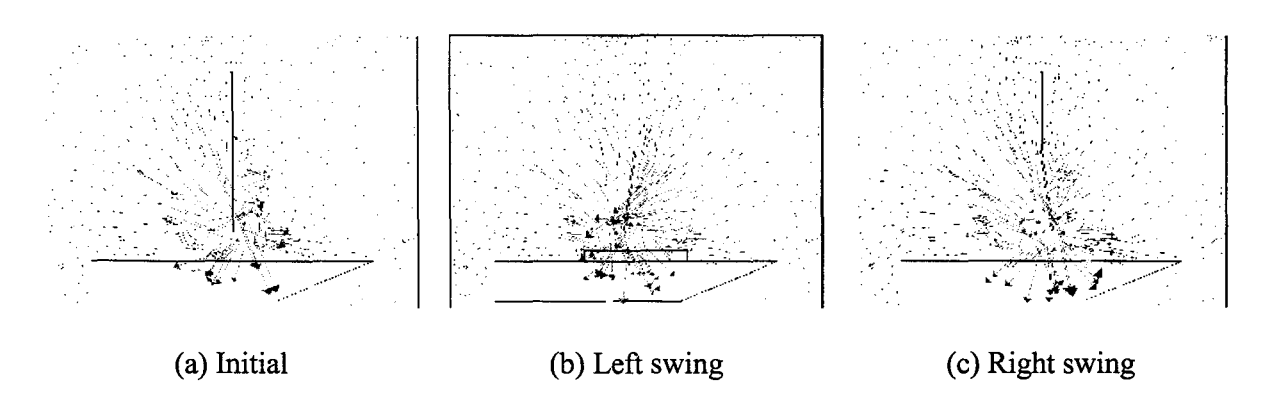


Fig. 10 Velocity vector for $\delta = 0.106$ at different time intervals

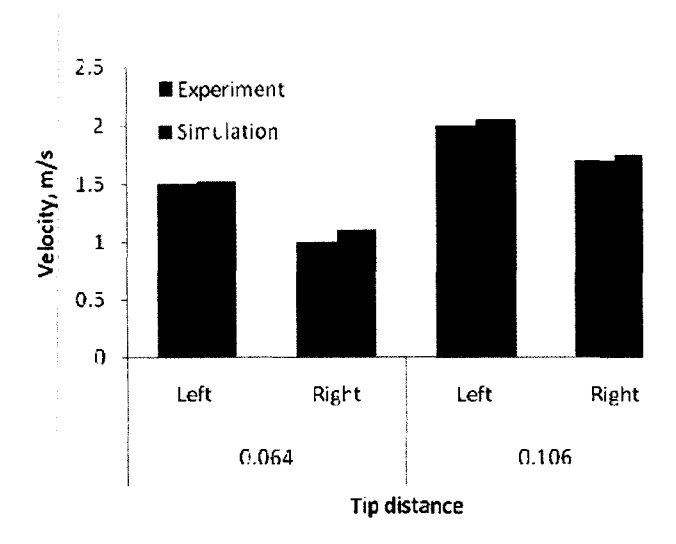


Fig. 11 Comparison of the computed maximum velocity with the experimental flow visualization

5.2 Heat transfer coefficient

At first, the temperature of the PLCC under natural convection (piezofan turned off) is set-up with a heat flux of 4.6kW/m^2 and maintained the same in all the experiments, without overheating the heat source. Whenever the temperatures in the heater showed no variation over a period (at t = 1800 s), it was assumed that steady-state operating conditions had been reached and it found to be 110°C . The heat transfer coefficient, h_{ave} is defined by using an energy balance between the power input and the heat removed from the surface of the heat source by convection, according to:

$$h_{ave} = \frac{Q}{A_h(T_h - T_a)} \tag{9}$$

where q is the power input to the heat source, A_h is the exposed surface area of the heater block. T_a is the temperatures from thermocouples used to measure the air temperature over the test section at different locations. Another thermocouple was used to monitor the temperature of the heat source (T_h) .

The piezofan is then turned on at t=3600s and the system was allowed to reach new steady-state temperatures for the heat source and surrounding air at the same input power, and the new heat transfer coefficient was calculated. The new steady state is reached at t=5100s, for both the cases. The piezofan is seen to cause a reduction in the heat source temperature from 110° C to 80° C and 60° C for $\delta=0.064$ and $\delta=0.106$ respectively. The temperature drop for the two different piezoelectric piezofan gap studied are plotted in Fig. 12. It is apparent that the heat removal rate is maximum at $\delta=0.106$, where there is 168% increase in the heat transfer coefficient, relative to the base case; for $\delta=0.064$, it is limited to only 61%. This is because, at $\delta=0.106$, the piezofan provides more air flow around the PLCC, compared to $\delta=0.064$.

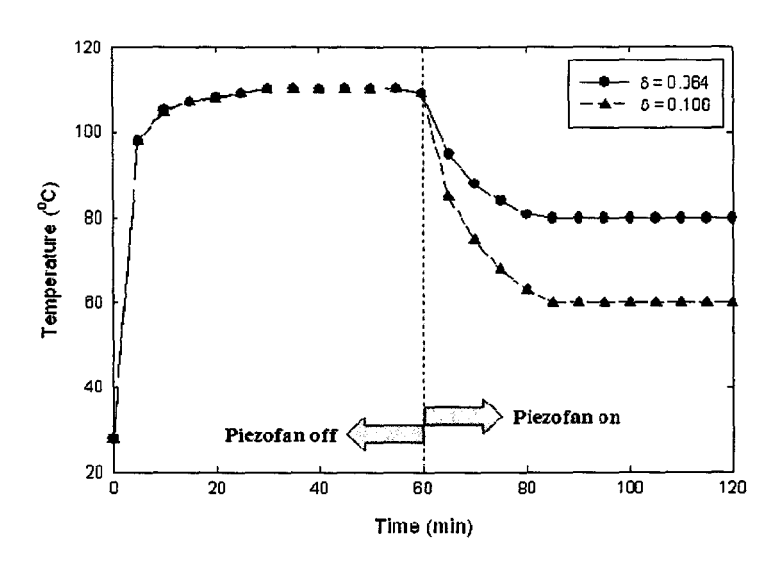


Fig. 12 Effect of non-dimensional gap, δ on PLCC surface temperature

Fig. 13 shows the temperature contours at different piezofan positions for $\delta = 0.064$ and 0.106 respectively. The heat from the heat source surface is slowly removed by the air flow that is induced by the piezofan. The temperature on the heat source decreases gradually since the piezoelectric piezofan is operating. It is presumed the heat convection has reached the steady state condition whenever the temperature gradient has no change with the time step. The contours dictate that the piezofan reduces the temperature on the PLCC. The temperatures are observed to be 84°C and 63°C for $\delta = 0.064$ and 0.106 respectively. The predicted heat transfer coefficients are 49% for $\delta = 0.064$ and 146% for $\delta = 0.106$. Lack of symmetry in contours about the main axis are observed, which may be attributed to the use of unstructured mesh which is chosen to facilitate the dynamic meshing. Fig. 14 shows the comparison of predicted and experimental heat transfer coefficients for $\delta = 0.064$ and $\delta = 0.106$. The predictions are in good agreement with the experimental results (discrepancy is within 10%).

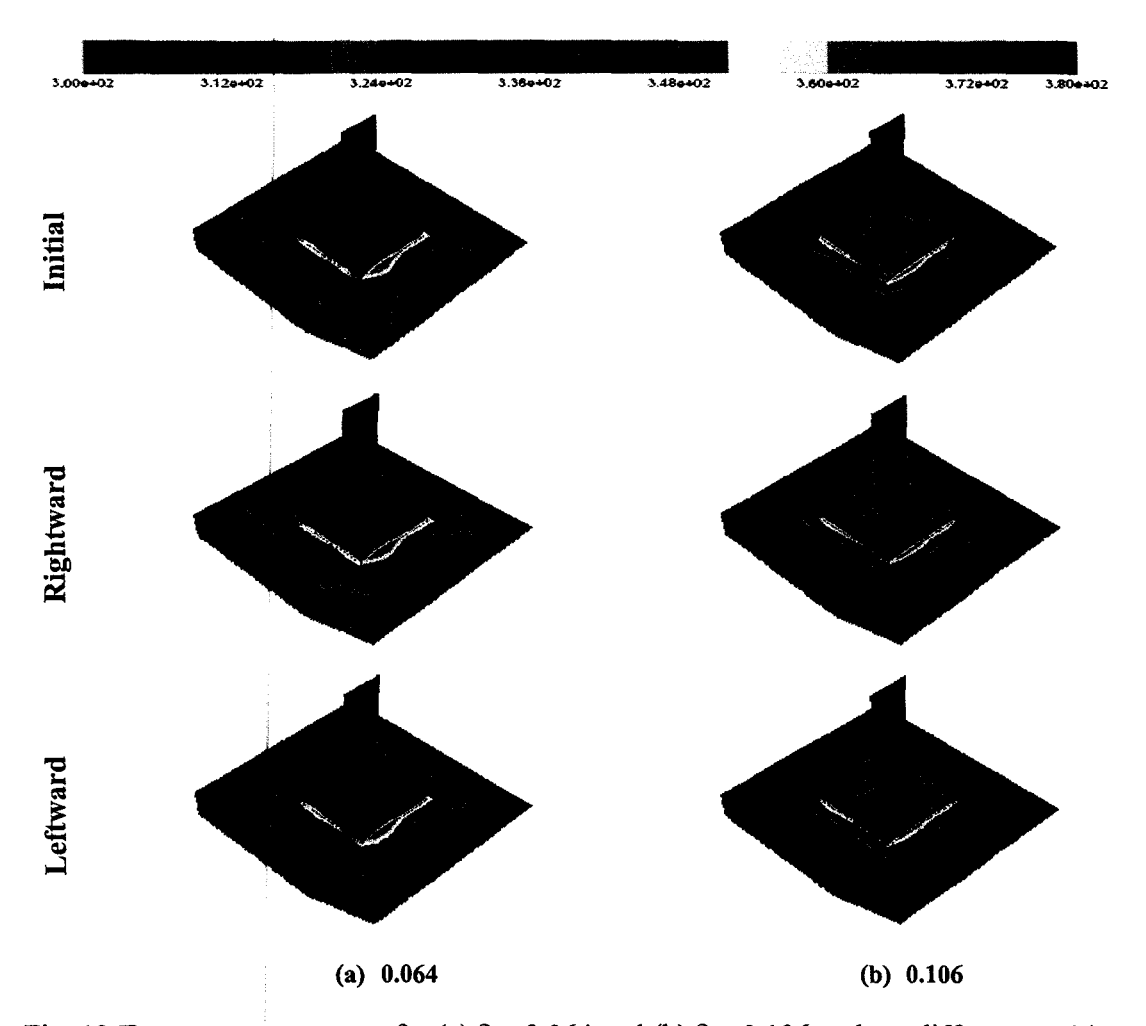


Fig. 13 Temperature contours for (a) $\delta = 0.064$ and (b) $\delta = 0.106$ at three different positions

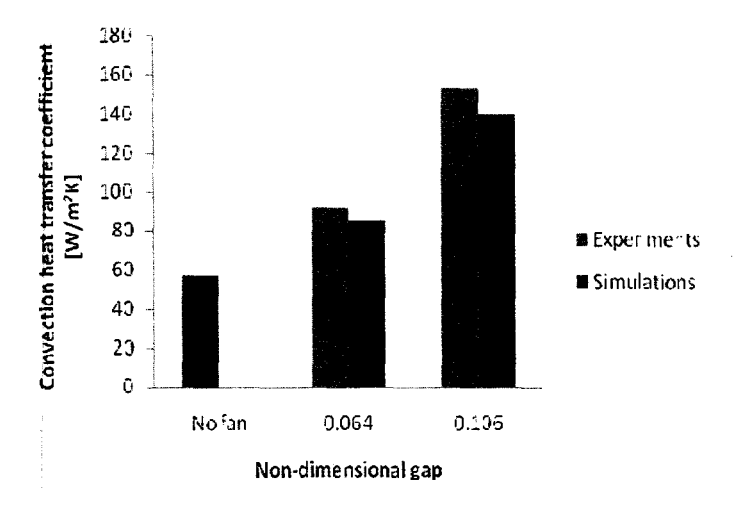


Fig. 14 Comparison of predicted and experimentally determined heat transfer coefficients

6. Conclusion

Experimental investigation and three dimensional numerical simulations are performed for a piezofan for two different gaps, and the thermal performance is compared with the base case (no fan). In numerical modeling, utmost care is exercised to emulate the realistic situation of a PLCC package. The piezofan operation is modeled using the dynamic meshes in FLUENT 6.3 software and the induced flow and heat convection involved are predicted. The piezofan swinging is observed to be of unsteady nature, which influenced the flow behavior on the PLCC surface. A gap of $\delta = 0.106$ yielded better heat transfer coefficient compared to the base case. The heat transfer coefficient predicted by CFD simulation also shown satisfactory agreement with the experimental data with a difference of 10%. Therefore, piezofan has shown to be a viable solution for the thermal management of PLCC packages. Similar experiments may be carried out for different gaps to arrive at the optimum gap, for various orientations of piezofan, and for more number of PLCC packages. The effect of enclosure for miniaturized systems is very crucial; so this issue may also be incorporated in future works.

REFERENCES

- Abdullah MK, Abdullah MZ, Ramana MV, Khor CY, Ahmad KA, Mujeebu MA, Ooi Y, Mohd Ripin Z (2009) Numerical and Experimental Investigations on Effect of Fan Height on the Performance of Piezoelectric Fan in Microelectronic Cooling, International Communications in Heat And Mass Transfer 36:51–58.
- Abdullah MK, Abdullah MZ, Ramana MV, Khor CY, Ahmad KA, Mujeebu MA, Ooi Y, Mohd Ripin Z (2008) Effect of Piezoelectric Fan Height on Flow and Heat Transfer for Electronics Cooling Applications, International Conference on Electronic Materials and Packaging, EMAP 2008, Taipei, Taiwan, Page(s): 165-170.
- Acikalin T, Garimella SV (2009) Analysis and Prediction of the Thermal Performance of Piezoelectrically Actuated Fans, Heat Transfer Engineering 30(6):487–498.
- Acikalin T, Wait SM., Basak S, Garimella SV, Raman A (2004) Experimental Investigation of the Thermal Performance of Piezoelectric Fans, Heat Transfer Engineering 25:4–14.
- Buermann P, Raman A, Garimella SV (2003) Dynamics and Topology Optimization of Piezoelectric Fans, IEEE Transactions on Components and Packaging Technologies 25(4):592-600.
- FLUENT© user's manual. Retrieved September 20, 2006 from the World Wide Web: http://www.fluentusers.com/fluent63/doc/ori/index.htm
- Garimella SV (2006) Advances in Mesoscale Thermal Management Technologies for Microelectronics, Microelectronics Journal 37:1165–1185.
- Kim, BJ., Rho, JS., and Jung, HK (2005) Optimal Design of Piezoelectric Cantilever Fan by Three-Dimensional Finite Element Analysis, KIEE International Transaction on Electrical Machinery and Energy Conversion Systems 5-B(1):90-94.
- Kimber M, Garimella SV, Raman A (2006) An Experimental Study of Fluidic Coupling Between Multiple Piezoelectric Fans, The Tenth Intersociety Conference on Thermal and Thermomechanical Phenomena in Electronics Systems, ITHERM 2006, SanDiego. Page(s): 333-340.

- Kimber M, Suzuki K, Kitsunai N, Seki K, Garimella SV (2008) Quantification of Piezoelectric Fan Flow Rate Performance and Experimental Identification of Installation Effects, 11th Intersociety Conference on Thermal and Thermomechanical Phenomena in Electronic Systems, ITHERM 2008, Florida. Page(s): 471 479.
- Kimber M, and Garimella SV, (2009) Measurement and prediction of the cooling characteristics of a generalized vibrating piezoelectric fan, International Journal of Heat and Mass Transfer 52:4470 4478.
- Kwon OD, Yoo JS, Yun YJ, Lee JS, Kang SH, Lim KJ (2005) A Research on the Piezoelectric Vibration Actuator for Mobile Phone, Proceedings of International Symposium on Electrical Insulating Materials, ISEIM 2005, Kitakyushu. Japan. 3:676-678.
- Liu SF, Huang RT, Sheu WJ, Wang CC (2009) Heat Transfer by a Piezoelectric Fan on a Flat Surface Subject to the Influence of Horizontal/Vertical Arrangement, International Journal of Heat and Mass Transfer 52:2565–2570.
- Meirovitch L (1997) Principals and techniques of Vibration, Englewood Cliffs: Prentice Hall.
- Melling A (1997) Tracer Particles and Seeding for Particle Image Velocimetry, Meas. Sci. Technology 8:1406–1416.
- Mohamed M, Deraman R, Abdullah MZ, Mujeebu MA, Abdullah MK (2008) Three Dimensional CFD Simulation For 8 PLCC Packages Mounted Inline on a Printed Circuit Board, Esteem, Volume 4, Number 1: 79-100.
- Sparrow EM, Niethammer JE, Chaboki A (1982) Heat Transfer And Pressure Drop Characteristics of Arrays of Rectangular Modules Encountered in Electronic Equipment, International Journal of Heat and Mass Transfer 25:961-973.
- Sparrow EM, Vemuri \$B, Kadle DS (1983) Enhanced and Local Heat Transfer, Pressure Drop and Flow Visualization for Array of Block Like in Electronic Equipment, International Journal of Heat and Mass Transfer 26(5):689-699.
- Toda M, Osaka S (1979) Vibrational Fan Using the Piezoelectric Polymer PVF₂, Proceedings of the IEEE, 67(8):1171-1173.
- Toda M, (1981) Voltage-induced Large Amplitude Bending Device-PVF Bimorph—Its Properties and Applications, Ferroelectrics 32, 127–133.
- Wait SM., Basak S, Garimella SV, Raman A (2007) Piezoelectric Fans Using Higher Flexural Modes for Electronics Cooling Applications, IEEE Transactions on Components and Packaging Technologies 30(1):119-128.
- Yoo JH, Hong JI, Cao W (2000) Piezoelectric Ceramic Bimorph Coupled to Thin Metal Plate as Cooling Fan for Electronic Devices, Sensors And Actuators A 79:8–12.

Full Pape

Heat Transfer Investigation on Effect of Multi-Piezoelectric Fan Locations/Arrangements with Simple Heat Sink for Microelectronic Cooling

M. K. Abdullah, N.C. Ismail, M. Z. Abdullah, M. A. Mujeebu, F. Hussin, H. Yusoff, M.B. Hashim and K. A. Ahmad

Aerodynamic and Advanced Cooling Laboratory, School of Mechanical and Aerospace Engineering Engineering Campus, Universiti Sains Malaysia 14300 Nibong Tebal, Penang, Malaysia Email: mkhalil@eng.usm.my

Abstract— An alternative cooling namely piezoelectric fan with relatively simple structures can be manipulated to generate airflow for cooling microelectronic devices. This viable solution has no electromagnetic noise, low power consumption and can be fitted to the confined space. The aim of this work is to investigate the finest option in term of locations (various height) and arrangements (vertical and horizontal locations) of multipiezoelectric fan that can be compliant in microelectronic devices. A simple heat sink with a single heat source is applied in the experiment and simulation. Predictive relationships (FLUENT 6.3) are used to describe the experimental trends and provide insight into the sensitivity of temperature and flow rate to these operating parameters. The numerical and experimental values are plotted and found in good agreement.

Keywords: Microelectronic cooling; location, multi-piezoelectric fan; heat transfer coefficient.

I. INTRODUCTION

A piezoelectric fan is a cantilever beam which consists of a piezoelectric material bonded into it. This piezoelectric material is typically bonded near the clamped end of the beam. The mechanism of contraction and expansion, generating shear forces between itself and the blade whenever an alternative input signal is applied to the piezoelectric material. These forces produce oscillations at the free end of the cantilever beam which creates motion in the surrounding fluid. This phenomenon has been maneuvered for enhancing the heat transfer between heat source and piezoelectric fan. The advantages of piezoelectric fan are no electromagnetic noise, low power consumption and limited space. Therefore, it can be adapted to operate at frequencies, which are too quiet to the human ear and can be built and modified to meet various geometric constraints for many applications. Recent research reveals that piezoelectric fans have received much attention owing to its capability as a thermal management solution [1].

A lot of researches on the performance of piezoelectric fans have been done. However, a few works have been reported on the application of the piezoelectric fan in the area of electronic cooling and are still underway. These fans first emerged in early seventies and it was introduced by Toda [2-3]. Simplified models have been developed for vibration prediction and flow field behavior. Ihara and Watanabe [4] investigated flows around the ends of oscillating flexible cantilevers. The comparison has been made between flow visualizations and simulation flow field which was developed Flow visualization by using discrete vortex method. experiments and simplified numerical simulation were conducted to gain insight into the flow induced by these piezoelectric fans [5-7]. In the first setup, experimentally mapped flow patterns were found to closely match those predicted by the model for the baffled fan while in the later; the advance flow measurements are carried out at different piezoelectric fan heights by using a particle image velocimetry (PIV) system.

One of the pioneer dealing with piezoelectric fans to heat transfer enhancement is Toda [2-3] which has been earlier. He found that the piezoelectric fans were able to cool on either side of a power transistor panel of a television receiver resulted in a 17°C decrease in temperature on the surface of the panel. Schmidt [8] experimented to determine the local and average transfer coefficients on a vertical surface cooled by using two piezoelectric fans resonating out of phase. It was noticeably showed that varying the distance between the fans and the surface and from one fan to another changed the transfer coefficients for the system. A further interest has been made by Acikalin et al. [9]. Piezoelectric fans are investigated as an active cooling technique in small-scale electronics cooling applications. Significant localized cooling was found, exceeding enhancements in convective heat transfer coefficients of 100% relative to natural convection.

Yoo et al. [10] studied on the possibility of replacing the rotary fan to the piezoelectric fans in some noise-sensitive.

Different vibrating metal plates were analyzed theoretically and showed that piezoelectric fans are also capable of generating jet flow for cooling purpose. Açikalin et al. [11] conducted a comparative study between piezoelectric fans, natural convection from a heat sink, and forced convection with axial fans. For a given power consumption; piezoelectric fans performed significantly better than axial fans, and compared to a natural convection heat sink; the piezoelectric fans were found to require less volume. On the other side, rotary fans are not preferred in the certain circumstance because of their high power consumption and noise generation. However, piezoelectric fans are not intended to replace rotary fans in larger devices, such as laptops and personal computers but it can be used for supplemental cooling in smaller devices [12].

Past research has focused on feasibility and performance characterization of a single fan, while arrays of such fans, which have important practical applications, have not been widely studied [13]. The two dimensional flow field generated from two flexible cantilevers dedicated to the fluid domain without considering heat transfer characteristics was analyzed experimentally by Ihara and Watanabe [4]. Mass transfer experiments on a vertical surface targeted by two piezoelectric fans were conducted by Schmidt [8]. Power-law correlations were found to reasonably describe both maximum and surface-averaged Sherwood numbers for three different distances from the vertical surface. In each case the Sherwood numbers formed contours that were symmetric about the midpoint of fan separation. Hosaka and Itao [14] and Basak and Raman [15] reported that the vibration characteristics of a vibrating cantilever are altered by the presence of a second oscillating beam depending on the vibration amplitude as well as the pitch and phase difference between neighboring cantilevers. Kimber et al. [16] confirmed experimentally by studying fluidic coupling between multi-piezoelectric fans. However, a number of aforementioned studies have demonstrated the potential of these fans as cooling solutions directly concentrated to the heat source and very little research has been conducted to better understand the behavior of multiple fans when attached with heat sink.

The present work considers the practically important configuration in term of locations and arrangements in which multi-piezoelectric fans are used in arrays with simple heat sink adapted, and where the complexity increases substantially in describing the fluidic and heat transfer behavior. Heat transfer experiments are conducted for two separate fan orientations; 90° and 0° (vertical and horizontal locations) and two different heights (0.5mm and 1.5mm). A detailed treatment of this topic is essential to providing insight into the underlying phenomena related to these fans, as well as to help in their implementation into practical designs.

II. MODELING

The governing equations of conservation of mass, momentum and energy have been applied in FLUENT in order to describe the fluid flow. The equations are displayed below. The general form of the mass conservation equation in *i*-th direction is:

$$\frac{\partial \rho}{\partial t} + \frac{\partial}{\partial x_i} (\rho u_i) = 0 \tag{1}$$

Conservation of momentum in *i*-th direction in an inertial (non-accelerating) reference frame is expressed by:

$$\frac{\partial}{\partial t}(\rho u_i) + \frac{\partial}{\partial x_j}(\rho u_i u_j) = -\frac{\partial P}{\partial x_i} + \frac{\partial \tau_{ij}}{\partial x_j} + \rho g_i + F_i$$
 (2)

Where, P is the static pressure, τ_{ij} is the viscous stress tensor and g_i and F_i are the gravitational acceleration and external body force in the i direction, respectively.

The conservation of energy equation in terms of h (static enthalpy) is:

$$\frac{\partial}{\partial t}(\rho h) + \frac{\partial}{\partial x_i}(\rho u_i h) = \frac{\partial}{\partial x_j}(k\frac{\partial T}{\partial x_i})$$
 (3)

Where T is the temperature and k is the thermal conductivity.

FLUENT allows to the users to simulate moving and deforming domains through the use of user define function (UDF). Dynamic meshes can be used to model flow where the shape of the domain is changing with time due to motion of the domain boundaries.

The integral form of the transport equation for a general scalar Φ , on an arbitrary control volume, V, on a moving mesh is written as,

$$\frac{d}{dt} \int_{V} \rho \Phi dV + \int_{\partial V} \rho \Phi (\vec{u} - \vec{u}_g) dA = \int_{\partial V} \Gamma \nabla \Phi dA + \int_{V} S_{\Phi} dV$$
 (4)

Where \vec{u} is the flow velocity vector and ug is the grid velocity of the moving meshes. The first and second terms on the left are the time derivative term and the convective terms. The terms on the right are the diffusive terms and the source terms. The term Γ represents the diffusion coefficient and S_{Φ} represents the source term of Φ . The term ∂V is used to represent the boundary of the control volume V and dA is the area movement.

All surfaces of the enclosure are isothermal and non-slip boundary conditions are applied at all solid surfaces. Similar setting on no-slip boundary conditions are also applied at the surfaces for the platform, heat sink and heat source. The detail descriptions are explained in Section 3.

III. DESCRIPTION OF THE MODEL AND COMPUTATIONAL TECHNIQUE

The model used in this simulation consists of a heater, simple heat sink and three piezoelectric fans mounted either

horizontally or vertically as shown in Fig. 1. The size of a heat source used is 3.0 cm \times 3.0 cm. The hybrid of tetrahedral and quad literal elements (about half million) are used in the present 3D analysis (see Fig. 2). A heat flux of 9166.67 W/m² has been set to the heat source. The heat sink is directly attached on the top of heater.

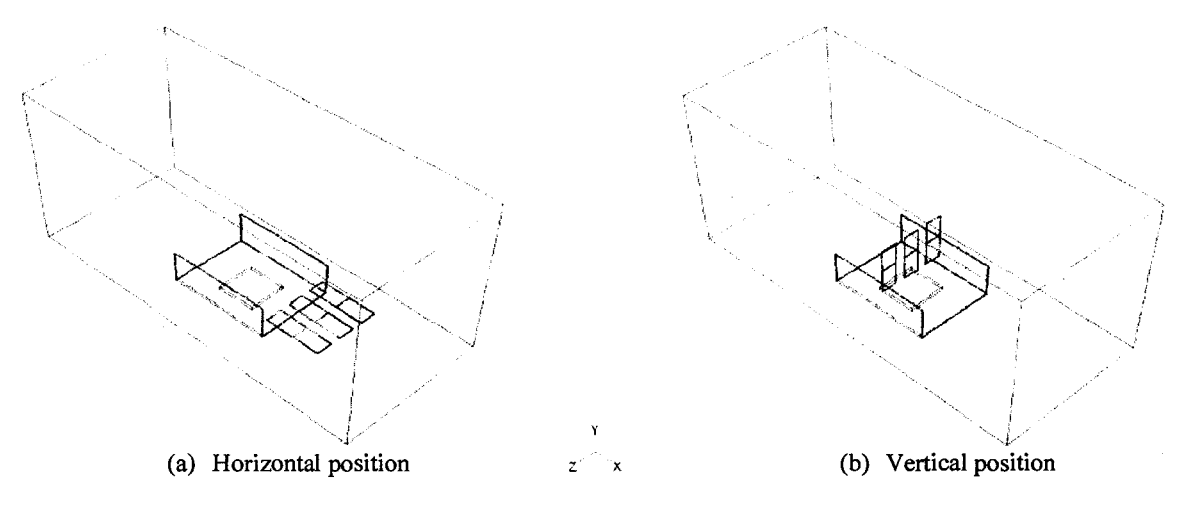


Fig. 1. Two positions of multi-piezoelectric fans with simple heat sink

The size of the computational domain is specified $28.0 \,\mathrm{cm} \times 14.8 \,\mathrm{cm} \times 12.0 \,\mathrm{cm}$ which is focused on heater, heat sink and multi-piezoelectric fans. The clamp of the piezoelectric fan is neglected and replaced by a simple adiabatic wall. The fan boundary is modeled as a moving

adiabatic wall whose location in time is set by a user-defined function in FLUENT. The fan is modeled as infinitesimally thin walls with no thermal conduction allowed through them. The left and right boundaries are set as outlet respectively.

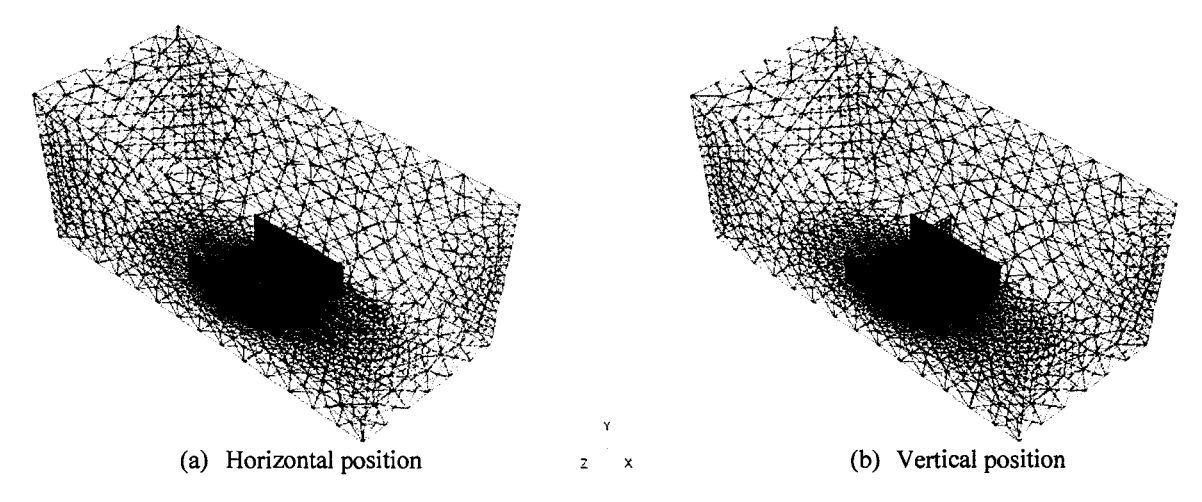


Fig. 2. Combination of tetrahedral and quad literal elements

The assumptions in the three-dimensional computational model include laminar, incompressible flow with radiation contributions since the temperature is below 100° C. First-order upwind discretization is used both for momentum and energy, with the SIMPLE scheme used for pressure-velocity coupling. A very small time step is applied, 1.0×10^{-4} s in order to capture the flow field correctly.

The heat transfer coefficient is calculated based on the average fluid temperature and the average heat source temperature. The total duration of the simulation is selected such that the heat transfer coefficient has reached a steady value during this period. It took 150,000 iterations, which corresponds to approximately seven days of computation time

per each case on a Pentium QuadCore processor (each 2.8 GHz) computer with 2.0 GB of memory.

IV. EXPERIMENTAL APPARATUS AND TEST SECTION

Fig. 3 shows the experimental apparatus used in the present study. The test section size of 25cm (H) × 12cm (W) × 80cm (L) made of glass have been fabricated for the study. A wood platform has been used for locating the heater since it has low thermal conductivity. The heat source is supplied by the heater. The heat loss through platform is assumed negligible. The heat source surface temperature is measured by the thermocouple which is soldered underneath of the heat source. Steady state condition is reached after 2 hours of the heating. A heat sink is bonded together to the heater with high thermal epoxy compound for high heat transfer occurred. Three piezoelectric fans are positioned at the angles of 90° (vertical) and 0° (horizontal) at the center and the trailing edges of heat sink. The piezoelectric fans under study are obtained from PiezoSystem Inc and its specifications are given in Table 1.

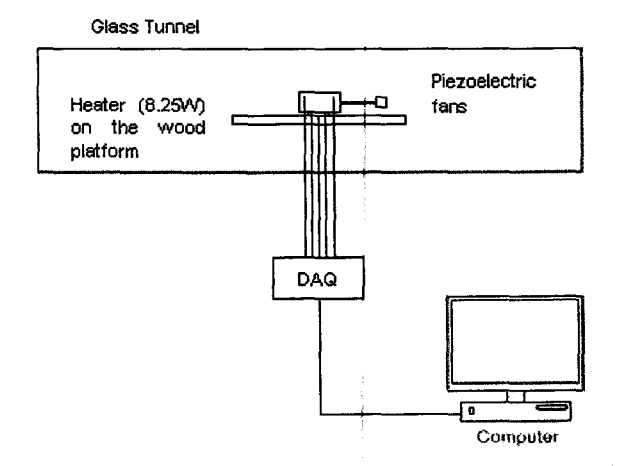


Fig. 3. Experimental setup used in the present study

Table 1 Specifications of the piezoelectric fan

Specification	Value
Material	Aluminum
Fan size (cm)	$4.7 (l_P) \times 1.2 (w_P) \times 0.04$
	(t_P)
Resonant frequency (Hz)	115
Power consumption of fan and circuit (mW)	42
Blade swing, peak to peak (cm)	0.95
Fan weight (gm)	2.0

V. RESULTS AND DISCUSSION

A. Experimental results and discussion

There are four experiments have been conducted in the present study; two sets for each locations and arrangements which have been identified individually as a Configuration A to D. The details are shown in the table below:

Table 2 Cases considered in the analysis

	Fan tip to heat source distance, d (cm)	
	0.5	1.5
Horizontal	Configuration A	Configuration C
Vertical_	Configuration B	Configuration D

Each configuration has five points of temperatures. However, temperature on the heat source (heater) is chosen for the case study. Fig. 4 shows the temperature profile obtained from the experiments. The total power input supplied to the heat source was 8.25 W.

The heater is turned on at t=0 s. The system reaches a steady state in natural convection whenever at t=2700 s at where the average temperature of the heat source under natural convection conditions around 85°C - 86°C . The piezoelectric fan is turned on at t=7200 s and a new steady state is reached after approximately 9000 s. The effect of multi-piezoelectric fans is clearly noticeable. A reduction in the average heat source temperature is around 28°C with the presence of multi-piezoelectric fans. The detail of temperatures obtained for the configurations are shown in Table 3.

Table 3 Temperature of configurations (experiment)

Configuration -	Temperature, °C
	Heater
Α	61.10
В	57.97
C	64.04
D	60.45

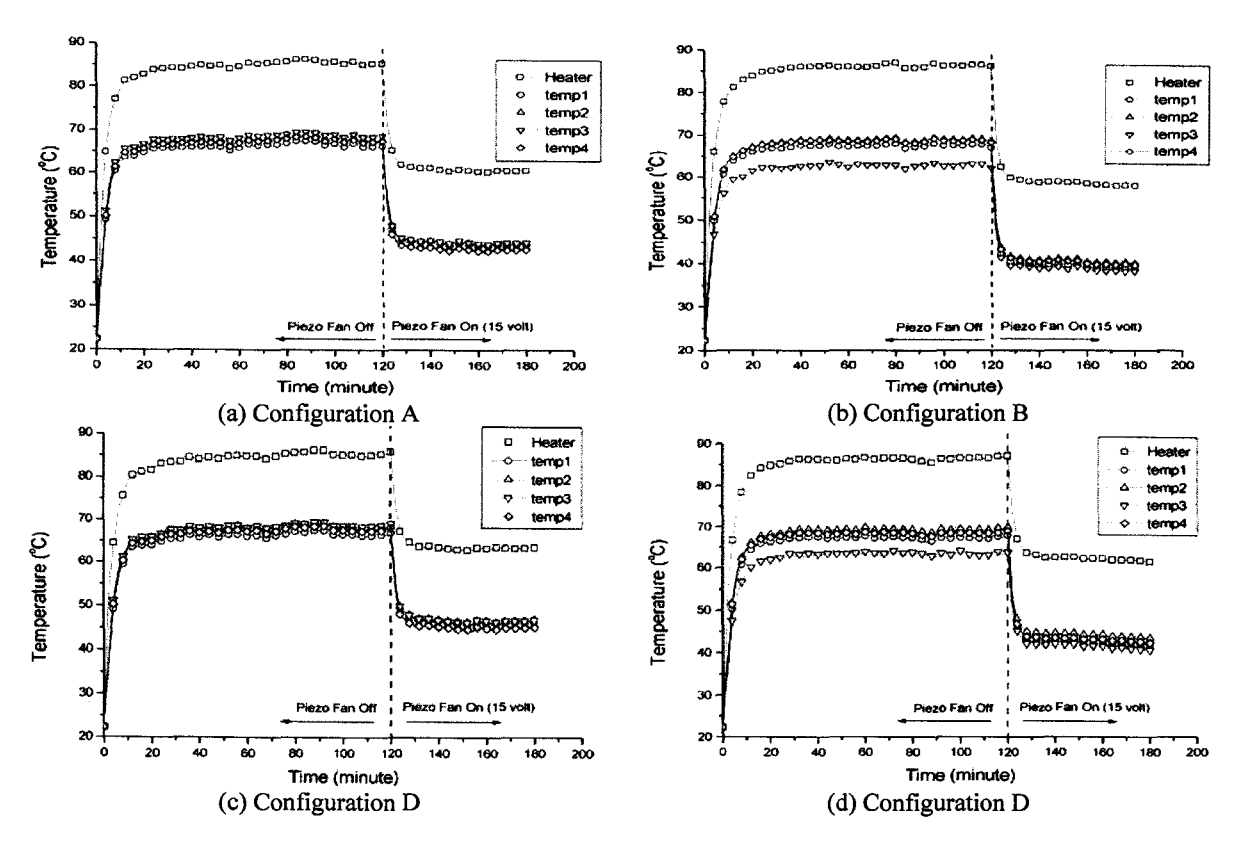


Fig. 4. Temperatures from a sample test in Configuration A

B. Configuration comparison

The steady-state heat transfer coefficients for four individual experiments from the configurations are shown in Fig. 5. The heat transfer coefficients are computed as

$$h_{ave} = \frac{Q_{in}}{A(T_{ave} - T_{co})} \tag{5}$$

In Eq. (5), Q_{in} is the heat input to the heat source, T_{ave} is the average heater surface temperature, T_{∞} is the ambient temperature, and A is the heat source area. Thermal losses from the heat source is assumed to be one-dimensional and varied depending on the final average heat source temperature reached in individual experiments.

From this figure, it is seen that the temperature reduction is highest for Configuration B and lowest for Configuration C. In all four configurations, the effect of fan arrangement on the temperature differentials is quite obvious compared to fan location. Plotted in this manner, it is clear that this effect persuaded the heat transfer significantly.

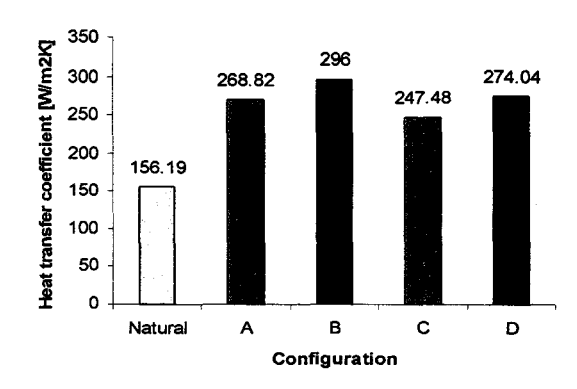


Fig. 5. Experimentally heat transfer coefficient

C. Numerical results and discussion

Simulations have been done for four configurations as mention early. The results are extracted whenever the temperature profile reached a steady state (150000 iterations). It means no temperature different are found even if the iterations increased. Fig. 6 shows the temperature results on the several configurations obtained from simulation.

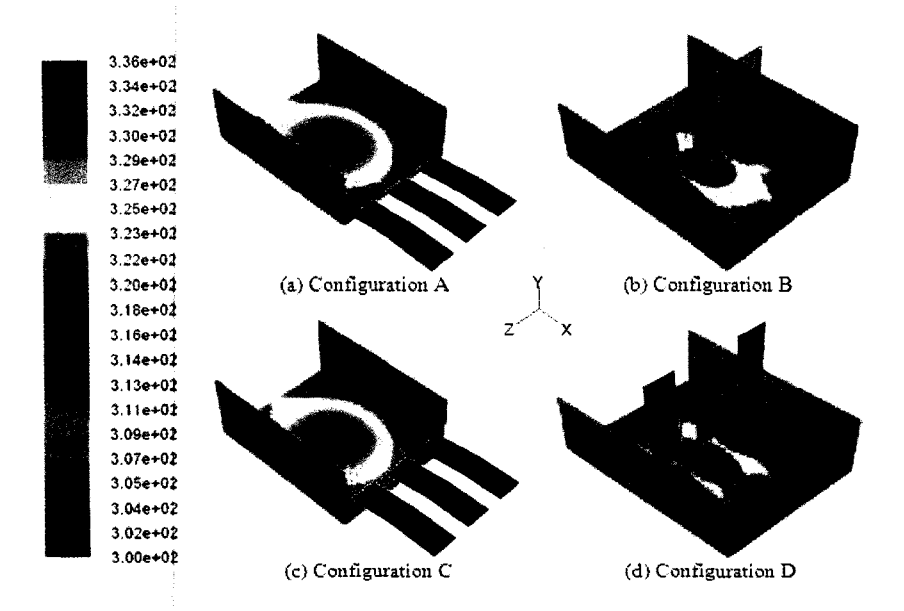


Fig. 6. Prediction of temperature contour on the several configurations

As expected, the effect of multi-piezoelectric fans is obviously evident. A temperature reduction in the average heat source surface temperature is around 25°C. The detail of temperatures obtained for those configurations are publicized in Table 4.

Table 4 Temperature of configurations (simulations)

Carfanadia	Temperature, °C
Configuration	Heater
A	62.52
В	61.53
C	63.16
D	61.60

D. Numerical results and discussion

A comparison of the four cases studied in the computations reveals a decrease in heat transfer coefficient with the arrangement of horizontal position and increasing distance between the fan and heat source and, as expected.

Predicted convective heat transfer coefficients from this study are compared to the experimental results in Fig. 7. A pattern of heat transfer coefficient obtained from simulation is conformed to the experiment. However, a huge different between simulation and experiment is observed on Configuration B even though their temperature different is very small (3.58°C). The main cause of this discrepancy is the amplitude effect is neglected in the numerical model, which is

expected to be especially pronounced in multi-piezoelectric fans.

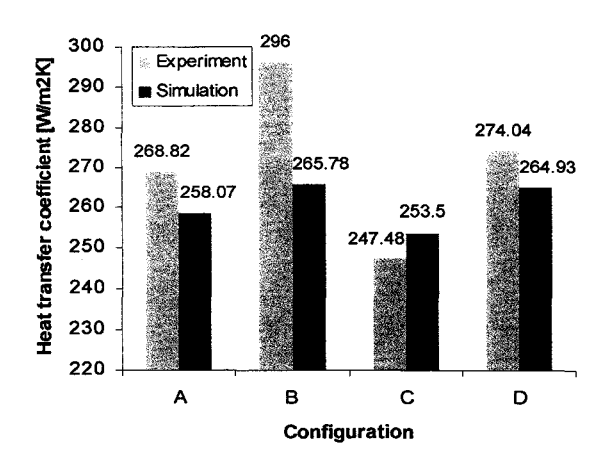


Fig. 7. Comparison of predicted and experimentally heat transfer coefficient

Meanwhile, the flow induced by the piezofan is more localized by stronger velocities in the vicinity of the heat source when the gap is small. As the piezofan moves up and down, forcing fluid to displace more rapidly as the piezofan passes a given position on the heat source. The closeness of the fan to the heat source leads to relatively high velocities and heat transfer coefficients. This fact is shown in Fig. 8.

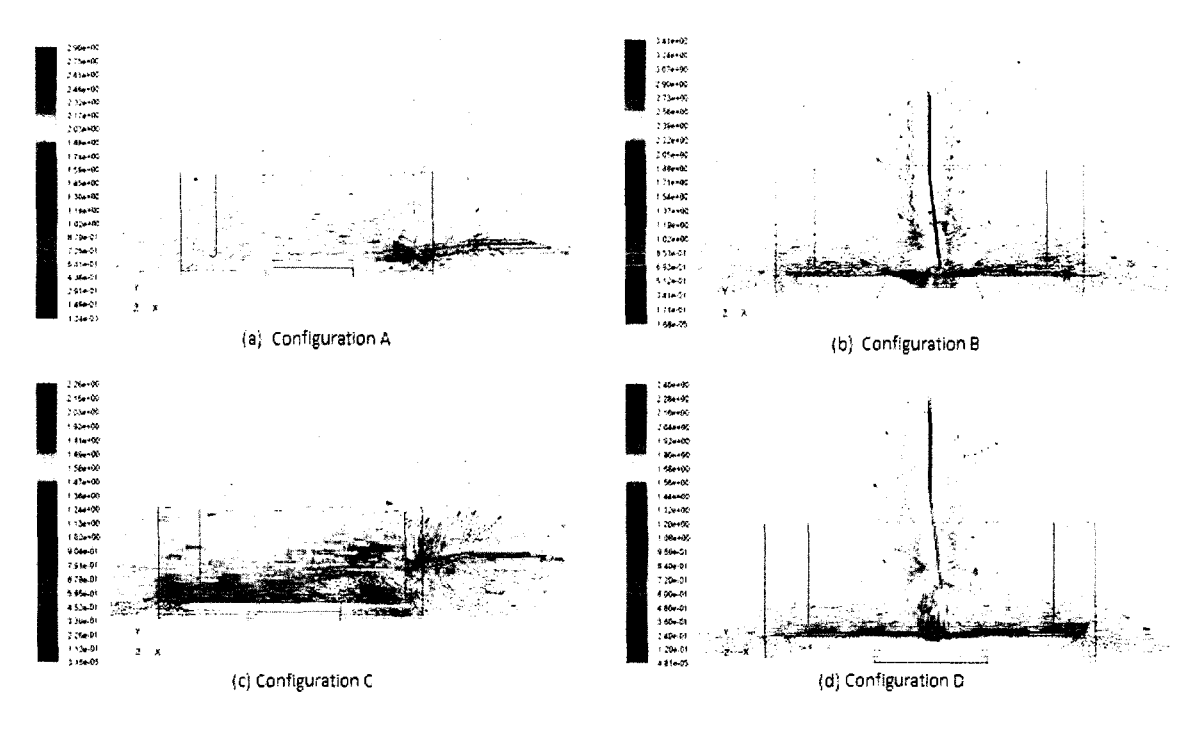


Fig. 8. Prediction of velocity vector on the several configurations

VI. CONCLUSION

Oscillating wall boundary condition with large deflection is modeled to the multi-piezoelectric fans operation resulting the flow and temperature fields' variation. Among the parameters investigated, location and arrangement between the fan and heat source have the greatest impact on the cooling capability of these fans. Effects of changes in the fan to heat source distance and the fan arrangement are investigated and compared against experimental results. It is observed that when the heat source is closed to the fan tip as well as vertical arrangement are greatly significant decreases in the heat transfer rates obtained. The multi-piezoelectric fans reduced the temperature of the heat source with heat sink by as much as 28°C, from values in natural convection of 86°C. Therefore, multi-piezoelectric fans have been proved to be a practicable solution for the thermal management of low-power electronics in applications such as laptops, cell phones, PDAs and LED packages.

REFERENCES

[1] Buermann, P., Raman, A., and Garimella, S.V., Dynamics and Topology Optimization of Piezoelectric Fans, *IEEE Transactionson Components and Packaging Technologies*, vol. 25, pp. 113–121, 2002.

- [2] Toda, M., 1979. Theory of air flow generation by a resonant type PVF2 Bimorph cantilever vibrator. Ferroelectrics 22, 911-918.
- [3] Toda, M., Voltage-Induced Large Amplitude Bending Device-PVF2 Bimorph—Its Properties and Applications, Ferroelectrics, vol. 32, pp. 127–133, 1981.
- [4] Ihara, A., and Watanabe, H., 1994. On the flow around flexible plates, oscillating with large amplitude. J. Fluid Struct. 8, 601–619.
- [5] Acıkalın, T., Raman, A., and Garimella, S.V., 2003. Twodimensional streaming flows induced by resonating, thin beams. J. Acoust. Soc. Am. 114, 1785–1795.
- [6] Abdullah MK, Abdullah MZ, Ramana MV, Khor CY, Ahmad KA, Mujeebu MA, Ooi Y, Mohd Ripin Z (2009), Numerical and Experimental Investigations on Effect of Fan Height on the Performance of Piezoelectric Fan in Microelectronic Cooling, International Communications in Heat And Mass Transfer 36 (2009) 51–58.
- [7] Abdullah MK, Abdullah MZ, Ramana MV, Khor CY, Ahmad KA, Mujeebu MA, Ooi Y, Mohd Ripin Z (2008), Effect of Piezoelectric Fan Height on Flow and Heat Transfer for Electronics Cooling Applications, International Conference on Electronic Materials and Packaging, EMAP 2008, Taipei, Taiwan, Page(s): 165-170.
- [8] Schmidt, R.R., 1994. Local and average transfer coefficients on a vertical surface due to convection from a piezoelectric fan. Procs. ITHERM, 41–49.
- [9] Acıkalın, T., Wait, S.M., Garimella, S.V., Raman, A., 2004. Experimental investigation of the thermal

- performance of piezoelectric fans. Heat Transfer Eng. 25, 4-14.
- [10] Yoo, J.H., Hong, J.I., Cao, W., 2000. Piezoelectric ceramic bimorph coupled to thin metal plate as cooling fan for electronic devices. Sensor Actuat. A Phys. 79, 8– 12.
- [11] Acıkalın, T., I. Sauciuc, Garimella, S. V., 2005, Piezoelectric actuators for low-form factor electronics cooling, in: Proceedings of the ASME intrPACK Conference, San Fransisco, CA, Vol 2, pp. 939-943.
- [12] Garimella, S. V., 2006, Advances in mesoscale thermal management technologies for microelectronics, Microelectronics Journal, 37, pp 1165–1185.
- [13] Kimber and Garimella, 2009, Cooling Performance of Arrays of Vibrating Cantilevers, Journal of Heat Transfer, Vol. 131, pp. 1-8.
- [14] Hosaka, H., and Itao, K., 2002, "Coupled Vibration of Microcantilever Array Induced by Airflow Force," ASME J. Vibr. Acoust., 124 (1), pp. 26-32.
- [15] Basak, S., and Raman, A., 2007, "Hydrodynamic Coupling Between Micromechanical Beams Oscillating in Viscous Fluids," Phys. Fluids, 19(1), pp. 017105.
- [16] Kimber, M., Garimella, S. V., and Raman, A., 2006, "An Experimental Study of Fluidic Coupling Between Multiple Piezoelectric Fans," International Society Conference on Thermal Phenomena, San Diego, CA, pp. 333–340.

Effect of piezoelectric fan height on flow and heat transfer for electronics cooling applications

¹M. K. Abdullah, ¹M. Z. Abdullah, ²S. F. Wong, ¹C. Y. Khor, ¹Y. Ooi, ¹K. A. Ahmad, ¹Z. Mohd
Ripin and ¹M. A. Mujeebu

¹Aerodynamic and Advanced Cooling Laboratory
School of Mechanical and Aerospace Engineering
Engineering Campus
Universiti Sains Malaysia
14300 Nibong Tebal, Penang
Malaysia

²Intel Technology (M) Sdn. Bhd.
Penang, Malaysia

ABSTRACT

Piezoelectric fan is used to remove the heat from the microelectronic devices, owing to their low power consumption, minimal noise emission and small in size. In the present study, a piezoelectric fan has been investigated to analyze performance. The paper also discusses the capability of piezoelectric fan to cool the microelectronic device and its performance. The simulation and experimental investigations have been made for two different positions of piezoelectric fan i.e. vertical and horizontal positions. The Fluent 6.2.3 software which is a computational fluid dynamics (CFD) code has been used in the simulation to predict the heat transfer coefficient and the flow fields. In the experimental set-up, two heaters in line arrangement have been used in the set-up. The flow measurements have been carried out by using the particle image velocimetry (PIV) system at different piezoelectric fan height. The heat transfer coefficients have been plotted and compared with the experimental values. The simulation results obtained are found in satisfactory agreement with the experimental results.

INTRODUCTION

With the advancement of science and technology, electronic products act more rapidly and perform more functions. Electronic products are also shrinking in size and weight, which has increased the volumetric heat generation rates and surface heat fluxes over their components. As the size of electronic component decreases, cooling by

fans has limited conventional components miniaturization. Hence, it is important to develop new cooling technology to improve performance of microelectronic components, which has motivated the usage of cantilever-type piezoelectric bimorph structure as a miniature fan. This is achieved by using a bimorph-type bending actuator, which consists of one or two thin piezoelectric ceramic layers bonded together. These piezoelectric bimorph structures have been investigated as an alternative cooling mechanism for cooling microelectronic components.

A number of works have been carried out with experiments as well as numerical simulation by using flexural waves [1]. The application of piezoelectric materials in sensors and actuators for actuating and controlling the smart structures were extensively studied by Crawly and Luis [2]. The potential convective heat transfer capability of an UFW generated by direct and inverse piezoelectric effect was experimentally investigated by Wu et al [3] and Loh et al. [4]. Yoo et al. [5] developed several types of piezoelectric fans using PZT, one of which resulted in a fan tip deflection of 3.55cm and air velocity of 3.1m/s measured 0.1cm away from the tip. Schmidt [6] used the naphthalene sublimation technique in experiments to determine the local and average transfer coefficients on a vertical surface cooled by two piezoelectric fans resonating out of phase. Changing the distance between fans, was found to noticeably change the heat transfer coefficients for the system. Acikalin et al. [7] developed a closed-form analytical solution

to predict the two-dimensional streaming flow from an infinite vibrating beam. The solution was used to develop a computational flow model for a baffled piezoelectric fan vibrating at its first mode of resonance in an infinite medium. Experimentally mapped flow patterns were found closely matched those predicted by the model for the baffled fan. The feasibility of using piezoelectric fans in small electronic cooling applications investigated by Wait et al. [8], Acikalin et al. [9] and Ramana et al. [10]. The visualization experiments were conducted to observe the flow induced by the piezo-fans. They also investigated thermal performance in two different arrangements and found the use of piezo-fans have enhanced the convective heat transfer coefficients.

In the present study, the piezoelectric fan is applied to cool two in inline heat sources horizontally mounted with no gap between them. The piezoelectric fan has been arranged at different height above the heat sources in order to obtain the effectiveness of cooling by the fan. The effect of piezoelectric fan height on the flow on the heat transfer coefficient is also presented.

DESCRIPTION OF MODEL

The model used in this simulation consists of an air chamber with the nozzle to a glass tunnel (test section). The size of a heat source used is 2.72 cm x 2.72 cm. The tetrahedral elements have been used in the present 2D analysis (see Figure 1). The dimension of the piezoelectric fan is given in Table 1. Both heat sources are supplied with a heat flux value of 4700 W/m² each for the heat transfer achieved at the heat source. In the model, the actual three-dimensional geometry of the experimental setup is simplified to a two-dimensional one as shown in Figure 1. The two-dimensional computational model considers the vertical midplane through the experimental test section as illustrated in Figure 2. Since gravity is normal to this two-dimensional plane, buoyancy effects are negligible and do not need to be included in the model.

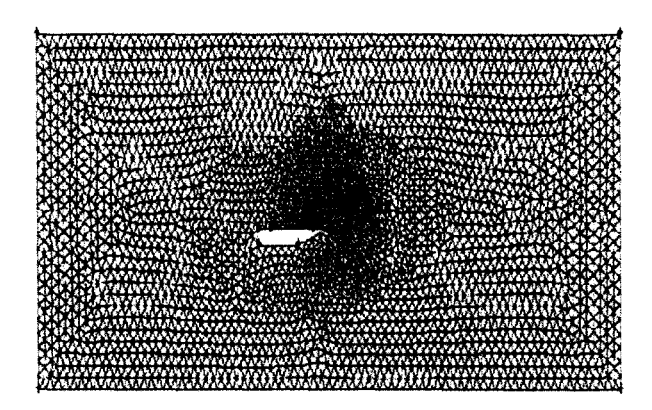


Figure 1 Mesh generation using tetrahedral elements

The size of the computational domain is similar to those used in the experiments (25 cm x 80 cm). The four sides of the enclosure shown in Figure 1 are set as isothermal walls in the numerical model. The clamp of the piezoelectric fan is neglected in the computational model, and instead replaced by a simple adiabatic wall as shown in the figure. The piezoelectric fan boundary condition is modeled as a moving adiabatic wall whose location in time is set by a user-defined function in FLUENT. The piezoelectric fan is modeled as infinitesimally thin walls with no thermal conduction allowed through them. The left and right boundaries are set as inlet and outlet boundary conditions respectively.

The enclosure includes two inline heat sources mounted horizontally embedded in the platform, as shown in Figure 3. Corresponding to the heat dissipation from both heat sources with a uniform heat flux of 4700 W/m² is applied to the exposed not insulated wall of the heat source in the numerical model (as shown in Figure 1). The other three walls of the heat source are considered to be adiabatic.

The assumptions in the two-dimensional computational model include laminar, incompressible flow with no buoyancy or radiation contributions. First-order upwind discretization is used both for momentum and energy, with the SIMPLE scheme used for pressure-velocity coupling. Although a second-order scheme would yield better accuracy, these schemes were not explored due to constraints on computational time. In order to capture the flow field correctly, a very small time step is required. For all the results presented here, a time step of 1.0 x 10⁻⁴s was used. Thus, 100 steps in time were needed for one cycle of fan vibration.

The heat transfer coefficient is calculated based on the average fluid temperature and the average heat source surface temperature. The total duration of the simulation is selected such that the heat transfer coefficient has reached a steady value during this period. This took 4,000 time steps, which corresponds to approximately 4 hours of computation time per case on a Pentium D processor (each 2.8 GHz) computer with 0.5 GB of memory. In this study, the coarser mesh 13,189 nodes, and run with time-step size of 0.0001 s has been used for Case A. The results presented below are obtained using a finer mesh with 15,575 nodes, with same time step of 0.0001 s (100 time steps per cycle of fan vibration.) The cycle-averaged and surface-averaged temperatures obtained with the coarse and fine meshes differed by 0.3 °C in Case B. With the coarse mesh, the cycle-averaged heat transfer coefficients predicted on the plate were approximately 2.5°/0 lower than the values obtained using the finer mesh.

EXPERIMENTAL APPARATUS AND TEST SECTION

Figure 2 shows the experimental apparatus used in the present study. The compressor (1) is used to atomize the corn oil particles in an atomizer (2). This oil particle is used as the seeding for the particle image velocimetry system. The air chamber (3) with the dimension of 1.5 x 1.5 x 1.5 m³ and has a test section (6) size of 25cm (H) x 6cm (W) x 80cm (L) made of glass have been fabricated for the study. The oil particles are settled in the air chamber and slowly drawn into the glass tunnel (test section).

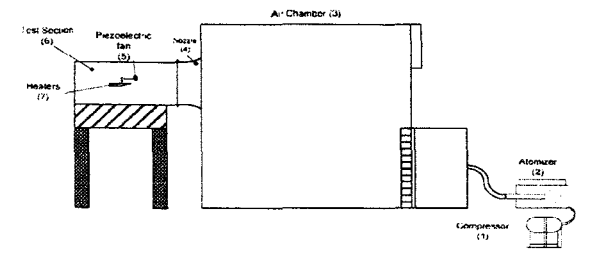


Figure 2 Experimental apparatus arrangement

Figure 3 illustrates the heaters arrangement. The heat source is supplied by the heater (7) and the piezoelectric fan (5). The piezoelectric fan has been located at two different positions i.e. horizontal and vertical positions as shown in Figure 3. The platform of heat sources (7) is made from wood which serves as insulator to minimize heat loss. Angles of 45° at leading and trailing edges are made to avoid the flow separation. The heat loss through platform is assumed negligible. The steady state condition is reached after 8 hours of the heating.

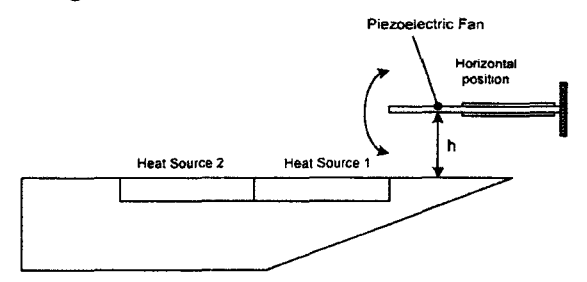
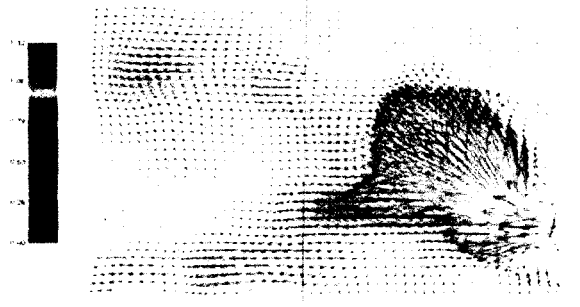


Figure 3 Schematic of the piezoelectric fan and heat source arrangements

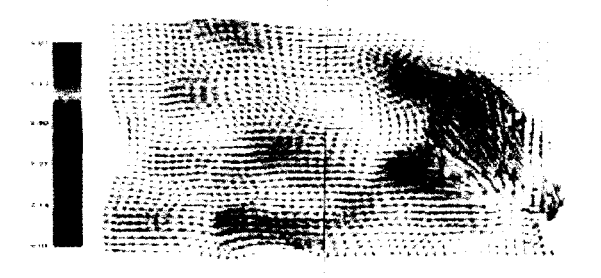
A Dantec 2D particle image velocimetry (PIV) system has been used to measure the velocity induced by a piezoelectric fan. The movement of seeding particle (atomization of corn oil) has been captured by a CCD camera where the camera is synchronized with a double pulse YAG laser and controlled by the computer via a PIV controller unit. The induced velocity is calculated by the software provided by the system.

RESULTS AND DISCUSSION

Figure 4 show the velocity vectors for case A, where the piezoelectric fan is located $h_p/l_p = 0.13$ from the heat source. The vectors are measured at 2 different time when the fan swings downward (Figure 4a) and upward (Figure 4b). The piezoelectric fan has been adjusted to the resonance mode, when it is operates the velocity is induced very much depending on the movement of piezofan. More induced velocity when the fan swings upward direction, it is observed that a higher volume of flow on the top surface of heat sources, where the maximum velocity reaches about 0.8m/s. Whereas, for the fan swing downward less volume of flow pass through on the top surface of heat source. The maximum velocity reaches at 0.4m/s.

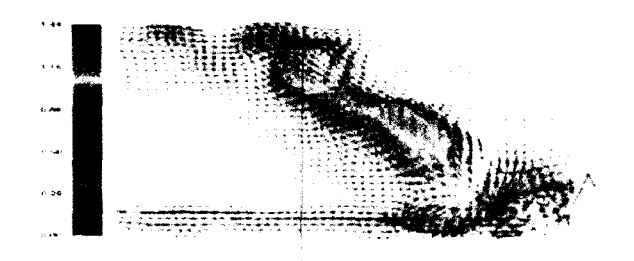


(a) Piezofan swing downwards



(b) Piezofan swing upwards Figure 4 Velocity vectors for Case A ($h/l_P=0.13$) induced by the piezofan

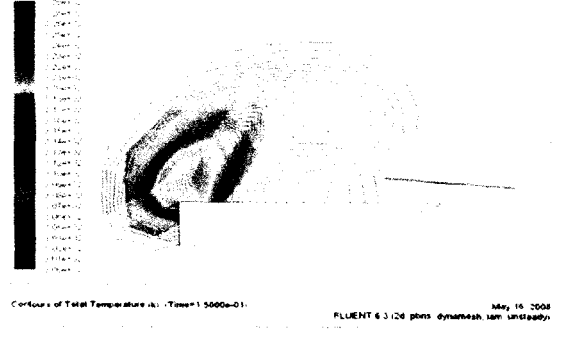
The velocity vectors for case B is shown in Figure 5 when the location of piezofan is located slightly higher at $h_p/l_p=0.23$ from the heat sources. The velocity vectors of higher magnitude are induced on the top surface of heat sources where the maximum velocity reaches up to 1.1m/s especially for the piezofan swings upward. For the piezofan swings downward, the velocity vectors slightly lower where the maximum velocity is about 1.0m/s. Thus, one can conclude that the heat transfer will be higher for case B compared to case A since the flow velocity increases with h/l_p on the heat source.



(b) Piezofan swing upwards

Figure 5 Velocity vectors for Case B ($h/l_P = 0.23$) induced by the piezofan

Figures 6a and 6b show the temperature contour for case A at different time intervals. The heat from the heat source surface is slowly removed to downstream by the air flow that induced by the piezofan. The temperature on the heat source decreases gradually since the piezoelectric fan is operating. The contours illustrate that the piezofan reduces the temperature on the heat source surface as much as 23° C. The double vortices of temperature can also be observed in the figure at t = 0.35s. Further the temperature on heat source surface reduces and temperature variation is small (less than 10%) for t = 0.35s and t = 0.4s. Thus, in the present study, it is assumed the heat convection is reached a steady state condition at t = 0.35s.



(a) t = 0.15s

(a) Piezofan swing downwards

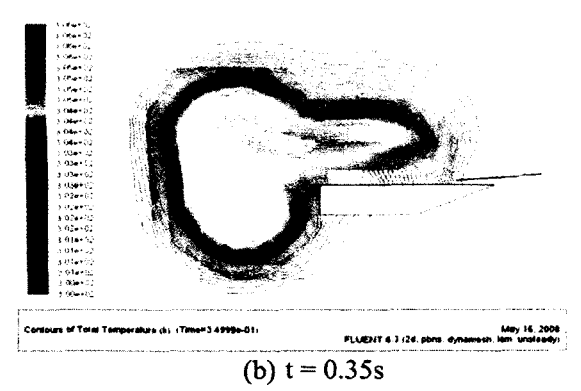
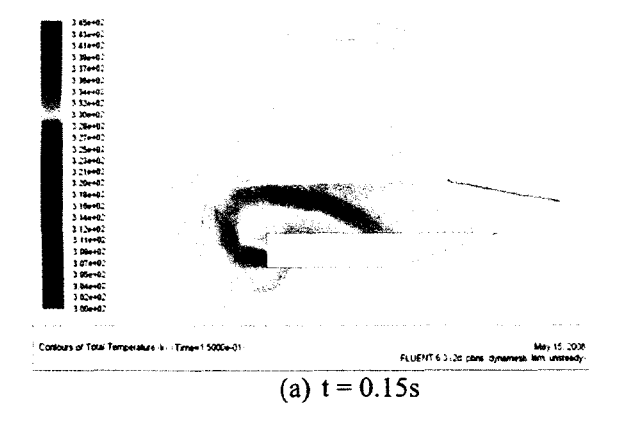


Figure 6(a)-(b) Temperature contours for Case A at different time interval

In case B $(h_p/l_p=0.23)$, Figures 7a and 7b show similar pattern with case A $(h_p/l_p=0.13)$. However, the heat transfer from the heat source to the air stream is higher compared to case A. The temperature on the heat source reduces with time, and just after t=0.35s the temperature is almost constant. The figures show the heat is slowly removed from the heat sources to downstream of the platform. The contour also shows that the temperature distribution is reached a steady condition at t=0.35s. The contours illustrated the piezofan reduces the temperature on the heat source surface as much as 25.1° C. It can be concluded that the height of piezofan has influenced the temperature drop on the heat source surface.



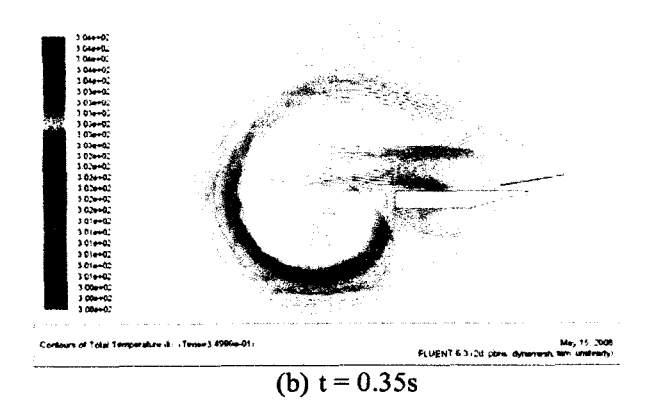


Figure 7(a)-(b) Temperature contours for Case B at different time interval

Two different heights of the piezoelectric fan are studied in the present work. The velocity vectors indicated comparatively more air flow over the heat sources for case B hence better heat convection performance. The results also show that the location of piezoelectric fan with $h_p/l_p=0.23$ has the bigger profile. Figure 8 shows the average heat convection coefficient for case B is $45.14 \text{W/m}^2 \text{K}$ and about 4% higher compare to case A. The heat transfer coefficient is calculated based on the average of heat source surface temperature using the equation:

$$h_{ave} = \frac{q}{(T_{ave} - T_{\infty})} \tag{5}$$

The results generally show that the piezoelectric fan height of $h_p/l_p=0.23$ above the heat source has better performance in the thermal management. The results predicted by the CFD software are found in good agreement with the experimental values (the difference is about 11% only).

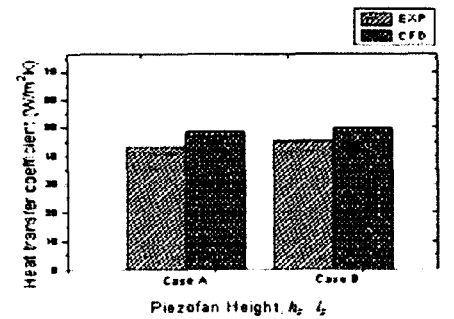


Figure 8 Heat transfer coefficients for cases A and B

CONCLUSIONS

The experimental and simulation studies have been made for a piezoelectric fan for two different heights above the heat source. The piezofan manages to reduce the temperature of the heat source by as much as 68.9°C. The piezoelectric fan operation is modeled using the dynamic meshes couple with a harmonic motion in FLUENT 6.2.3 software and has predicted the induced flow and heat convection involved. The results showed that the height of piezofan from the heat source has influenced the heat transfer coefficient. A height of $h_p/l_p = 0.23$ has increased about 4% in heat transfer coefficient compared to $h_0/l_p = 0.13$. The piezofan swinging is unsteady phenomena and influenced the flow behavior on heat source surface. The heat transfer coefficient predicted by CFD simulation has shown good agreement with the experimental data with difference of 11%.

REFERÊNCES

- [1] P. I.Ro, Loh, Feasibility of using flexure waves as a cooling mechanism, IEEE Transactions on Industrial Electronics 48 (1) (2001) 143-149.
- [2] E. F. Crawly, and D. J.Luis, Use of piezoelectric actuator as elements of intelligent structures, AIAA Journal 25 (1987) 1373-1385.
- [3] T. Wu, P.I. Ro, A. I. Kingon, J. F. Mulling, Piezoelectric resonating structures for microelectronic cooling, Smart Materials and Structures 12 (2003) 181-187.
- [4] B. G. Loh, S. Hyun, P. I.Ro, C. Kleinstreuer, Acoustic streaming induced by ultrasonic flexural vibrations and associated enhancement of convective heat transfer, Journal of Acoustics Society of America 111 (2002) 875-883.
- [5] J. H. Yoo, J. I. Hong, W. Cao, Piezoelectric ceramic bimorph coupled to thin metal plate as cooling fan for electronic devices", Sensor Actuators, A. Phys. 79 (2000) 8-12.
- [6] R. R. Schmidt, Local and average transfer coefficients on a vertical surface due to convection from a piezoelectric fan", Proc. ITHERM, Washington, D.C. 1994, pp. 41-49.
- [7] T. Acikalin, A. Raman, S. V.Garimella, A. Raman, Two dimensional streaming flows

- induced by resonating thin beam", J. Acoustic Society of America 114 (2003) 1785-1795.
- [8] S. M. Wait, T. Acikalin, S. V. Garimella, A. Raman, Piezoelectric fans for the thermal management of electronics", Proc. Sixth ISHMT/ASME Heat and Mass Transfer Conference, Kalpakkam, India, January 5-7, 2004. Paper No. HMT-2004-C76, pp. 447-452.
- [9] T.Acikalin, S. V. Garimella, A. Raman, J.Petroski, Characterization and optimization of the thermal performance of miniature piezoelectric fans", Int. J. Heat and Fluid Flow 28 (2007) 806-820.
- [10] M. V. Ramana, I. P. Almanar, M. Z. Abdullah, Z. Mohd Ripin, K. N. Seetharamu, Design and optimization of piezoelectric fans for cooling of microelectronic devices", Int. Journal of Microelectronic and Packaging Society 4(3) (2007) 121-129.



STUDY ON PIEZOELECTRIC FAN HEIGHT ON THE COOLING PERFORMANCE OF PLCC ELECTRONIC PACKAGE



M.K. Abdullah, M.B. Hashim, M.Z. Abdullah, M.A. Mujeebu, K.A. Ahmad, and F. Ismail

UNIVERSITI SAINS MALAYSIA

The Accelerated Program For Excellence University

7

INTRODUCTION

Plezoelectric fan generally consists of a patch of piezoelectric material bonded to a flexible cantilever blade. An alternating vortage is applied to the piezoelectric patch, it expands and contracts in the lengthwise direction, causing bending moments at both ends of the patch. These moments drive the attached blade to oscillate at the same frequency. These fans use very little power and can be developed to meet vanious geometric constraints for many applications. It clearly enhances the heat transfer when compared to natural convection. This technology is desirable because it is noiseless at the frequencies of operation, and is compact, lightweight, and durable.

2

PROBLEM DEFINITION

The continuing increase of power densities in microelectronics and simultaneous drive to reduce the size and weight of electronic products have led to crucial thermal management issues in the industry. Inappropriate thermal management of the electronic device degrades its performance significantly. The conventional cooling devices such as rotary fan and heat sink are popular in the current market. Ironically, they are not so suitable for portable devices such as laptop and mobile phone owing to space and power limitations. Plastic Leaded Chip Carrier (PLCC) arrangement is an alternative that can be used in portable electronic devices to improve thermal performance hence electronic performance. However, a PLCC alone cannot resolve the issue since it also requires a cooling mechanism. One of the viable solutions is piezoelectric fan. It is an innovative design which is gaining acceptance as fessible solution for portable electronic products.

3

PIEZOFAN POTENTIAL

The potential offered by piezoelectric fans for the thermal management of low-power electronics components, PLCC is assessed experimentally as well as numerically. Two different experimental configurations are measured in order to map the effects of piezoelectric fan gaps on the heat transfer from a small heat source. The numerical simulation is done by using PLUENT 6.3. The piezoelectric fan is applied to cool a single heat source, mounted vertically.

4

EXP./SIMUL. SETUP

The model used in this simulation consists of a glass tunnel (test section), heater, heater platform and piezoelectric fan. A glass tunnel of size 25cm (H) × 8cm (W) × 80cm (L) is constructed to act as the test section. The specifications of piezofan are given in Table 1. Figure 1 shows the three-dimensional geometry of the experimental setup and it is similar to the simulation setup. The fan boundary is modeled as a moving wall whose location in time is set by a user-defined function in FLUENT. The combinations of tetrahedral and hexahedral elements are used in the present 3-D analysis. The flow is assumed as laminar and incompressible with no radiation contributions. First-order upwind discretization is used both or momentum and energy, with the SIMPLE scheme used for pressure-velocity coupling. The heat transfer coefficient based on the average fluid and heat source surface temperatures is calculated. The total duration of the simulation is selected such that the heat transfer coefficient has reached a steady value during this period. This took 150,000 time steps, which corresponds to approximately 4 days of computation time per each case on a Pentium Quadcore processor (2.8 GHz) computer with 2-GB of memory.

Table 1 Specifications of the plezofan

Specification	Value
Material	Aluminum
Fansize (cm)	$4.7(I_P) \times 1.2(w_P) \times 0.04(I_P)$
Resonant frequency (Hz)	115
Power consumption of fan and circuit (mW)	42
Blade swing, peak to peak (cm)	0.95
Fan weight (gm)	2.0
Heater size (cm)	2.0 × 2.0
Heat flux (W/m²)	4594

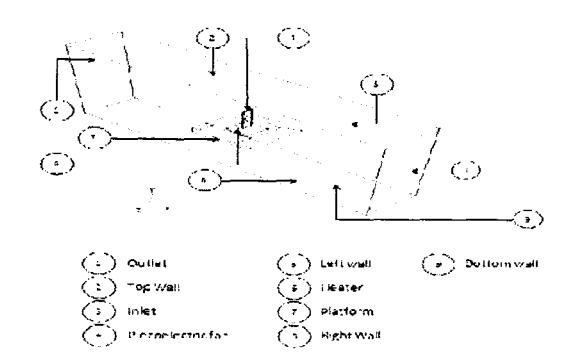


Figure 1: Iso-view of experimental/simulation setup

5 RESULT & DISCUSSION

The goal of this study is to analyze the temperature distribution, flow and average heat convection coefficient for non-dimensional gaps of 0.064 and 0.106. The non-dimensional gap is defined as a gap between tip of the piezodan and heat source surface over the length of piezofan. Figure 2 shows the temperature contours at different piezofan positions. The heat from the heat source surface is slowly removed by the air flow that is induced by the piezofan. It is presumed the heat convection is reached the steady state condition whenever the temperature gradient has no change with the time step. The temperatures are observed to be 84°C and 63°C for gaps 0.064 and 0.106 respectively.

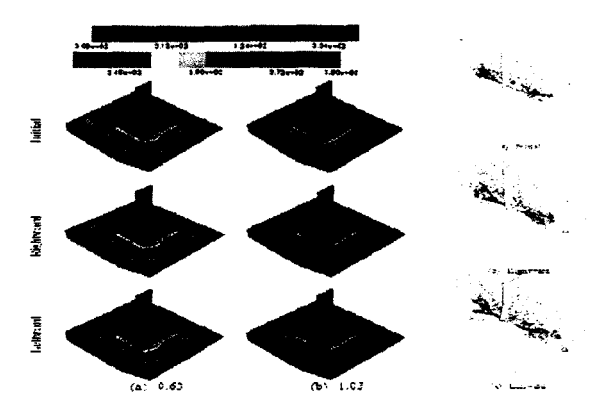


Figure 2: Temperatures contours and velocity vector at three different positions

The vectors are chosen at three different positions such as, the fan at the initial position (undeflected), swing lethward and swing rightward where it has entrain a larger amount of fluid. Two regions of circulation would be expected as can be seen in figures. These symmetric circulation zones above and below the vibrating piezofan are attributed to the rapid leftward and rightward swings. For the gap of 0.064, the maximum velocity when the fan swings left is found to be 1.52m/s and for right swing, it is 1.1m/s. Meanwhile, the maximum velocities during leftward and right ward swings are observed to be 2.05m/s and 1.75m/s respectively for the gap of 0.106. It clearly shows that with the gap of 0.106, the fluid motion has enough physical space and more of the energy of the excited fluids is used to diffuse heat from the PLCC causing the observed localized cooling effect.

5

MODEL VALIDATION

The effect of change in gaps on the PLCC surface temperature is shown in Figure 3 which causes a reduction in the heat source temperature from 110°C to 80°C and 60°C for 0.064 and 0.106 respectively. Predicted convective heat transfer coefficients for non-dimensional gaps are compared with the experimental results as shown in Figure 4 which shows that the predicted results are in satisfactory agreement with the experimental values. The results also indicate that the piezofan provides enhanced cooling relative to the natural convection; increase of 61% and 168% for gaps 0.064 and and 0.106 respectively. 0.106 respectively.

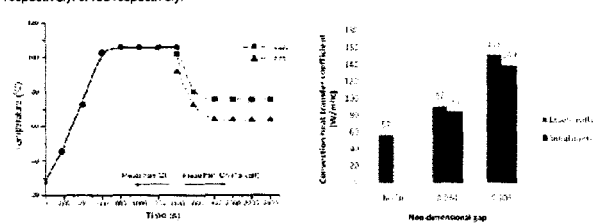


Figure 3: Effect of fan gaps on PLCC

Figure 4: Comparison of predicted and experimentally determined heat transfer coefficients

6

CONCLUSION

The results showed that certain gap of piezofan from the heat source has influenced the heat transfer coefficient. Therefore, piezoelectric fans have been shown to be a viable solution for the thermal management of PLCC packages.

Acknowledgement

This work is supported by the Universiti Sains Malaysia under contract of FRGS 97-ET-7-007-006-ET and

Researcher Information

Assoc. Prof. Dr. Mohd Zulkifly Abdullah Advance Cooling Laboratory School of Mechanical Engineering, Universiti Sains Malaysia, Engineering Campus, 14300 Nibong Tebal, Seberang Perai Selatan, Penang, Malaysia. Teh 604-598